

**STATE AND PARAMETER ESTIMATION IN NONLINEAR LUMPED
AND DISTRIBUTED PARAMETER CIRCUITS USING REAL-TIME
STOCHASTIC FILTERING ALGORITHMS**

A Thesis Submitted to

Delhi Technological University

for the Award of Degree of

Doctor of Philosophy

In

Electronics and Communication Engineering

By

Amit Kumar Gautam

(Enrollment No.: 2K15/PhD/EC/03)

Under the Supervision of

Dr. Sudipta Majumdar

Assistant Professor



Department of Electronics and Communication Engineering

Delhi Technological University (Formerly DCE)

Bawana Road, Delhi-110042, India.

July, 2023

© Delhi Technological University–2023

All rights reserved.

DECLARATION

I declare that the research work reported in this thesis entitled “**State and Parameter Estimation in Nonlinear Lumped and Distributed Parameter Circuits using Real-Time Stochastic Filtering Algorithms**” for the award of the degree of *Doctor of Philosophy in Electronics and Communication Engineering* has been carried out by me under the supervision of *Dr. Sudipta Majumdar*, Department of Electronics and Communication Engineering, Delhi Technological University, Delhi, India.

The research work embodied in this thesis, except where otherwise indicated, is my original research. This thesis has not been submitted by me earlier in part or full to any other University or Institute for the award of any degree or diploma. This thesis does not contain other person’s data, graphs or other information, unless specifically acknowledged.

Date :

(Amit Kumar Gautam)

Enrollment no.: 2K15/PhD/EC/03

Department of ECE

Delhi Technological University,

Delhi-110042, India



DELHI TECHNOLOGICAL UNIVERSITY

(Formerly Delhi College of Engineering)

Shahbad Daultapur, Bawana Road, Delhi-110042, India

CERTIFICATE

This is to certify that the research work embodied in the thesis entitled "**State and Parameter Estimation in Nonlinear Lumped and Distributed Parameter Circuits using Real-Time Stochastic Filtering Algorithms**" submitted by **Mr. Amit Kumar Gautam** with enrollment number (**2K15/PhD/EC/03**) is the result of his original research carried out in the Department of Electronics and Communication Engineering, Delhi Technological University, Delhi, for the award of **Doctor of Philosophy** under the supervision of **Dr. Sudipta Majumdar**.

It is further certified that this work is original and has not been submitted in part or fully to any other University or Institute for the award of any degree or diploma.

This is to certify that the above statement made by the candidate is correct to the best of our knowledge.

(Dr. Sudipta Majumdar)

Supervisor

Department of ECE

Delhi Technological University,

Delhi-110042, India

(Dr. O. P. Verma)

Professor & Head

Department of ECE

Delhi Technological University,

Delhi-110042, India

ACKNOWLEDGEMENTS

First and foremost I wish to express my sincere gratitude to my supervisor Dr. Sudipta Majumdar, Department of Electronics and Communication Engineering, Delhi Technological University (DTU), Delhi for her inspiring guidance and support during my research work, and for giving me the freedom to explore my own ideas. It is indeed a great pleasure for me to work under her supervision. I appreciate all her contributions of time and ideas to make my Ph.D. experience productive and stimulating. The joy and enthusiasm she has for her research was contagious and motivational for me.

Secondly, I wish to thank Prof. Harish Parthasarathy, Department of Electronics and Communication Engineering, Netaji Subhas University of Technology, Delhi for his everlasting support and guidance in my Ph.D.

I sincerely thank Prof. O. P. Verma, Professor and Head, Department of ECE, DTU for providing me the necessary facilities and valuable suggestions during the progress of the work. I would like to thank Professor N. S. Raghava, Professor Neeta Pandey, Professor S. Indu and Dr. Rajesh Birok for continuous support throughout my Ph.D.

I owe a deep sense of gratitude to Dr. Rahul Bansal for continuous support and encouragement during my Ph.D.

I want to acknowledge Mr. Jitendra, Mr. Rehan, Mr. Shashank, Dr. Asheesh, Mr. Rajiv, Dr. Akhilesh and Mr. Amarendra for their constant support and encouragement. I express my thanks to all research scholars of the Department of ECE.

I would like to give special thanks to Himani Swarup as a whole for her continuous support and understanding when undertaking my research and writing my thesis. Your prayer for me was what sustained me this far.

I gratefully acknowledge the academic branch and administration of DTU for providing the environment and facilities to carry out my research work. I also express my thanks to office staff of Department of ECE for all kinds of support. I also gratefully acknowledge the University Grants Commission (UGC) of India, for providing fellowship (Junior research fellowship (JRF) and senior research fellowship (SRF)) that made my Ph.D. work possible.

Last but not the least, I thank the almighty God for showing me the right path to complete this Ph.D. thesis.

Date :

(Amit Kumar Gautam)

Place : Delhi, India.

Dedicated to

Brijesh Gautam

&

Himani Swarup

Contents

Declaration	i
Certificate page	ii
Acknowledgements	iii
List of Abbreviations	x
List of Symbols	xii
List of figures	xiii
List of tables	xvi
1 Introduction	1
1.1 Literature survey	2
1.2 Literature gap	3
1.3 Objectives	4
1.4 A Brief Contextual Review of State Estimation	4
1.4.1 Kalman Filter	6
1.4.2 Extended Kalman Filter	7
1.4.3 Iterated Extended Kalman Filter	9
1.4.4 Unscented Kalman Filter	10
1.5 Perturbation Thoery	12
1.6 Stochastic Differential Equations	13
1.7 Volterra Series	15
1.8 Least Mean Square Algorithm	15
1.9 Recursive Least Squares Algorithm	16
1.10 Organization of the Thesis	17
2 Nonlinear Modeling of Analog Circuits Using Perturbation Theory	20
2.1 Volterra Model of Silicon Controlled Rectifier	22
2.1.1 Mathematical Modeling	22

2.1.2	Simulation Results	26
2.1.3	Conclusions	27
3	State Estimation of Higher Order RC Circuit	29
3.1	State Space Model	30
3.2	Implementation of EKF algorithm	32
3.3	Simulation Results using EKF Method	33
3.4	Simulation Results using UKF Method	36
3.5	Conclusions	39
4	State Estimation of Single-Phase Rectifier Circuit	40
4.1	State Space Model	41
4.2	Implementation of EKF algorithm	42
4.3	Simulation Results using EKF Method	43
4.4	Simulation Results using IEKF Method	46
4.5	Simulation Results using UKF	49
4.6	Conclusions	49
5	State Estimation of Transistor Circuit	52
5.1	State Estimation of CE Amplifier Circuit	54
5.1.1	State Space Model	54
5.1.2	Implementation of EKF and IEKF	56
5.1.3	Simulation Results	57
5.1.4	Conclusions	59
5.2	State Estimation of DA Circuit using Unscented Kalman Filter	60
5.2.1	State Space Model	60
5.2.2	Implementation of UKF	64
5.2.3	Simulation Results	66
5.2.4	Conclusions	68
6	State Estimation and Parameter Estimation of Transmission Line	71
6.1	State Estimation and Parameter Estimation of Single-Phase nonuniform Transmission Line	74
6.1.1	State Space Model	74
6.1.2	Modeling of NTL using Frequency Domain Analysis	84
6.1.3	State and Parameter Estimation for Transmission Line Circuit	86
6.1.4	Simulation Results	88
6.1.5	Conclusions	95
6.2	State Estimation and Parameter Estimation of Three-Phase Transmission Line	97
6.2.1	Modeling of Three-Phase Transmission Line	97

6.2.2	Modeling of Transposed/Untransposed Transmission Line	99
6.2.3	Modeling of NTL using Frequency Domain Analysis	106
6.2.4	State Estimation for Transmission Line	107
6.2.5	Simulation Results	110
6.2.6	Conclusions	111
7	Conclusions and Future Scope	118
7.1	Conclusions	118
7.2	Scope for Future Work	122
	List of Publications	123
	Bibliography	125

Abstract

This thesis documents our investigation of state and parameter estimation of lumped and distributed parameter circuits using real-time stochastic filtering algorithms. We used Kalman filter (KF) and its variants for this purpose. The complete study consists of investigation of three related problems. The state and parameter estimation of nonlinear circuits require accurate mathematical modeling of the circuit. Therefore, the first problem is to derive the mathematical model of nonlinear circuits. In the case of nonlinear system, it is difficult to obtain a closed form input-output equation. In this case, we try to obtain an approximate nonlinear input-output relation. For this purpose, we used Volterra and perturbation theory. Besides these, we also used the bipolar junction transistor (BJT) models and transmission line models to obtain mathematical expressions that include nonlinearity. The second problem is to choose an appropriate estimation algorithm that involves less mathematical computation. For example, Particle filter (PF) can also be used and it may give better results than KF, but it requires additional computations for this purpose. The H-infinity based filtering has faster convergence than KF, but the computation complexity is higher than KF. In this work, the computational complexity of extended Kalman filter (EKF), iterated extended Kalman filter (IEKF) and unscented Kalman filter (UKF) has been compared for a typical circuit. The third problem is to choose some mathematical tools to reduce the mathematical complexity. We used Kronecker product for sparse matrix representation and compact representation.

In the following, we present a chapter-wise summary of the thesis.

Chapter 1 begins with a literature survey. Section 1.2 and 1.3 present the literature gap and objectives. The contextual review of state estimation is mentioned in section 1.4. Theory of KF, EKF, IEKF and UKF are presented in sections 1.4.1, 1.4.2, 1.4.3, and 1.4.4 respectively. Further, a brief theory of perturbation method, stochastic differential equations (SDE), Volterra series, least mean square (LMS) algorithm and

recursive least squares (RLS) algorithm are presented in sections 1.5, 1.6, 1.7, 1.8 and 1.9 respectively. Section 1.10 presents the organization of the thesis.

Chapter 2 deals with the implementation of perturbation theory along with Ebers-Moll model of BJT to derive the linear and nonlinear closed form Volterra expression between input and output of silicon controlled rectifier (SCR) circuit. It also presents the computation of the distortion occurring due to linear part only.

Chapter 3 includes state estimation of the higher order RC low pass filter (LPF) and RC high pass filter (HPF) circuit using EKF and UKF methods and compared the estimation performance with LMS algorithm.

Chapter 4 deals with the state estimation of single-phase rectifier circuit using EKF, IEKF and UKF methods and compared the estimation performance with LMS algorithm.

Chapter 5 presents the state estimation of BJT based common emitter (CE) and Darlington amplifier (DA) circuits using EKF, IEKF and UKF methods. In the first part, we estimated the output voltage of CE BJT circuit using IEKF and compared the performance of IEKF with EKF method. In the second part, we present the application of UKF for output voltage estimation of DA circuit. This work uses Kronecker product for vector multiplication. We compared the UKF estimation results with EKF and IEKF methods.

In **Chapter 6**, we present the modeling and real-time state and parameter estimation of nonuniform transmission lines (NTL) of single-phase and three-phase transposed and untransposed circuits. For modeling purpose, we used transmission line model, Fourier series expansion and Kronecker product. In first problem, state-space model of the single-phase NTL circuit has been derived. As Telegrapher's equations used for modeling the NTL are a function of space and time, the Fourier series expansion of the voltage and current have been used to obtain the time-dependent equations. The measurements have been obtained by solving the eigenvector problem. The frequency-domain analysis is used to obtain the state-space equations. For this, the four distributed parameters of the line are expanded in Fourier series. We compared the estimation performance of KF, EKF and UKF with RLS method. Secondly, we present KF based state estimation and EKF and UKF based parameter estimation for three-phase NTL. For this, state space model for three-phase transposed and untransposed NTL has been obtained. Clarke transformation matrix has been utilized for phase to sequence transformation which allows to represent the three-phase trans-

mission line (TL) into fully transposed TL. Measurement model for current and voltage vectors along the line are expressed in terms of Fourier series. Also, the frequency domain analysis is used to obtain the eigenvalue and eigenvector for measurement model. The voltage and current of NTL are expanded in Fourier series to obtain the sparse matrix formulation using Kronecker product. Kronecker product representation of discrete unitary trans-forms results in computer efficient implementation. This work implements the analysis of nonlinearity effect in transmission lines using perturbation theory. For this, the nonlinearity of the transmission line is included by perturbing the voltage and current of the line. Also, we compared the estimation performances with RLS method.

Finally, some concluding remarks are presented in **Chapter 7** and some future work direction is also presented.

List of Abbreviations

- BJT:** *Bipolar junction transistor*
- CE:** *Common emitter*
- DA:** *Darlington amplifier*
- ESD:** *Electrostatic discharge*
- EKF:** *Extended Kalman filter*
- HWR:** *Half wave rectifier*
- HPF:** *High pass filter*
- IEKF:** *Iterated extended Kalman filter*
- KF:** *Kalman filter*
- KCL:** *Kirchhoff's current law*
- KVL:** *Kirchhoff's voltage law*
- LT:** *Laplace transform*
- LMS:** *Least mean square*
- LPF:** *Low pass filter*
- MSE:** *Mean square error*
- NTL:** *Nonuniform transmission lines*
- PF:** *Particle filter*
- PDF:** *Probability density function*
- RLS :** *Recursive least squares*
- RMSE:** *Root mean square error*
- SNR:** *Signal to noise ratio*
- SCR:** *Silicon controlled rectifier*
- SDE:** *Stochastic differential equations*
- TL:** *Transmission line*
- UKF:** *Unscented Kalman filter*
- UT:** *Unscented transformation*

List of symbols

σ^2 : Variance

Σ : Covariance

ε, σ : Perturb value

η : State vector

∇ : Gradient

β : Current amplification factors

α_F : Forward current gain

α_R : Reverse current gain

V_T : Thermal voltage

ϕ, Ψ : Nonlinear functions

$*$: Convolution operator

δ : Unit impulse function

\times : Multiplication

$'$: Derivative

\hat{x} : Estimated value of x

R_L : Load resistance

R_S : Series Resistance

L_S : Series inductance

C : Capacitance

R_C : Collector resistance

R_E : Emitter resistance

C_B : Base capacitance

C_C : Collector capacitance

C_E : Emitter capacitance

I_S : Saturation current

N_F : Emission coefficient

N_j : Gaussian noise

B_j : Brownian motion process

\otimes : Kronecker product

C_w : Covariance of system noise

C_v : Covariance of measurement noise

W_N : Weight matrix

ξ : Real and imaginary terms

\forall : For all

Ω : Impedance matrix

ω : Angular frequency

List of Figures

2.1	Circuit diagram of SCR.	22
2.2	Anode currents of SCR output.	27
2.3	Simulation diagram of HWR circuit using SCR.	28
2.4	Input and output voltage across series RC component.	28
3.1	a) RC low pass filter, b) RC high pass filter.	31
3.2	Estimated output voltage of RC filter for sinusoidal wave.	34
3.3	Estimated output voltage of RC filter for square wave.	35
3.4	Comparison of output voltage estimation of LPF using noisy input with a) $\mu = 0, \sigma^2 = 0.1$, b) $\mu = 0, \sigma^2 = 0.5$, c) $\mu = 0, \sigma^2 = 1.0$, Comparison of output voltage estimation of HPF using noisy input with d) $\mu = 0, \sigma^2 = 0.1$, e) $\mu = 0, \sigma^2 = 0.5$, f) $\mu = 0, \sigma^2 = 1.0$	37
3.5	Comparison of estimation error for LPF using noisy input with a) $\mu = 0, \sigma^2 = 0.1$, b) $\mu = 0, \sigma^2 = 0.5$, c) $\mu = 0, \sigma^2 = 1.0$, Comparison of estimation error for HPF using noisy input with d) $\mu = 0, \sigma^2 = 0.1$, e) $\mu = 0, \sigma^2 = 0.5$, f) $\mu = 0, \sigma^2 = 1.0$	38
4.1	Circuit diagram of single-phase FWR.	41
4.2	Estimated voltage using EKF and LMS methods for noisy signal with a) $\mu = 0, \sigma^2 = 0.1$, b) $\mu = 0, \sigma^2 = 0.5$, c) $\mu = 0, \sigma^2 = 1.0$, d) $\mu = 0, \sigma^2 = 2.0$	44
4.3	Estimated current using EKF and LMS methods for noisy signal with a) $\mu = 0, \sigma^2 = 0.1$, b) $\mu = 0, \sigma^2 = 0.5$, c) $\mu = 0, \sigma^2 = 1.0$, d) $\mu = 0, \sigma^2 = 2.0$	45
4.4	Estimated voltage using EKF and IEKF methods for a) noiseless input signal, b) signal with $\mu = 0, \sigma^2 = 0.1$, c) signal with $\mu = 0, \sigma^2 = 0.5$, d) signal with $\mu = 0, \sigma^2 = 1.0$	47
4.5	Estimated current using EKF and IEKF methods for a) noiseless input signal, b) signal with $\mu = 0, \sigma^2 = 0.1$, c) signal with $\mu = 0, \sigma^2 = 0.5$, d) signal with $\mu = 0, \sigma^2 = 1.0$	48
4.6	Comparison of capacitor voltage and diode current estimation using UKF and EKF methods.	50
5.1	Diagram of CE amplifier circuit.	54
5.2	a) Input signal, b) Estimated output for the noiseless input using the IEKF and EKF methods with PSPICE simulation, c) Estimated output for the noisy input using the IEKF and EKF methods with PSPICE simulation.	58

5.3	Circuit diagram of Darlington pair amplifier.	60
5.4	a) Input sinusoidal voltage. Comparison of output voltage estimation of DA using EKF, IEKF and UKF methods for noisy input with b) $\mu = 0$, $\sigma^2 = 0.1$, c) $\mu = 0$, $\sigma^2 = 0.5$, d) $\mu = 0$, $\sigma^2 = 1.0$	68
6.1	Circuit diagram of a nonuniform transmission line.	75
6.2	Voltage estimation using KF and RLS methods with Gaussian noise input, (a) $\mu=0$, $\sigma^2 = 0.1$, (b) $\mu=0$, $\sigma^2 = 0.5$	89
6.3	Parameters estimation using EKF and RLS methods with Gaussian noise input, (a) $\mu=0$, $\sigma^2 = 0.1$, (b) $\mu=0$, $\sigma^2 = 0.5$	90
6.4	Circuit diagram of a three-phase transmission line.	97
6.5	Comparison of line currents using Gaussian noisy input ($\mu = 0$ and $\sigma^2 = 0.1$) with RLS, KF and UKF methods.	111
6.6	Comparison of line currents using Gaussian noisy input ($\mu = 0$ and $\sigma^2 = 0.25$) with RLS, KF and UKF methods.	112
6.7	Comparison of line currents using Gaussian noisy input ($\mu = 0$ and $\sigma^2 = 0.5$) with RLS, KF and UKF methods.	112
6.8	Comparison of line voltages using Gaussian noisy input ($\mu = 0$ and $\sigma^2 = 0.1$) with RLS, KF and UKF methods.	113
6.9	Comparison of line voltages using Gaussian noisy input ($\mu = 0$ and $\sigma^2 = 0.25$) with RLS, KF and UKF methods.	113
6.10	Comparison of line voltages using Gaussian noisy input ($\mu = 0$ and $\sigma^2 = 0.5$) with RLS, KF and UKF methods.	116

List of Tables

2.1	Percentage of distortion errors for various input values.	27
3.1	Comparison of SNR value for different methods.	33
3.2	Performance of different methods for LPF.	36
3.3	Performance of different methods for HPF.	36
4.1	Comparison of capacitor voltage (v_C) estimation using different methods. 43	
4.2	Comparison of diode current (i_D) estimation using different methods. .	44
4.3	Comparison of capacitor voltage (v_C) estimation using different methods. 46	
4.4	Comparison of diode current (i_D) estimation using different methods. .	47
4.5	Comparison of capacitor voltage (v_C) estimation using different methods. 49	
4.6	Comparison of diode current (i_D) estimation using different methods. .	51
5.1	Comparison of SNR value using EKF and IEKF methods.	58
5.2	Comparison of parameters using EKF and IEKF methods.	58
5.3	Comparison of SNR (dB) of DA for different methods.	69
5.4	RMSE of output voltage estimation using EKF, IEKF and UKF methods.	69
5.5	Computational complexity for EKF method.	69
5.6	Computational complexity for IEKF method.	70
5.7	Computational complexity for UKF method.	70
5.8	Comparison of MSE with different values of $C_{w,k}$ and $C_{v,k}$ using trial and error method.	70
6.1	Comparison of RMSE for R, X, B using RLS and EKF methods.	89
6.2	Comparison of standard deviation of parameter errors (σ_e) for R, X, B using RLS and EKF methods.	91
6.3	Comparison of SNR (dB) and RMSE for line voltage (v) estimation using KF and RLS methods.	91
6.4	Unknown Parameters of Estimation Methods.	109
6.5	Comparison of RMSE for line currents and line voltages using RLS, KF and UKF methods.	114

6.6 Comparison of standard deviation of the parameter errors (σ_e) for line currents and line voltages using RLS, KF and UKF methods. 115

6.7 Comparison of RMSE for different parameters in transposed line using RLS, EKF and UKF methods. 115

6.8 Comparison of RMSE for different parameters in untransposed line using RLS, EKF and UKF methods. 116

Chapter 1

Introduction

Real-time estimation is important for control and regularity of the system. Fast dynamic state and parameter estimators are important for proper lumped and distributed parameter circuit monitoring. State estimation methods estimate and predict the desired state variables of a dynamic system using noisy measurements. State estimation is helpful for suppression of physical process where states cannot be measured directly or the disturbance have a significant role. This thesis documents our investigation of state and parameter estimation of lumped and distributed parameter circuits using real-time stochastic filtering algorithms. We used KF method and its variants for this purpose. The complete study consists of investigation of three related problems. The state and parameter estimation of nonlinear circuits require accurate mathematical modeling of the circuit. Therefore, the first problem is to derive the mathematical model of nonlinear circuits. In the case of a nonlinear system, it is difficult to obtain a closed-form input-output equation. In this case, we try to obtain an approximate nonlinear input-output relation. For this purpose, we used Volterra and perturbation theory. Besides these, we also used the BJT models and transmission line models to obtain mathematical expressions that include nonlinearity. The second problem is to choose an appropriate estimation algorithm that involves less mathematical computation. For example, PF method can also be used and it may give better results than KF method but it requires additional computations for this purpose. The H-infinity based filtering has faster convergence than KF method, but the computation complexity is higher

than KF method. In this work, the computational complexity of EKF, IEKF and UKF methods has been compared for a typical circuit. The third problem is to choose some mathematical tools to reduce the mathematical complexity. We used Kronecker product for sparse matrix representation and compact representation. This chapter discusses the basics of state estimation methods such as KF, EKF, IEKF, UKF, LMS and RLS algorithms.

1.1 Literature survey

Literature survey is presented in various chapters. Nonlinear circuit analysis can be done using different methods [1] - [10]. Kuntman [1] used the Ebers-Moll model of the transistor to obtain the optimum source resistance of the amplifier circuit. To obtain the nonlinear nodal solution, Newton Raphson method has been used. Fong and Meyer [2] presented the Volterra model of common emitter amplifier and differential pair transconductance using large signal model. Song *et al.* [3] used Volterra model together with memory polynomial model for compensation of nonlinear distortion of a power amplifier. Though Volterra series is the extension of linear system theory, large number of parameters related to the Volterra series limits the practical application of this model having modest memory. Also, Volterra series has the disadvantage that modeling using this requires immoderate computations as the determination of unknown coefficients increases exponentially with degree of non-linearity and the Volterra filter length. The perturbation theory has the advantage of simple implementation as the method is applied by continuously improving the previously obtained approximate solution of a problem. It is implemented by a small deformation of a system that is exactly solvable. Wu *et al.* [4] used the perturbation technique to get the amount of asymmetry and nonuniformity during the transfer from differential to a common mode in a differential circuit. Afifi and Dusseaux [5] implemented perturbation method on scattering of electromagnetic wave to obtain coherent and incoherent intensities. Mishra and Yadava [6] studied the effect of internal and external noise perturbations in chaotic Colpitts oscillator. Liu *et al.* [7] presented a robust KF method in which a random perturbation is taken into account. These random perturbations of parameters have been considered in state and measurement matrices, which are known as state-dependent multiplicative noises. Thuan and Huong [8] studied the effect of nonlinear perturbations on stability and passivity of delayed switched systems, as the instability

of system leads to poor performance of the dynamic system. Buonomo and Schiavo [9] derived the nonlinear distortion in analog circuits using perturbation theory that uses single and two-tone input signals. Wang *et al.* [10] presented perturbation projection vector modeling of an oscillator which is based on memristor and used it for pattern recognition. Wang *et al.* [11] studied the effect of nonlinear perturbation. Lakshmanan *et al.* [12] presented the effect of the nonlinear perturbation on uncertain systems.

1.2 Literature gap

(i) Estimation required for real time process:- Real-time estimation of lumped and distributed parameter circuits are important for the reliable operation of systems as the state and parameter change with time and environmental condition. Integration of renewables, power electronics technology and new regulation of the market has increased the complexity of power systems. This requires the proper monitoring and control of power systems. There exist filters which can be used for nonlinear systems. But, most of the noises are modeled as Gaussian noise. So, the use of KF method and its variants is appropriate for estimations. For this purpose, modeling of these circuits is obtained by stochastic differential equations and their estimation is performed by real-time stochastic filtering algorithms.

(ii) Requirement of nonlinear modeling for precise estimation:- Due to linearization of nonlinear systems around the operating point of states, performance and stability are not assured for all operating conditions. The use of linearized equation in place of nonlinear equation results in improper analysis of the system. So, it requires the nonlinear mathematical modeling of systems. The use of Volterra representation and perturbation theory is useful for this purpose.

(iii) Mathematical tools require to reduce the computation complexity:- The mathematical derivations of nonlinear systems lead to mathematical complexity. Mathematical tools such as Kronecker product and its properties are useful to reduce the complexity of mathematical derivation. Kronecker product helps sparse representation of matrices and compact representation of mathematical expressions.

1.3 Objectives

In this work, the following have been used for real-time estimation for lumped and distributed parameter circuits :-

1. Volterra series, perturbation theory, transistor models and transmission line models to obtain the nonlinear mathematical expressions of the system.
2. KF, EKF, IEKF and UKF methods for state and parameter estimation purposes.
3. Kronecker product to reduce the mathematical complexity and compact representation of the mathematical expressions.

1.4 A Brief Contextual Review of State Estimation

The KF, PF and H-infinity filter are some of the state estimation methods in which KF is the most popular method. KF versions have been applied in various areas such as control system, robotics, etc. [13] - [23]. But, the limitation of KF method is that it can be used for linear systems only. The KF method evaluates the minimum mean square error (MSE) estimate of the random vector that represents the system states. The KF dynamics are derived in the frame work of Gaussian probability density function (pdf). These dynamics result from iterative use of prediction and filtering. The KF method can be implemented for systems having linear state dynamics and observation dynamics. But, nonlinearity in system model or observation model results in non Gaussian pdfs. The variations of KF method that can be used for nonlinear systems are: - EKF, IEKF, UKF, PF and H-infinity filter [24]. These filters use different approaches to handle the nonlinearity. The EKF method uses the linearization of both the transition and measurement functions of the nonlinear system, which involves computation of Jacobian matrices. But, EKF method has two important shortcomings. The shortcomings are :-1) difficulty in determining the Jacobian, 2) These linearization results in filter instability, when sufficient small time step intervals are not used. Also, EKF method has limitation in prorogating the constraints through the state and covariance calculation. EKF and IEKF are analytical methods as the approximation is based on Taylor's series expansion. IEKF algorithm resembles the conventional EKF algorithm. The linearization of the prediction function is same for both the filters but the only difference is in how the updated estimate is computed. To remove these

shortcomings of EKF and IEKF methods, Julier *et al.* [25] and Simon [26] proposed UKF method which is based on the fact that it is easier to approximate a probability density function than a nonlinear function. It utilizes the statistical properties of Gaussian variables having nonlinear transformation. The mean and variance are computed using the unscented transformation (UT), which avoids the computation of Jacobians.

UKF method is an advanced version of KF method. It uses more accurate approximations to compute multi-dimensional integral as compared to EKF method. A set of sample points known as sigma points are used for state distribution in UKF method. These sigma points capture the posterior mean and variance of the state distribution. Using a selected set of points, the UKF method accurately map the probability distribution of the measurement model. UKF method [27]- [28] is based on statistical approach, which overcomes the limitations of EKF method. UKF method is used in many applications. In [29], Ahmeid *et al.* introduced a new method based on KF method for real-time estimation to converter. The KF performance is improved using adaptive tuning methods. Hoffmann *et al.* [30] used EKF method for grid impedance and voltage estimation of power converter of electric network. The noise presented at the connection point has been taken into account. This work also considered the use of EKF method in distorted voltage waveform environment. In [31], Nadarajan *et al.* used EKF method for state and parameter estimation of stator winding fault in brushless synchronous generator. The model-based method is used and simplified the model for online implementation. In [32], Yazdanian *et al.* used EKF method for parameter estimation of ringdown signal. The method can be implemented for both constant and time-varying parameters. In [33], Bogdanski *et al.* presented identification of vehicle handling dynamics and presented review of UKF, EKF, and PF methods showed that all three filters are suitable in real time for online estimation. For this, the paper used simple and efficient model to obtain the independent parameters. Tian *et al.* [34] proposed UKF based estimation for battery system which uses modified equivalent circuit model. The method presents low computational cost and improved estimation simultaneously. In [35], Ghahremani *et al.* implemented UKF method in synchronous machine. Simple and effective propagation of probability density function in UKF improved the estimation purpose.

1.4.1 Kalman Filter

KF is the least mean square error estimator for linear and Gaussian dynamic systems where the state transition and observation models include additive Gaussian noise. By propagating the mean and covariance at each time step, the KF method computes the unknown state [26], [36]. The two steps of the KF method are :- (i) prediction step, and (ii) updation step.

A discrete-time linear system is represented by the following equations :-

$$\mathbf{x}_{n+1} = \mathbf{F}_n \mathbf{x}_n + \mathbf{B}_n \mathbf{u}_n + \mathbf{G}_n \mathbf{w}_n \quad (1.1)$$

$$\mathbf{z}_n = \mathbf{H}_n \mathbf{x}_n + \mathbf{v}_n \quad (1.2)$$

where $\mathbf{x}_n \in \mathbb{R}^k$ and $\mathbf{z}_n \in \mathbb{R}^m$ are state model and measurement model at time n respectively. $\mathbf{F}_n \in \mathbb{R}^{k \times k}$, $\mathbf{B}_n \in \mathbb{R}^{k \times l}$ and $\mathbf{H}_n \in \mathbb{R}^{m \times m}$ are the system transition matrix, input matrix and output matrix respectively. \mathbf{u}_n is a known input vector. $\mathbf{w}_n \in \mathbb{R}^l$ and $\mathbf{v}_n \in \mathbb{R}^m$ are the system and measurement uncorrelated Gaussian noise with the following assumptions :- $\bar{\mathbf{w}}_n = 0$, $\bar{\mathbf{v}}_n = 0$, $\overline{\mathbf{w}_n \mathbf{w}_n^T} = \mathbf{C}_{w_n}$, $\overline{\mathbf{v}_n \mathbf{v}_n^T} = \mathbf{C}_{v_n}$, $\overline{\mathbf{w}_n \mathbf{v}_j^T} = \mathbf{0} \forall n \& j$. KF steps are :-

1. **Initialization:** Initialize $\hat{\mathbf{x}}_0 = \bar{\mathbf{x}}_0$, $\Sigma_0 = \Pi_0$, \mathbf{C}_{w_0} and \mathbf{C}_{v_0} .

2. **State prediction:**

(a) Computation of predicted state as :-

$$\hat{\mathbf{x}}_{n+1|n} = \mathbf{F}_n \hat{\mathbf{x}}_{n|n} + \mathbf{B}_n \mathbf{u}_n \quad (1.3)$$

(b) Computation of covariance matrix of prediction error as :-

$$\Sigma_{n+1|n} = \mathbf{F}_n \Sigma_{n|n} \mathbf{F}_n^T + \mathbf{C}_{w_n} \quad (1.4)$$

3. **Measurement update:**

(a) Computation of Kalman gain as :-

$$\mathbf{K}_{n+1} = \Sigma_{n+1|n} \mathbf{H}_n^T (S)^{-1} \quad (1.5)$$

where $S = \mathbf{H}_n \Sigma_{n+1|n} \mathbf{H}_n^T + \mathbf{C}_{v_n}$

(b) Updation of estimated state as :-

$$\hat{\mathbf{x}}_{n+1|n+1} = \hat{\mathbf{x}}_{n+1|n} + \mathbf{K}_{n+1}(\mathbf{z}_n - \mathbf{H}_n(\hat{\mathbf{x}}_{n+1|n})) \quad (1.6)$$

(c) Computation of covariance error matrix as :-

$$\Sigma_{n+1|n+1} = (\mathbf{I} - \mathbf{K}_{n+1}\mathbf{H}_n)\Sigma_{n+1|n} \quad (1.7)$$

where $n+1|n$ and $n+1|n+1$ are a priori and a post estimate.

1.4.2 Extended Kalman Filter

EKF is the modified version of KF method. EKF is broadly used for estimation purpose in various applications [24], [37], [38]. It uses linearized model of the nonlinear system to implement Kalman filtering. The linearization process uses the partial derivative or Jacobian matrices of nonlinear function of the model. Using a priori and posteriori error covariance, the estimation process is defined in terms of the linearized observation model. The algorithm starts with initialization of mean value of the state vector and covariance matrix.

A discrete-time nonlinear system is represented as :-

$$\mathbf{x}_{n+1} = \mathbf{f}_n(\mathbf{x}_n, \mathbf{u}_n) + \mathbf{G}_n \mathbf{w}_n \quad (1.8)$$

$$\mathbf{z}_n = \mathbf{h}_n(\mathbf{x}_n) + \mathbf{v}_n \quad (1.9)$$

where $\mathbf{f}_n(\cdot) \in \mathbb{R}^k$ and $\mathbf{h}_n(\cdot) \in \mathbb{R}^m$ denote the time variant nonlinear functions. EKF algorithm is a nonlinear version of KF algorithm and has been designed for nonlinear state estimation. It includes updation in time and measurement at time n after initialization. EKF linearizes the nonlinear function $\mathbf{f}_n(\cdot)$ and $\mathbf{h}_n(\cdot)$ using Taylor series. (1.8) and (1.9) has been approximated using Taylor series expansion as :-

$$\mathbf{x}_{n+1} \cong \mathbf{f}_n(\hat{\mathbf{x}}_{n|n}) + \mathbf{F}_n \delta_n + \text{Higher order terms} \quad (1.10)$$

$$\mathbf{z}_n \cong \mathbf{h}_n(\mathbf{f}_n(\hat{\mathbf{x}}_{n|n})) + \mathbf{H}_n \delta_n + \text{Higher order terms} \quad (1.11)$$

where $\delta_n = \mathbf{x}_n - \hat{\mathbf{x}}_n$. δ_n denotes the priori estimated error. \mathbf{P}_n denotes the covariance error at time n . EKF steps are :-

1. **Initialization:** Initialize $\hat{\mathbf{x}}_0 = \bar{\mathbf{x}}_0$, $\Sigma_0 = \Pi_0$, \mathbf{C}_{w_0} and \mathbf{C}_{v_0} .

2. **State prediction:**

(a) Computation of Jacobian matrix as :-

$$\mathbf{F}_n = \left. \frac{\partial \mathbf{f}_n(\mathbf{x}_n, \mathbf{u}_n)}{\partial \mathbf{x}} \right|_{\mathbf{x}=\hat{\mathbf{x}}_{n|n}} \quad (1.12)$$

(b) Computation of state as :-

$$\hat{\mathbf{x}}_{n+1|n} = \mathbf{f}_n(\hat{\mathbf{x}}_{n|n}) \quad (1.13)$$

(c) Computation of predicted covariance of error as :-

$$\Sigma_{n+1|n} = \mathbf{F}_n \Sigma_{n|n} \mathbf{F}_n^T + \mathbf{C}_{w_n} \quad (1.14)$$

3. **Measurement update:**

(a) Computation of Jacobian matrix as :-

$$\mathbf{H}_n = \left. \frac{\partial \mathbf{h}_n(\mathbf{x}_n, \mathbf{u}_n)}{\partial \mathbf{x}} \right|_{\mathbf{x}=\hat{\mathbf{x}}_{n|n}} \quad (1.15)$$

(b) Computation of Kalman gain as :-

$$\mathbf{K}_{n+1} = \Sigma_{n+1|n} \mathbf{H}_n^T (S)^{-1} \quad (1.16)$$

where $S = \mathbf{H}_n \Sigma_{n+1|n} \mathbf{H}_n^T + \mathbf{C}_{v_n}$

(c) Updation of estimated state as :-

$$\hat{\mathbf{x}}_{n+1|n+1} = \hat{\mathbf{x}}_{n+1|n} + \mathbf{K}_{n+1} (\mathbf{z}_n - \mathbf{h}_n(\hat{\mathbf{x}}_{n+1|n})) \quad (1.17)$$

(d) Computation of covariance error matrix as :-

$$\Sigma_{n+1|n+1} = (\mathbf{I} - \mathbf{K}_{n+1} \mathbf{H}_n) \Sigma_{n+1|n} \quad (1.18)$$

1.4.3 Iterated Extended Kalman Filter

IEKF algorithm is the improved version of EKF method. The IEKF technique [24] does the same linearization as the EKF method for \mathbf{f}_n , $\hat{\mathbf{x}}_{n+1|n}$ and $P_{n+1|n}$. The only difference is that in IEKF, linearization of g_n is based on the updated state estimation of $\hat{\mathbf{x}}_{n+1|n+1}$ rather than the predicted state estimate $\hat{\mathbf{x}}_{n+1|n}$. In IEKF, v_n is formulated as :-

$$\mathbf{v}_n = \mathbf{g}_n(\mathbf{z}_n, \mathbf{x}_n) \quad (1.19)$$

where \mathbf{g}_n is nonlinear function. In addition to additive white noise, measurement model becomes

$$\mathbf{z}_n = \mathbf{h}_n(\mathbf{x}_n) + \zeta_n \mathbf{v}_n \quad (1.20)$$

Therefore

$$\mathbf{v}_n = (\zeta_n)^{-1}(\mathbf{z}_n - \mathbf{h}_k(\mathbf{x}_n)) \quad (1.21)$$

where ζ_n denotes the invertible matrix. IEKF algorithm steps have been mentioned as :-

1. Initialization:

- (a) Set threshold value ε , $\Sigma_0 = \Pi_0$, \mathbf{C}_{w_n} and \mathbf{C}_{v_n} .
- (b) Set $i = 0$ and initialize $\hat{\mathbf{x}}_{0,n|n} = \hat{\mathbf{x}}_0$.

2. Prediction:

- (a) Calculate $\hat{\mathbf{x}}_{n+1|n}^0$ and $\hat{P}_{n+1|n}^i$ as depicts in (1.13)-(1.14) and increment $i = i + 1$.

3. Update step:

- (a) Linearization of error model as :-

$$H_n^i = \frac{\partial g_n(z_n, \hat{\mathbf{x}}_{n|n}^i)}{\partial x} \quad (1.22)$$

- (b) Computation of Kalman gain :-

$$K_{n+1}^i = \Sigma_{n+1|n} H_n^{iT} (H_n^i \Sigma_{n+1|n} H_n^{iT} + C_{v_n})^{-1} \quad (1.23)$$

(c) Updation of state as :-

$$\hat{x}_{n+1|n+1}^i = \hat{x}_{n+1|n}^i + K_{n+1}^i \left(g_n \left(z_n, \hat{x}_{n+1|n}^{i-1} \right) + h_{i,k} \left(\hat{x}_{n+1|n}^i - \hat{x}_{n+1|n+1}^{i-1} \right) \right) \quad (1.24)$$

Repeat until

$$\left(\hat{x}_{n+1|n}^i - \hat{x}_{n+1|n+1}^{i-1} \right) \parallel < \varepsilon \quad (1.25)$$

. Set $i_0 = i$ and computation of updated estimate as :-

$$\hat{x}_{n+1|n}^i = \hat{x}_{n+1|n+1}^{i_0} \quad (1.26)$$

Computation of covariance of updated estimate as :-

$$\Sigma_{n+1|n+1} = (I - K_n^{i_0} H_{n+1}^{i_0}) \Sigma_{n+1|n}. \quad (1.27)$$

1.4.4 Unscented Kalman Filter

UKF algorithm uses UT [39] to formulate the nonlinear transformation of a random variable \mathbf{x} by assuming its mean value $\bar{\mathbf{x}}$ and covariance Σ_0 . UT consist of sigma point denoted by Ω_i . UT steps are as follows :-

1. Calculation of sigma points for $i = 2L + 1$ as :-

$$\begin{aligned} \Omega_0 &= \hat{\mathbf{x}}_n \\ \Omega_i &= \hat{\mathbf{x}}_n + (\eta \sqrt{\Sigma_n})_i, \quad i = 1, \dots, L \\ \Omega_i &= \hat{\mathbf{x}}_n - (\eta \sqrt{\Sigma_k})_i, \quad i = L + 1, \dots, 2L \end{aligned} \quad (1.28)$$

where $\eta = \sqrt{L + \lambda}$. L and λ are the number of state and scaling constant respectively.

2. The weights associated to i^{th} column of matrix \mathbf{x} are :-

$$\begin{aligned} \Upsilon_0^{(m)} &= \frac{\lambda}{\eta}, \\ \Upsilon_0^{(c)} &= \frac{\lambda}{\eta} + (1 - \alpha^2 + \beta), \\ \Upsilon_i^{(m)} &= \Upsilon_i^{(c)} = \frac{\lambda}{2\eta}, \quad i = 1, \dots, 2L \end{aligned} \quad (1.29)$$

Here, α and β indicate tuning parameter and positive weighing parameter respectively.

3. Updation of time propagation using transformed sigma points as :-

$$\mathcal{Z}_i = \varphi(\Omega_i, \mathbf{u}_n), \quad i = 1, \dots, 2L \quad (1.30)$$

4. Calculation of priori state and covariance error as :-

$$\bar{\mathbf{z}} = \sum_{i=0}^{2L} \Upsilon_i^{(m)} \mathcal{Z}_i \quad (1.31)$$

$$\Sigma_{\mathbf{z}} = \sum_{i=0}^{2L} \Upsilon_i^{(c)} (\mathcal{Z}_i - \bar{\mathbf{z}})(\mathcal{Z}_i - \bar{\mathbf{z}})^T \quad (1.32)$$

5. The cross-covariance of \mathbf{x} and \mathbf{z} is estimated as :-

$$\Sigma_{\mathbf{xz}} = \sum_{i=0}^{2L} \Upsilon_i^{(c)} (\Omega_i - \bar{\mathbf{z}})(\mathcal{Z}_i - \bar{\mathbf{z}})^T \quad (1.33)$$

The steps for UKF algorithm are :-

1. Initialize $\hat{\mathbf{x}}_0 = \bar{\mathbf{x}}_0$, $\Sigma_0 = \Pi_0$.
2. Sigma point calculation: Computation of sigma point Ω_i according to (1.28).
3. Time updation: (i) For $i = 1, \dots, 2L$, computation of $\mathcal{Z}_{i,n+1|n}$ according to (1.30).
 (ii) Calculation of predicted mean $\bar{\mathbf{z}}_{n+1|n}$ using (1.31).
 (iii) Calculation of predicted covariance $\Sigma_{\hat{\mathbf{z}}} = \Sigma_{\mathbf{z}} + C_{w_n}$ using (1.32).
 (iv) For $i = 1, 2, \dots$, computation of propagating sigma points as :-

$$\mathbf{Z}_{i,n+1|n} = h(\mathcal{Z}_{i,n+1|n}, \mathbf{u}_n) \quad (1.34)$$

(v) Calculation of estimated output as :-

$$\hat{z}_{n+1|n} = \sum_{i=0}^{2L} \Upsilon_i^{(m)} Z_{i,n+1|n} \quad (1.35)$$

(vi) The cross-covariance of x and z is computed as :-

$$\Sigma_{zz} = \sum_{i=0}^{2L} \Upsilon_i^{(c)} (Z_i - \hat{z}_n)(Z_i - \hat{z}_n)^T \quad (1.36)$$

4. Measurement updation :- (i) Computation of Kalman gain as :-

$$K_{n+1} = (\Sigma_{\hat{z}} + C_{v_k}) \Sigma_{xz}^{-1} \quad (1.37)$$

(ii) Updation of state as :-

$$\hat{x}_{n+1|k+1} = \hat{x}_{n+1|n} + K_{n+1} (z_n - \hat{z}_{n+1|n}) \quad (1.38)$$

(iii) Calculation of covariance of updated estimate as :-

$$\Sigma_{n+1|n+1} = \Sigma_{n+1|n} - K_{n+1} \Sigma_{z_n} K_n^T \quad (1.39)$$

1.5 Perturbation Thoery

Perturbation theory is used to model a small deformation of a system that is exactly solvable. It is implemented on a system that can not be solved exactly. It uses the mathematical method of approximation to obtain the solution to a deformed system. It is the method that continuously improves the previously obtained approximate solution to a problem. In this way, the method allows to implement the computational efficiency of idealized systems to more realistic problems. Also, it presents analytic insight into complex problems. This method includes a small term ' ε ' to solve the equation as :-

$$A = A_0 + \varepsilon A_1 + \varepsilon^2 A_2 + \dots \quad (1.40)$$

where A_0 is the known solution to the exactly solvable problem and A_1, A_2, \dots are nonlinear terms. The use of only linear model for nonlinear system presents error between the actual response and linear approximation, so nonlinear model is important.

Nonlinear closed form input-output relation is also important for design and simulation of complex circuits as transfer of physical description into mathematical form is required for simulation.

Perturbation theory is widely used for different applications. Buonomo and Schiavo [40] used perturbation method for periodic response of forced nonlinear circuit and also considered the harmonic distortion. Majumdar *et al.* [41] implemented perturbation technique to Ebers-Moll modeled transistor amplifier circuit. This method has been used to derive the closed-form Volterra series. Rathee *et al.* [42] proposed perturbation-based Fourier series model for representation of nonlinear distortion in circuits. This method has the advantage of simple implementation. Rathee and Parthasarathy [43] used perturbation method to decompose the driving force and circuit state into linear and nonlinear components. Further, the nonlinear circuit is represented by a nonlinear differential equation, in which the fluctuations are modeled using $\hat{\text{Ito}}$ stochastic differential equations. The results obtained in this way are compared with perturbation-based deterministic differential equations. This comparison presents the noise component. Dang *et al.* [44] used perturbation method for space variance of range envelope in synthetic aperture radar. In [45], perturbation method is implemented on 64-PSK.

1.6 Stochastic Differential Equations

In general, a continuous nonlinear SDE [36] is represented by :-

$$\frac{d}{dt}\mathbf{x}_t = \mathbf{f}(\mathbf{x}_t, \mathbf{w}_t, t); t \geq t_0 \quad (1.41)$$

where $\mathbf{f}(\cdot)$ is a nonlinear function of time t . \mathbf{w}_t is the random input function. Consider the initial condition \mathbf{x}_{t_0} . The integral of (1.41) is well defined when \mathbf{f} and \mathbf{w}_t are restricted. (1.41) can be written as :-

$$\mathbf{x}_t - \mathbf{x}_{t_0} = \int_{t_0}^t \mathbf{f}(\mathbf{x}_t, \mathbf{w}_t, t) dt \quad (1.42)$$

The SDE with an additive white Gaussian function is expressed as :-

$$\frac{d}{dt}\mathbf{x}_t = \mathbf{f}(\mathbf{x}_t, t) + \mathbf{G}(\mathbf{x}_t, t)\mathbf{w}_t; t \geq t_0 \quad (1.43)$$

$$d\mathbf{x}_t = \mathbf{f}(\mathbf{x}_t, t)dt + \mathbf{G}(\mathbf{x}_t, t)\mathbf{w}_t dt \quad (1.44)$$

where $\mathbf{G}(\cdot)$ is matrix function and independent of \mathbf{w}_t . Integrating (1.44), we obtain

$$\mathbf{x}_t - \mathbf{x}_{t_0} = \int_{t_0}^t \mathbf{f}(\mathbf{x}_t, t) dt + \int_{t_0}^t \mathbf{G}(\mathbf{x}_t, t) d\mathbf{B}(t) \quad (1.45)$$

where $\mathbf{w}_t = \frac{d\mathbf{B}(t)}{dt}$. $\mathbf{B}(t)$ is the Brownian motion process. The first integral in (1.45) is defined as the mean square Riemann integral. The second integral can be defined only in the mean square sense by $It\hat{o}$ because it has random component and is known as $It\hat{o}$ SDE. Let $i(t)$ and $v(t)$ denote line current and voltage Fourier series coefficient vector respectively with size $(2N+1) \times 1$ where the Fourier series truncation is from $-N$ to $+N$. Let θ denotes the distributed parameter vector of Fourier series coefficients. It is assumed that by taking the real and imaginary parts, in the voltage, current and parameters Fourier series coefficients, the SDE becomes real. Then, $\left[v(t)^T, i(t)^T, \theta(t)^T \right]^T = \eta(t)$ becomes state vector and state equation has been formed as :-

$$d\mathbf{x}(t) = \mathbf{f}(\theta(t))\eta(t)dt + \mathbf{G}(\theta(t))\mathbf{B}(t) \quad (1.46)$$

where $\mathbf{B}(t)$ is a Brownian motion vector derived from the line loading. The measurement model involves measuring only a small subset of the voltage and current Fourier series coefficients. Thus the measurement model is of the form

$$d\mathbf{z}(t) = \mathbf{H}\eta(t)dt + d\mathbf{v}(t) \quad (1.47)$$

where \mathbf{H} is a sparse matrix of ones and zeroes. It should be kept in mind that measurement of a given Fourier component may not be possible. But, it is possible to measure the current and voltage vector at a finite set of spatial points along the line and express these spatio temporal measurements in terms of the spatial Fourier series coefficients. For example, $v(t, z)$ can be measured as :-

$$v(t, z) = \sum_{n \in \mathcal{Z}} v_n(t) e^{j2\pi n z / d} \quad (1.48)$$

and likewise for $i(t, z)$. The measured process $[v(t, z_1), \dots, v(t, z_n), i(t, z_1), \dots, i(t, z_n)]^T$ can then be expressed as a matrix of size $2n \times (2(2N+1))$ multiplied by the Fourier coefficient vector $[v_n(t); i_n(t) : -N \leq n \leq N]^R$. Thus \mathbf{H} gets modified.

1.7 Volterra Series

Volterra series gives the input-output relation of a nonlinear, causal, time-invariant system with fading memory. Volterra series is an extension of linear convolution and nonlinear power series. The Volterra discrete time domain series is expressed as :-

$$y(n) = \sum_{p=1}^P \sum_{i_1=1}^M \dots \sum_{i_p=1}^M h_p(i_1, \dots, i_p) \prod_{j=1}^p x(n - i_j) \quad (1.49)$$

where input $x(n)$ and output $y(n)$ are considered for system. $h_p(\cdot)$ is the p^{th} order Volterra kernels.

1.8 Least Mean Square Algorithm

The LMS algorithm's objective is to minimize the MSE to achieve the desired signal at the receiving end. It is based on the gradient-based method of steepest descent. LMS algorithm is used in various applications [46]- [50]. LMS has the advantage of being easy to compute and not requiring matrix inversion. LMS method is based on a linear regression approach to estimate the unknown parameters.

Let $x(n)$ denotes signal at receiver end and output signal $y(n)$ depends on $x(n)$ as :-

$$y(n) = W^H * x(n) \quad (1.50)$$

W is the weighted coefficient $W = [W_1 \dots W_p]$ and $x = [x_1(n) \dots x_p(n)]$. where p denotes the number of input element and H denotes the hermitian transpose. The error between a desired signal $d(n)$ and received signal $y(n)$ is :-

$$e(n) = d(n) - y(n) \quad (1.51)$$

The LMS algorithm is used to minimize the error. Weight is updated using steepest decent as :-

$$W(n+1) = W(n) + \frac{1}{2} \mu [-\nabla J(n)] \quad (1.52)$$

where μ is step size ($0 \leq \mu \leq 1$). The gradient vector $\nabla J(k)$ is expressed as :-

$$\nabla J(n) = -2r(n) + 2R(n)W(n) \quad (1.53)$$

where $r(n)$ and $R(n)$ denote cross-correlation and covariance between $d(n)$ and $x(n)$ which is expressed as :-

$$r(n) = d^*(n) * x(n) \quad (1.54)$$

$$R(n) = x(n) * x^H(n) \quad (1.55)$$

Substituting (1.54)-(1.55) into (1.53), we get

$$W(n+1) = W(n) + \mu x(n)e^*(n) \quad (1.56)$$

1.9 Recursive Least Squares Algorithm

The RLS is adaptive filtering. It obtains the filter coefficients in recursive manner. It uses the minimization of weighted least square cost function criteria to obtain the filter weights by considering the input signal as the deterministic signal. It has widespread applications in engineering including signal processing and communication. Various form of this algorithm is also used in literature for parameter estimation and system identification purpose. The two classes of least squares method are :-

- (i) Iterative method for offline identification.
- (ii) Recursive methods for online identification.

The least squares have applications in control and function fitting, estimation and system identification. The RLS filter is used in different applications [51] - [54].

RLS computes the state recursively and gives the optimal solution in the mean squared sense [55]. In the RLS algorithm, the past errors are rounded-off and present state computations are propagated to the future instant which results in error accumulation. Consider the desired signal \mathbf{d}_k and optimum solution $\mathbf{W}_k = [W_1 \ W_2 \dots \ W_{M-1}]^T$. The desired signal is given by

$$\mathbf{d}_k = \mathbf{y}_k^T \mathbf{W}_k + \mathbf{w}_k^{(R)} \quad (1.57)$$

where $\mathbf{y}_k = [y_k \dots y_{k-M+1}]^T$ is the observation vector, $\mathbf{w}_k^{(R)}$ is the zero mean white Gaussian noise. The aim of the RLS algorithm is to estimate \mathbf{W}_k such that sum of

weighted mean square error $\sum_{j=1}^k \lambda^{k-j} [\mathbf{d}_j - \mathbf{W}_k \mathbf{y}_j^T]^2$ is minimized. Here λ is forgetting factor. Consider the correlation matrix $\mathbf{C}_k = \sum_{i=1}^k \lambda^{k-i} \mathbf{y}(i) \mathbf{y}^T(i) = \lambda \mathbf{C}_{k-1} + \mathbf{y}(k) \mathbf{y}^T(k)$. $\mathbf{P}_k^{(R)}$ is the inverse correlation matrix given by $\mathbf{P}_k^{(R)} = \mathbf{C}_k^{-1}$. The steps involved in RLS algorithm are

$$\zeta_k = \mathbf{d}_k - \mathbf{y}_k^T \mathbf{W}_k \quad (1.58)$$

$$\mathbf{K}_k^{(R)} = \frac{\mathbf{P}_{k-1}^{(R)} \mathbf{y}_k}{1 + \mathbf{y}_k^T \mathbf{P}_{k-1}^{(R)} \mathbf{y}_k} \quad (1.59)$$

$$\mathbf{W}_k = \mathbf{W}_{k-1} + \mathbf{K}_k^{(R)} \zeta_k. \quad (1.60)$$

$$\lambda_k = 1 - \frac{(1 - \mathbf{y}_k^T \mathbf{K}_k^{(R)}) \zeta_k^2}{\chi} \quad (1.61)$$

$$\mathbf{P}_k^{(R)} = \lambda_k^{-1} \mathbf{P}_{k-1}^{(R)} - \lambda_k^{-1} \mathbf{K}_k^{(R)} \mathbf{y}_k^T \mathbf{P}_{k-1}^{(R)} \quad (1.62)$$

where ζ denotes estimation error, $\mathbf{K}_k^{(R)}$ is the RLS gain. χ is constant value. The variable forgetting factor is used to stabilize $\mathbf{P}_k^{(R)}$ as it is sensitive to any disturbance that causes the increase in estimation error. This algorithm can be easily derived using the so called matrix inversion lemma.

1.10 Organization of the Thesis

The organization of the problems investigated in the thesis is as follows :-

Chapter 2 deals with the implementation of perturbation theory to derive the linear and nonlinear closed form Volterra expression between the input and output of SCR circuit. It also presents the computation of the distortion occurring due to linear part only.

Chapter 3 includes state estimation of the higher order RC LPF and RC HPF circuit using EKF and UKF methods and compared the estimation performance with LMS algorithm.

Chapter 4 deals with the state estimation of single-phase rectifier circuit using EKF, IEKF and UKF methods and compared the estimation performance with LMS algorithm.

Chapter 5 presents the state estimation of the following circuits using EKF, IEKF and UKF methods :-

- (i) CE-based BJT circuit.
- (ii) BJT-based DA circuit.

In the first part, we estimated the output voltage of CE BJT circuit using IEKF method and compared the performance of IEKF method with EKF method. The state space model of CE BJT circuit has been obtained using Kirchhoff's current law (KCL) and Ebers-Moll model of the transistor. In second part, we present the application of UKF method for output voltage estimation of DA circuit. Implementation of UKF algorithm requires state-space model of DA circuit, which has been obtained using Kirchhoff's voltage law (KVL), KCL and Gummel-Poon model of BJT. This work uses Kronecker product for vector multiplication. We compared the UKF estimation results with EKF and IEKF methods. We present the brief description of few recent methods of state estimation and compared estimation using EKF, IEKF and UKF methods.

In **Chapter 6**, we present the formulation of NTL dynamics modeling using Fourier series expansion and Kronecker product along with the state and parameter estimation using KF and EKF methods. The following circuits have been used for estimation purposes :-

- (i) Single-phase NTL circuit.
- (ii) Three-phase transposed and untransposed NTL circuit.

In first problem, state-space model of the single-phase NTL circuit has been derived. As Telegrapher's equations used for modeling the NTL are a function of space and time, the Fourier series expansion of the voltage and current have been used to obtain the time-dependent equations. Kronecker product has been used for representation of Fourier unitary transform. The measurements have been obtained by solving the eigenvector problem. The frequency-domain analysis is used to obtain the state-space equations. For this, the four distributed parameters of the line are expanded in Fourier series.

Secondly, we present KF-based state estimation and EKF and UKF-based parameter estimation for three-phase NTL. For this, state space model for three-phase transposed and untransposed NTL has been obtained by including Fourier series expansion of state and Gaussian noise vectors in the SDEs. Clarke transformation matrix has been utilized for phase to sequence transformation which allow to represent the three-phase TL into fully transposed TL. Measurement model for current and voltage vectors along the line are expressed in terms of Fourier series. Also, the frequency domain analysis is used to obtain the eigenvalue and eigenvector for measurement model. The voltage and current of NTL are expanded in Fourier series to obtain the sparse

matrix formulation using Kronecker product. Kronecker product representation of discrete unitary transforms results in computer efficient implementation. This work implements the analysis of nonlinearity effect in transmission lines using perturbation theory. For this, the nonlinearity of the transmission line is included by perturbing the voltage and current of the line. Also, we compared the estimation performances with RLS method. This chapter also discusses a few recent methods used for state and parameter estimation and their disadvantages.

Finally, some concluding remarks are presented in **Chapter 7** and some future work direction is also presented.

Chapter 2

Nonlinear Modeling of Analog Circuits Using Perturbation Theory

This chapter ¹ presents the modeling of SCR circuit using perturbation theory (Chapter 1.5). Generally, nonlinear circuit components are approximated by linear model for different applications. But, use of linear model causes signal distortion, which affects the performance of the nonlinear circuit component. This requires nonlinear closed-form expression of circuit components. For the simulation of on-chip circuits, an accurate model of the SCR is necessary. Although models are available based on the experimentally reported behaviour of the SCR, nonlinear closed-form relationships between the SCR's input and output are unavailable. Further, these models were developed using the existing device models, which affects the overall SCR model. However, the model developed in this work makes it possible to use a single block as an SCR model in software like SIMULINK, which offers flexibility and access to all the SCR circuit parameters [56]. The derived equation can be applied to the SCR model for computer-aided design. Typically, the SCR model is effective for designing systems that prevent electrostatic discharge (ESD) [57]. Tap changing transformers based on thyristor are used in various applications ranging from very high power aluminum potline to small hydrogen electrolyzer for gas station. [58] used

¹The result of this chapter is based on the following research paper (i) Amit Kumar Gautam and Sudipta Majumdar, "Volterra model of silicon controlled rectifier," in International Conference on Functional Materials, Characterization, Solid State Physics, Power, Thermal and Combustion Energy, AIP Conference Proceedings 1859, 020060, pp.1-8, 2017.

SCR for ICS's ESD protection that is operated in K/Ka band (26.540 GHz) and used in short range communication. [59] applied SCR for ESD issue of differential low noise amplifier that is used in RF receiver. [58] proposed inductor assisted light activated silicon controlled rectifier (LASCR) for ESD protection of the Gigahertz ICs in nanoscale CMOS technologies. In the design of integrated circuits, simulation is essential. It reduces the amount of time needed for circuit design. Before manufacturing the chips, it also provides circuit verification, testing, and early modifications. However, mathematical expressions of the circuit are necessary for accurate simulation. Additionally, the device's nonlinearity property is an important feature, therefore we used the Ebers-Moll model and perturbation theory to obtain closed form nonlinear expressions of SCR input and output.

SCR are commonly used as front-end devices in recent adjustable-speed drive system [60]. [61] used SCR as a reliable switch in high rating power electronics. [62] used SCR as a bridge-type fault current limiter. The p-channel laterally diffused metal-oxide-semiconductor (PLDMOS) works as a high voltage power SCR [63]. In IC applications, electrostatic discharge (ESD) is a major reliability problem. SCR provides significant ESD (anti-electrostatic device) robustness per length [[64], [65], [66]]. The stacked high holding voltage silicon controlled rectifier (HHVSCR) is proposed by [67] for ESD protection. The laterally diffused metal-oxide-semiconductor (LDMOS) transistor, which is used in RF and microwave communication power amplifier modules, has also been used in high voltage integrated circuits (IC) [65]. Further, Various systems including power management IC, dc-dc converters, LED and liquid crystal display, drivers power electronic modules and automotive microcontrollers (MCUs) use LDMOS transistors. SCR stacking architectures with high holding voltage are useful for a battery monitoring 60 V pins IC. In continuous torus, the circuit is triggered by SCR [68]. Altolaquirre [69] introduced the quad-silicon controlled rectifier which is a revolutionary electrostatic discharge prevention device. According to [70], SCR is also used in line commuted converters (LCC) for controlling the speed of DC motors.

Volterra modeling (Chapter 1.7) of SCR using Ebers-Moll model with perturbation method has been presented in section 2.1.1. To observe the effect of nonlinear expression, simulation results have been presented in section 2.1.2. Also, the distortion error has been computed by varying input amplitude and frequency is shown in Table 2.1.

2.1 Volterra Model of Silicon Controlled Rectifier

2.1.1 Mathematical Modeling

The SCR circuit shown in Figure 2.1 contains input resistance R_g and output resistance R_{E1} . Q_1 and Q_2 represent the transistors with current amplification factors β_1 and β_2 respectively. The gate voltage V_g is applied to Q_2 as the trigger voltage. v denotes the sinusoidal input voltage. Following equations represent the circuit dynamics using

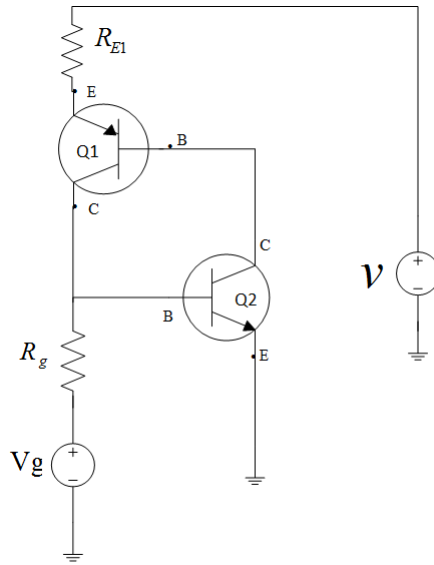


Figure 2.1: Circuit diagram of SCR.

KCL and KVL as :-

$$-v + i_{1e} \times R_{E1} + v_{1eb} + v_{2ce} = 0 \quad (2.1)$$

$$-V_g + (i_{2b} - i_{1c}) \times R_g + v_{2be} = 0 \quad (2.2)$$

$$\left(1 + \frac{1}{\beta_1}\right) \times i_{1c} - i_{1e} = 0 \quad (2.3)$$

The three state variables namely v_{1e} , v_{1b} , v_{1c} are obtained by equating the values of $v_{2b} = v_{1c}$, $v_{2e} = 0$, $v_{2c} = v_{1b}$. Emitter, collector and base current are denoted as i_e , i_c

and i_b respectively. (2.4)-(2.5) represent the Ebers-Moll model [41] of BJT circuit.

$$i_c = \alpha_F I_{ES} \left[\exp \frac{v_{be}}{V_T} - 1 \right] - I_{CS} \left[\exp \frac{v_{bc}}{V_T} - 1 \right] \quad (2.4)$$

$$i_e = -I_{ES} \left[\exp \frac{v_{be}}{V_T} - 1 \right] + \alpha_R I_{CS} \left[\exp \frac{v_{bc}}{V_T} - 1 \right] \quad (2.5)$$

where α_F and α_R are forward current gain and reverse current gain. I_{ES} and I_{CS} denote leakage current at emitter terminal and leakage current at collector terminal. V_T denotes thermal voltage. (2.4) and (2.5) for both transistors are now separated into linear and nonlinear parts as :-

$$\begin{aligned} i_{1c} &= a_{11}v_{1b}^{(0)} + a_{12}v_{1c}^{(0)} + a_{13}v_{1e}^{(0)} + \varepsilon \psi_1(v_b, v_c, v_e) \\ &= a_{11}v_{1b}^{(0)} + a_{12}v_{1c}^{(0)} + a_{13}v_{1e}^{(0)} + \varepsilon (b_{11}v_{1b}^{2(0)} + b_{12}v_{1c}^{2(0)} + b_{13}v_{1e}^{2(0)} + b_{14}v_{1b}^{2(0)}v_{1e}^{2(0)} + b_{15}v_{1b}^{2(0)}v_{1c}^{2(0)}) \end{aligned} \quad (2.6)$$

$$\begin{aligned} i_{2c} &= a_{21}v_{2b}^{(0)} + a_{22}v_{2c}^{(0)} + a_{23}v_{2e}^{(0)} + \varepsilon \psi_2(v_b, v_c, v_e) \\ &= a_{21}v_{2b}^{(0)} + a_{22}v_{2c}^{(0)} + a_{23}v_{2e}^{(0)} + \varepsilon (b_{21}v_{2b}^{2(0)} + b_{22}v_{2c}^{2(0)} + b_{23}v_{2e}^{2(0)} + b_{24}v_{2b}^{2(0)}v_{2e}^{2(0)} + b_{25}v_{2b}^{2(0)}v_{2c}^{2(0)}) \end{aligned} \quad (2.7)$$

$$\begin{aligned} i_{1e} &= c_{11}v_{1b}^{(0)} + c_{12}v_{1c}^{(0)} + c_{13}v_{1e}^{(0)} + \varepsilon \phi_1(v_b, v_c, v_e) \\ &= c_{11}v_{1b}^{(0)} + c_{12}v_{1c}^{(0)} + c_{13}v_{1e}^{(0)} + \varepsilon (d_{11}v_{1b}^{2(0)} + d_{12}v_{1c}^{2(0)} + d_{13}v_{1e}^{2(0)} + d_{14}v_{1b}^{2(0)}v_{1e}^{2(0)} + d_{15}v_{1b}^{2(0)}v_{1c}^{2(0)}) \end{aligned} \quad (2.8)$$

$$\begin{aligned} i_{2e} &= c_{21}v_{2b}^{(0)} + c_{22}v_{2c}^{(0)} + c_{23}v_{2e}^{(0)} + \varepsilon \phi_2(v_b, v_c, v_e) \\ &= c_{21}v_{2b}^{(0)} + c_{22}v_{2c}^{(0)} + c_{23}v_{2e}^{(0)} + \varepsilon (d_{21}v_{2b}^{2(0)} + d_{22}v_{2c}^{2(0)} + d_{23}v_{2e}^{2(0)} + d_{24}v_{2b}^{2(0)}v_{2e}^{2(0)} + d_{25}v_{2b}^{2(0)}v_{2c}^{2(0)}) \end{aligned} \quad (2.9)$$

where the parameters ψ_1 , ψ_2 , ϕ_1 and ϕ_2 are nonlinear function. ε uses a small value that accounts for the circuit's nonlinearity. Comparing the equations (2.4), (2.6), (2.7) and (2.5), (2.8), (2.9), the values of a_{ij} and b_{ij} are :-

$$\begin{aligned} a_{11} &= \frac{\alpha_{F1} I_{ES1} - I_{CS1}}{V_T}, & a_{12} &= \frac{I_{CS1}}{V_T}, & a_{13} &= -\frac{\alpha_{F1} I_{ES1}}{V_T}, & b_{11} &= \frac{\alpha_{F1} I_{ES1} - I_{CS1}}{2V_T^2} \\ b_{12} &= -\frac{I_{CS1}}{2V_T^2}, & b_{13} &= \frac{\alpha_{F1} I_{ES1}}{2V_T^2}, & b_{14} &= -\frac{\alpha_{F1} I_{ES1}}{V_T^2}, & b_{15} &= \frac{I_{CS1}}{V_T^2}, \\ a_{21} &= \frac{\alpha_{F2} I_{ES2} - I_{CS2}}{V_T}, & a_{22} &= \frac{I_{CS2}}{V_T}, & a_{23} &= -\frac{\alpha_{F2} I_{ES2}}{V_T}, & b_{21} &= \frac{\alpha_{F2} I_{ES2} - I_{CS2}}{2V_T^2}, \\ b_{22} &= -\frac{I_{CS2}}{2V_T^2}, & b_{23} &= \frac{\alpha_{F2} I_{ES2}}{2V_T^2}, & b_{24} &= -\frac{\alpha_{F2} I_{ES2}}{V_T^2}, & b_{25} &= \frac{I_{CS2}}{V_T^2}, \\ c_{11} &= \frac{\alpha_{R1} I_{CS1} - I_{ES1}}{V_T}, & c_{12} &= -\frac{\alpha_{R1} I_{CS1}}{V_T}, & c_{13} &= \frac{I_{ES1}}{V_T}, & d_{11} &= \frac{\alpha_{R1} I_{CS1} - I_{ES1}}{2V_T^2}, \\ d_{12} &= \frac{\alpha_{R1} I_{CS1}}{2V_T^2}, & d_{13} &= -\frac{I_{ES1}}{2V_T^2}, & d_{14} &= \frac{I_{ES1}}{V_T^2}, & d_{15} &= -\frac{\alpha_{R1} I_{CS1}}{V_T^2}, \\ c_{21} &= \frac{\alpha_{R2} I_{CS2} - I_{ES2}}{V_T}, & c_{22} &= -\frac{\alpha_{R2} I_{CS2}}{V_T}, & c_{23} &= \frac{I_{ES2}}{V_T}, & d_{21} &= \frac{\alpha_{R2} I_{CS2} - I_{ES2}}{2V_T^2}, \end{aligned}$$

$$d_{22} = \frac{\alpha_{R_2} I_{CS_2}}{2V_T^2}, \quad d_{23} = -\frac{I_{ES_2}}{2V_T^2}, \quad d_{24} = \frac{I_{ES_2}}{V_T^2}, \quad d_{25} = -\frac{\alpha_{R_2} I_{CS_2}}{V_T^2}$$

where ε is assumed to be unity.

$$v_b = v_b^{(0)} + \varepsilon v_b^{(1)} \quad (2.10)$$

$$v_e = v_e^{(0)} + \varepsilon v_e^{(1)} \quad (2.11)$$

$$v_c = v_c^{(0)} + \varepsilon v_c^{(1)} \quad (2.12)$$

Substituting values of v_b , v_e and v_c from (2.10)-(2.12) and i_c , i_e from (2.6)-(2.9) into (2.1)-(2.3), we get

$$v = R_{E_1} c_{11}(v_{1b}^{(0)} + \varepsilon v_{1b}^{(1)}) + R_{E_1} c_{12}(v_{1c}^{(0)} + \varepsilon v_{1c}^{(1)}) + R_{E_1} c_{13}(v_{1e}^{(0)} + \varepsilon v_{1e}^{(1)}) + R_{E_1} \varepsilon (d_{11} v_{1b}^{2(0)} + d_{12} v_{1c}^{2(0)} + d_{13} v_{1e}^{2(0)} + d_{14} v_{1b}^{(0)} v_{1e}^{(0)} + d_{15} v_{1b}^{(0)} v_{1c}^{(0)} + (v_{1e}^{(0)} + \varepsilon v_{1e}^{(1)})) \quad (2.13)$$

$$V_g = \left(\frac{R_g a_{21}}{\beta_2} \right) (v_{2b}^{(0)} + \varepsilon v_{2b}^{(1)}) + \left(\frac{R_g a_{22}}{\beta_2} \right) (v_{2c}^{(0)} + \varepsilon v_{2c}^{(1)}) + \left(\frac{R_g}{\beta_2} \right) \varepsilon (b_{21} v_{2b}^{2(0)} + b_{22} v_{2c}^{2(0)} + b_{23} v_{2e}^{2(0)} + b_{24} v_{2b}^{(0)} v_{2e}^{(0)} + b_{25} v_{2b}^{(0)} v_{2c}^{(0)} - R_g a_{11} (v_{1b}^{(0)} + \varepsilon v_{1b}^{(1)}) - R_g a_{12} (v_{1c}^{(0)} + \varepsilon v_{1c}^{(1)}) - R_g a_{13} (v_{1e}^{(0)} + \varepsilon v_{1e}^{(1)}) - R_g \varepsilon (b_{11} v_{1b}^{2(0)} + b_{12} v_{1c}^{2(0)} + b_{13} v_{1e}^{2(0)} + b_{14} v_{1b}^{(0)} v_{1e}^{(0)} + b_{15} v_{1b}^{(0)} v_{1c}^{(0)})) \quad (2.14)$$

$$\left(1 + \frac{1}{\beta_1} \right) [a_{11} (v_{1b}^{(0)} + \varepsilon v_{1b}^{(1)}) + a_{12} (v_{1c}^{(0)} + \varepsilon v_{1c}^{(1)}) + a_{13} (v_{1e}^{(0)} + \varepsilon v_{1e}^{(1)}) + \varepsilon (b_{11} v_{1b}^{2(0)} + b_{12} v_{1c}^{2(0)} + b_{13} v_{1e}^{2(0)} + b_{14} v_{1b}^{(0)} v_{1e}^{(0)} + b_{15} v_{1b}^{(0)} v_{1c}^{(0)})] - c_{11} (v_{1b}^{(0)} + \varepsilon v_{1b}^{(1)}) - c_{12} (v_{1c}^{(0)} + \varepsilon v_{1c}^{(1)}) - c_{13} (v_{1e}^{(0)} + \varepsilon v_{1e}^{(1)}) - \varepsilon (d_{11} v_{1b}^{2(0)} + d_{12} v_{1c}^{2(0)} + d_{13} v_{1e}^{2(0)} + d_{14} v_{1b}^{(0)} v_{1e}^{(0)} + d_{15} v_{1b}^{(0)} v_{1c}^{(0)}) = 0 \quad (2.15)$$

The linear and nonlinear components of voltages are obtained by comparing the coefficient of ε in (2.13) - (2.15). The linear components are expressed as :-

$$v = R_{E_1} c_{11} v_{1b}^{(0)} + R_{E_1} c_{12} v_{1c}^{(0)} + (1 + R_{E_1} c_{13}) v_{1e}^{(0)} \quad (2.16)$$

$$V_g = R_g \left(\frac{a_{22}}{\beta_2} - a_{11} \right) v_{1b}^{(0)} + \left(1 - R_g a_{12} + \frac{R_g a_{21}}{\beta_2} \right) v_{1c}^{(0)} - R_g a_{13} v_{1e}^{(0)} \quad (2.17)$$

$$\left\{ \left(1 + \frac{1}{\beta_1} \right) a_{11} - c_{11} \right\} v_{1b}^{(0)} + \left\{ \left(1 + \frac{1}{\beta_1} \right) a_{12} - c_{12} \right\} v_{1c}^{(0)} + \left\{ \left(1 + \frac{1}{\beta_1} \right) a_{13} - c_{13} \right\} v_{1e}^{(0)} = 0 \quad (2.18)$$

Equation (2.19) represents state vector as :-

$$X_0(s) = [v_{1b}, v_{1c}, v_{1e}, v_{2b}, v_{2c}, v_{2e}]^T \quad (2.19)$$

The Laplace transform (LT) equation obtain the following solution as :-

$$X_0(s) = F^{-1}(s)G(s)v(s) + F^{-1}(s)H(s)V_{CC} \quad (2.20)$$

where

$$F = \begin{bmatrix} c_{11}R_{E_1} & c_{12}R_{E_1} & 1 + c_{13}R_{E_1} \\ (-a_{11} + \frac{a_{22}}{\beta_2})R_g & \frac{R_g a_{21}}{\beta_2} + 1 - R_g a_{12} & -a_{13}R_g \\ -c_{11} + (1 + \frac{1}{\beta_1})a_{11} & -c_{12} + (1 + \frac{1}{\beta_1})a_{12} & -c_{13} + (1 + \frac{1}{\beta_1})a_{13} \end{bmatrix}.$$

$$Z_i(s) = F^{-1}(s)G(s) \quad (2.21)$$

$$v_{1b}^{(0)}(t) = v * z_1(t) + \phi_1(t) \quad (2.22)$$

$$v_{1c}^{(0)}(t) = v * z_2(t) + \phi_2(t) \quad (2.23)$$

$$v_{1e}^{(0)}(t) = v * z_3(t) + \phi_3(t) \quad (2.24)$$

where convolution operator is represented by '*' notation. Representing (2.21) in terms of LT as :-

$$Z_1(s) = \frac{F_{11}}{|F|}, \quad Z_2(s) = \frac{F_{12}}{|F|}, \quad Z_3(s) = \frac{F_{13}}{|F|}, \quad \phi_1(s) = \frac{F_{21}}{|F|}V_g, \quad \phi_2(s) = \frac{F_{22}}{|F|}V_g, \quad \phi_3(s) = \frac{F_{23}}{|F|}V_g.$$

where $\phi(t)$ represents the inverse LT of $F^{-1}(s)H(s)V_{CC}$. The small signal equivalent model's impulse responses are :-

$$v_{1b}^{(0)}(t) = v * \delta(t) \times K_1 + K_2 \times V_g \times \delta(t) \quad (2.25)$$

$$v_{1c}^{(0)}(t) = v * \delta(t) \times K_3 + K_4 \times V_g \times \delta(t) \quad (2.26)$$

$$v_{1e}^{(0)}(t) = v * \delta(t) \times K_5 + K_6 \times V_g \times \delta(t) \quad (2.27)$$

where $\delta(t)$ denotes unit impulse function.

$$K_1 = \frac{F_{11}}{|F|}, \quad K_2 = \frac{F_{21}}{|F|}, \quad K_3 = \frac{F_{12}}{|F|}, \quad K_4 = \frac{F_{22}}{|F|}, \quad K_5 = \frac{F_{13}}{|F|}, \quad K_6 = \frac{F_{23}}{|F|}$$

Now comparing the coefficients of ε^1 , we obtain the expressions of nonlinear components

as :-

$$u_1(t) = b_{11}v_{1b}^{2(0)} + b_{12}v_{1c}^{2(0)} + b_{13}v_{1e}^{2(0)} + b_{14}v_{1b}^{(0)}v_{1e}^{(0)} + b_{15}v_{1b}^{(0)}v_{1c}^{(0)} \quad (2.28)$$

$$u_2(t) = b_{21}v_2^{2(0)} + b_{22}v_{1c}^{2(0)} + b_{23}v_{1e}^{2(0)} + b_{24}v_{2b}^{(0)}v_{2e}^{(0)} + b_{25}v_{2b}^{(0)}v_{1c}^{(0)} \quad (2.29)$$

$$u_3(t) = d_{11}v_{1b}^{2(0)} + d_{12}v_{1c}^{2(0)} + d_{13}v_{1e}^{2(0)} + d_{14}v_{1b}^{(0)}v_{1e}^{(0)} + d_{15}v_{1b}^{(0)}v_{1c}^{(0)} \quad (2.30)$$

$$u_4(t) = d_{21}v_{2b}^{2(0)} + d_{22}v_{1c}^{2(0)} + d_{23}v_{1e}^{2(0)} + d_{24}v_{2b}^{(0)}v_{2e}^{(0)} + d_{25}v_{2b}^{(0)}v_{1c}^{(0)} \quad (2.31)$$

$$v_1^{(1)}(B)(s) = \left[\frac{R_g F_{21} - (1 + \frac{1}{\beta_1}) F_{31}}{|F|} \right] U_1(s) - \left[\frac{R_g F_{21}}{|F| \beta_2} \right] U_2(s) + \left[\frac{F_{31} - R_{E1} F_{11}}{|F|} \right] U_3(s) \quad (2.32)$$

$$v_1^{(1)}(C)(s) = \left[\frac{R_g F_{22} - (1 + \frac{1}{\beta_1}) F_{32}}{|F|} \right] U_1(s) - \left[\frac{R_g F_{22}}{|F| \beta_2} \right] U_2(s) + \left[\frac{F_{32} - R_{E1} F_{12}}{|F|} \right] U_3(s) \quad (2.33)$$

$$v_1^{(1)}(E)(s) = \left[\frac{R_g F_{23} - (1 + \frac{1}{\beta_1}) F_{33}}{|F|} \right] U_1(s) - \left[\frac{R_g F_{23}}{|F| \beta_2} \right] U_2(s) + \left[\frac{F_{33} - R_{E1} F_{13}}{|F|} \right] U_3(s) \quad (2.34)$$

$$v_{1b}^{(1)}(t) = K_7 \times (u_1(t) * \delta(t)) + K_8 \times (u_2(t) * \delta(t)) + K_9 \times (u_3(t) * \delta(t)) \quad (2.35)$$

$$v_{1c}^{(1)}(t) = K_{10} \times (u_1(t) * \delta(t)) + K_{11} \times (u_2(t) * \delta(t)) + K_{12} \times (u_3(t) * \delta(t)) \quad (2.36)$$

$$v_{1e}^{(1)}(t) = K_{13} \times (u_1(t) * \delta(t)) + K_{14} \times (u_2(t) * \delta(t)) + K_{15} \times (u_3(t) * \delta(t)) \quad (2.37)$$

where

$$K_7 = \left[\frac{R_g F_{21} - (1 + \frac{1}{\beta_1}) F_{31}}{|F|} \right], \quad K_8 = \left[\frac{R_g F_{21}}{|F| \beta_2} \right], \quad K_9 = \left[\frac{F_{31} - R_{E1} F_{11}}{|F|} \right], \quad K_{10} = \left[\frac{R_g F_{22} - (1 + \frac{1}{\beta_1}) F_{32}}{|F|} \right],$$

$$K_{11} = \left[\frac{R_g F_{22}}{|F| \beta_2} \right], \quad K_{12} = \left[\frac{F_{31} - R_{E1} F_{11}}{|F|} \right], \quad K_{13} = \left[\frac{R_g F_{23} - (1 + \frac{1}{\beta_1}) F_{33}}{|F|} \right], \quad K_{14} = \left[\frac{R_g F_{23}}{|F| \beta_2} \right],$$

$$K_{15} = \left[\frac{F_{33} - R_{E1} F_{13}}{|F|} \right].$$

2.1.2 Simulation Results

From the circuit shown in Figure 2.1, the linear (zeroth order) and first order nonlinear output voltages have been plotted in MATLAB for various input voltages and frequencies which is shown in Figure 2.2. The percentage distortion due to linear term only has been calculated using (2.38). Table 2.1 shows the distortion error by varying the value

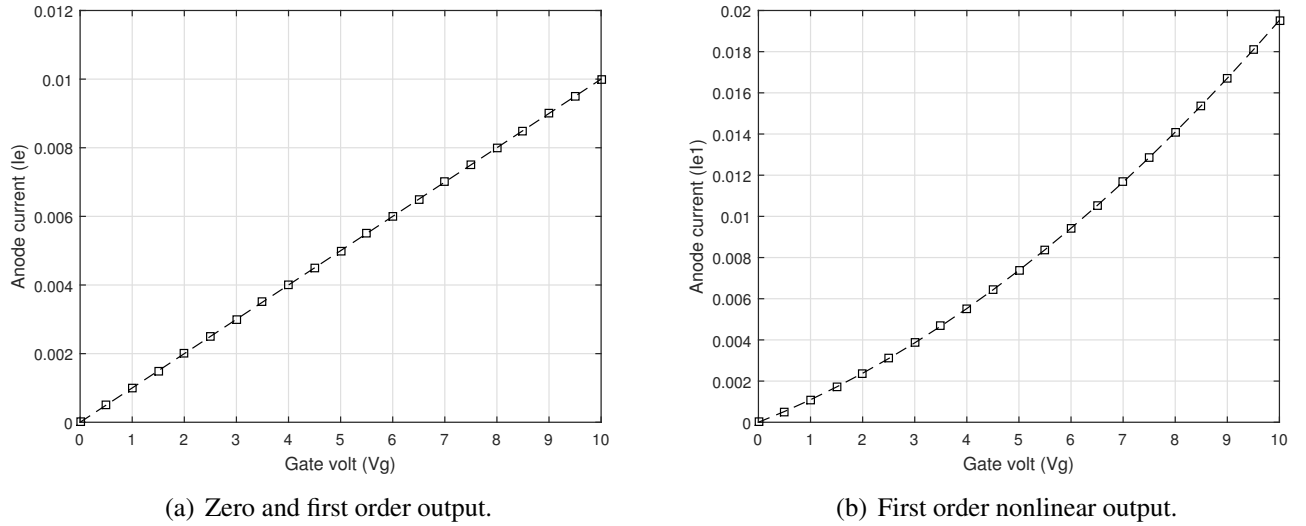


Figure 2.2: Anode currents of SCR output.

of amplitude and frequency of input signal. Percentage distortion is expressed as :-

$$\text{Percentage distortion} = \frac{I_{e1} - I_e}{I_{e1}} \times 100\% \quad (2.38)$$

The result shows the significance of nonlinearity. In SIMULINK software, the resulting equations are used as a half wave rectifier (HWR) circuit. The input output voltages are presented in Figure 2.4.

Table 2.1: Percentage of distortion errors for various input values.

S.No.	Peak amplitude (Volts)	Distortion error(%)
1	0.70	0.3883%
2	0.90	0.4640%
3	1.00	0.5028%
4	1.30	0.6117%
5	1.50	0.6729%

2.1.3 Conclusions

In this chapter, the closed form nonlinear expressions of SCR has been derived. The derived expressions have been used to plot the SCR characteristic in MATLAB. The use of closed form expressions to model SCR in SIMULINK provides direct access to circuit parameters, which is helpful for designing and analysis of new circuits.

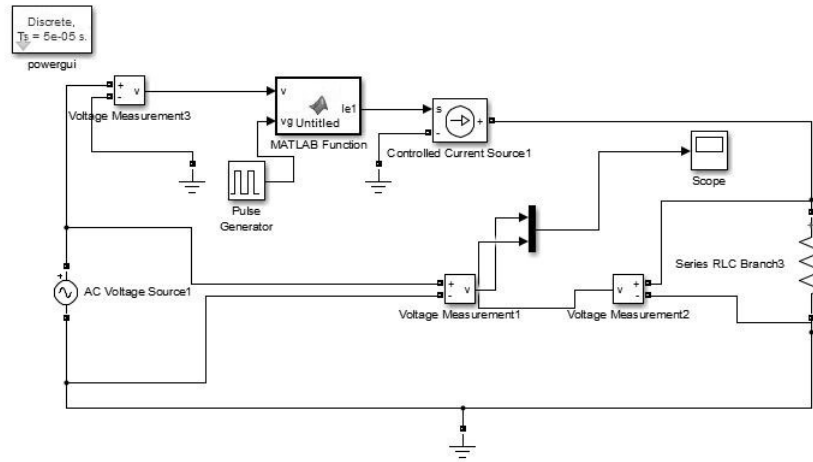


Figure 2.3: Simulation diagram of HWR circuit using SCR.

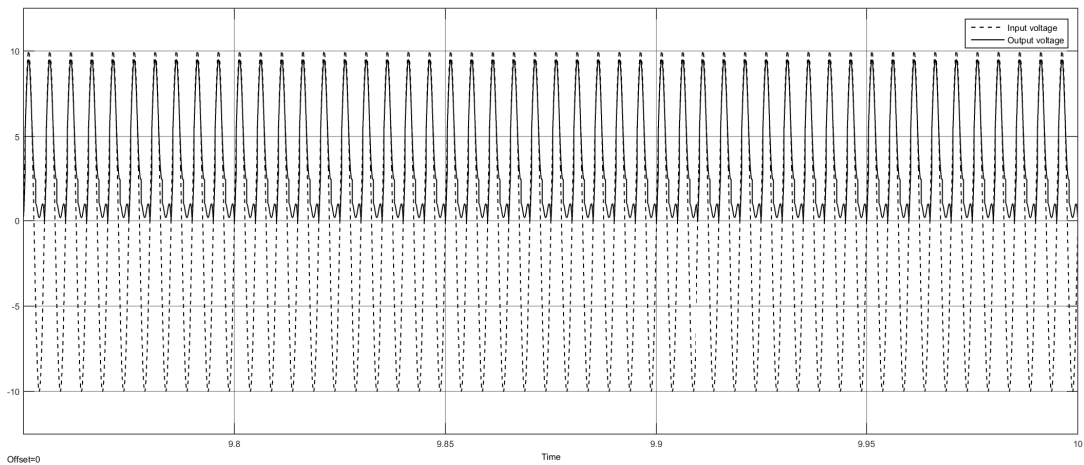


Figure 2.4: Input and output voltage across series RC component.

Chapter 3

State Estimation of Higher Order RC Circuit

This chapter ¹ presents the implementation of different versions of KF algorithm on higher order RC LPF and HPF circuits for state estimation. For this, the state space model of the circuit is obtained using KCL.

In the previous chapter, the closed form Volterra expression of SCR has been derived. In this chapter, state space model of the circuit has been derived as required by KF methods.

The Major contributions of the proposed work are :- (i) state estimation of the analog RC circuit using different versions of KF have been computed. (ii) state-space model of dynamic analog RC circuits has been obtained using KVL and KCL. (iii) input voltage is modeled as the zero mean white noise. (iv) The output results of different versions of KF algorithm have been compared with each other. Simulation results demonstrate the effectiveness of the proposed method.

Parameter estimation is an important area in the field of science and technology. Various estimation techniques have been used by researcher. There are two basic parameter estimation methods: - 1) methods based on optimization approaches and 2) methods based on stability theory. Differential evolution, particle swarm optimization

¹The result of this chapter is based on the following research papers (i) Amit Kumar Gautam and Sudipta Majumdar, "Parameter estimation of RC circuits using extended Kalman filter," International Journal of Advanced in Management, Technology and Engineering Sciences, ISSN no. 2249-7455, vol. 8, no. 1, pp. 83-91, 2018, (ii) Amit Kumar Gautam and Sudipta Majumdar, "State estimation of RC filter using unscented Kalman filters," International Journal of Innovative Technology and Exploring Engineering, ISSN no. 2278-3075, vol. 9, no. 9, pp. 91-96, 2020.

are examples of optimization-based methods and Lyapunov stability method, synchronization approach based on Lasalle's principle are stability-based estimation methods. The parameter estimation methods based on the deterministic minimizes error function between model output and measurement data. Various methods have been used for parameter estimation of systems. In [71], the effects of white noise perturbation on the parameters of electrical network have been analyzed and least square estimation has been used after transferring the deterministic model into stochastic models. [72] presented the total least square estimation of signal parameter via rotation invariance method. [73] proposed an extended stochastic gradient (ESG) filtering and multi-innovative filtering for parameter estimation. [74] proposed a parameter estimation of permanent magnet synchronous machine using a dynamic particle swarm optimization method.

RC LPF has many applications. It is used as a discrete-time repetitive controller for a fly-back inverter in continuous conduction mode. The RC LPF has been also used for tracking and rejection of periodic signals in a typical frequency range. In [75], RC circuit has application in micro-electromechanical systems (MEMS) sensor that includes a ring oscillator, an RC controlled pulse generator together with a self-tuned inverter converter. The RC HPF reduces the bandwidth of noise source. [76] proposed RC LPF with good asymptotic behavior in the pass band. In [77], the RC LPF is also used in a flexible continuous time delta sigma modulator. [78] presents RC filter implementation in chopper stabilized thin film transistor low noise amplifier, which is used for electroencephalogram (EEG) signal acquisition and biomarker extraction system. In [79], it is used in linear periodically time-varying filter circuit which is used in spectrum scanner.

The state space representation of higher order RC LPF and RC HPF using KCL has been derived in section 3.1. Section 3.2 presents implementation of EKF method to RC LPF and RC HPF circuits. Simulation results of RC circuits using EKF and UKF methods are presented in sections 3.3 and 3.4 respectively.

3.1 State Space Model

A second-order dynamic LPF with R and C components is shown in Figure 3.1(a). Let $u_1(t)$ be the input sinusoidal signal. $V_{c_1}(t)$ is capacitor voltages across C_1 and $V_{c_2}(t)$ is the capacitor voltages across C_2 . The state space model for the circuit shown in

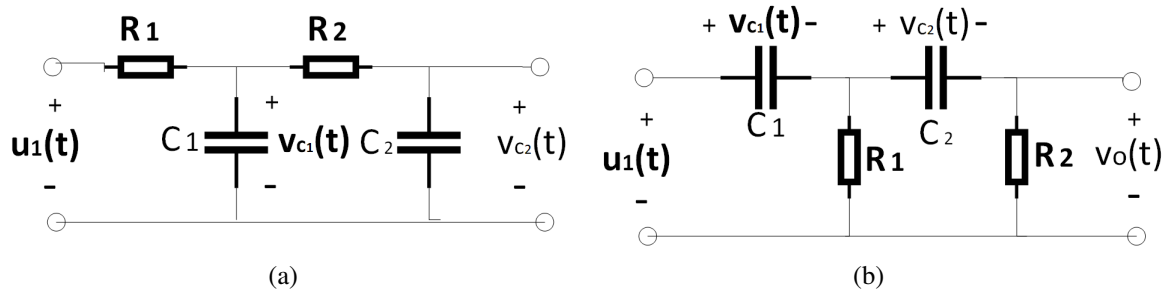


Figure 3.1: a) RC low pass filter, b) RC high pass filter.

Figure 3.1 (a) is obtained by using KCL. The equations are as follows :-

$$\frac{v_{c1}(t)}{R_1} - \frac{u_1(t)}{R_1} + \frac{v_{c1}(t)}{R_2} - \frac{v_{c2}(t)}{R_2} + C_1 \frac{dv_{c1}(t)}{dt} = 0 \quad (3.1)$$

$$\frac{v_{c2}(t)}{R_2} - \frac{v_{c1}(t)}{R_2} + C_2 \frac{dv_{c2}(t)}{dt} = 0 \quad (3.2)$$

Representing (3.1)-(3.2) as state space model, we have

$$\begin{bmatrix} \dot{v}_{c1}(t) \\ \dot{v}_{c2}(t) \end{bmatrix} = \begin{bmatrix} -\frac{1}{C_1} \left(\frac{1}{R_1} + \frac{1}{R_2} \right) & \frac{1}{R_2 C_1} \\ \frac{1}{R_2 C_2} & -\frac{1}{R_2 C_2} \end{bmatrix} \begin{bmatrix} v_{c1}(t) \\ v_{c2}(t) \end{bmatrix} + \begin{bmatrix} \frac{1}{R_1 C_1} \\ 0 \end{bmatrix} u_1(t) \quad (3.3)$$

where ' symbol represents $\frac{d}{dt}$. The output voltage of RC LPF can be written as :-

$$\mathbf{z} = \mathbf{v}_{c2}(t) \quad (3.4)$$

Representing (3.3)-(3.4) as state space model, we have

$$\frac{d}{dt} \mathbf{x} = \mathbf{F} \mathbf{x} + \mathbf{B} \mathbf{u} \quad (3.5)$$

where \mathbf{x} and \mathbf{u} are state and input vector respectively.

$$\mathbf{F} = \begin{bmatrix} -\frac{1}{C_1} \left(\frac{1}{R_1} + \frac{1}{R_2} \right) & \frac{1}{R_2 C_1} \\ \frac{1}{R_2 C_2} & -\frac{1}{R_2 C_2} \end{bmatrix}, \mathbf{B} = \begin{bmatrix} \frac{1}{R_1 C_1} & 0 \end{bmatrix}^T \quad (3.6)$$

\mathbf{z} is the measurement model given as :-

$$\mathbf{z} = \mathbf{H} \mathbf{x} + \mathbf{C} \mathbf{u} \quad (3.7)$$

where \mathbf{H} denotes the measurement matrix as :-

$$\mathbf{H} = \begin{bmatrix} 0 & 1 \end{bmatrix} \text{ and } \mathbf{C} = \begin{bmatrix} 0 \end{bmatrix} \quad (3.8)$$

Similarly, state-space model for RC HPF shown in Figure 3.1 (b) can be represented as :-

$$\frac{d}{dt} \begin{bmatrix} v_{c1}(t) \\ v_{c2}(t) \end{bmatrix} = \begin{bmatrix} -\frac{1}{C_1}(\frac{1}{R_1} + \frac{1}{R_2}) & -\frac{1}{R_2 C_1} \\ -\frac{1}{R_2 C_2} & -\frac{1}{R_2 C_2} \end{bmatrix} \begin{bmatrix} v_{c1}(t) \\ v_{c2}(t) \end{bmatrix} + \begin{bmatrix} \frac{1}{C_1}(\frac{1}{R_1} + \frac{1}{R_2}) \\ \frac{1}{R_2 C_2} \end{bmatrix} u_2(t) \quad (3.9)$$

$$\mathbf{z} = \begin{bmatrix} -1 & -1 \end{bmatrix} \begin{bmatrix} v_{c1}(t) \\ v_{c2}(t) \end{bmatrix} + u_2(t) \quad (3.10)$$

The matrices \mathbf{F} , \mathbf{B} , \mathbf{H} and \mathbf{C} for RC HPF are :-

$$\mathbf{F} = \begin{bmatrix} -\frac{1}{C_1}(\frac{1}{R_1} + \frac{1}{R_2}) & -\frac{1}{R_2 C_1} \\ -\frac{1}{R_2 C_2} & -\frac{1}{R_2 C_2} \end{bmatrix}, \mathbf{B} = \begin{bmatrix} \frac{1}{C_1}(\frac{1}{R_1} + \frac{1}{R_2}) \\ \frac{1}{R_2 C_2} \end{bmatrix}, \mathbf{H} = \begin{bmatrix} -1 & -1 \end{bmatrix}^T, \mathbf{C} = \begin{bmatrix} 0 & 1 \end{bmatrix} \quad (3.11)$$

3.2 Implementation of EKF algorithm

The state model in (3.5) and (3.7) can be discretized using first-order exponential method. The transformed equations are expressed as :-

$$\mathbf{x}_{k+1} = \mathbf{F}_k \mathbf{x}_k + \mathbf{B}_k \mathbf{u}_k + \mathbf{G}_k \mathbf{w}_k \quad (3.12)$$

$$\mathbf{z}_k = \mathbf{H}_k \mathbf{x}_k + \mathbf{C}_k \mathbf{u}_k + \mathbf{D}_k \mathbf{v}_k \quad (3.13)$$

(3.12) and (3.13) are discrete representation of equations (3.5) and (3.7) respectively obtained using $t = kT_s$, where $k = 1, 2, 3, \dots$ where T_s is sampling time. The matrices \mathbf{F}_k , \mathbf{B}_k , \mathbf{C}_k and \mathbf{H}_k are obtained by discretizing \mathbf{F} , \mathbf{B} , \mathbf{H} and \mathbf{C} respectively. They are :-

$$\mathbf{F}_k = e^{T_s} = I + F T_s = \begin{bmatrix} 1 - \frac{T_s}{C_1}(\frac{1}{R_1} + \frac{1}{R_2}) & \frac{T_s}{R_1 C_1} \\ \frac{T_s}{R_2 C_2} & 1 - \frac{T_s}{R_2 C_2} \end{bmatrix} \quad (3.14)$$

$$\mathbf{B}_k = B T_s = \begin{bmatrix} \frac{T_s}{R_1 C_1} & 0 \end{bmatrix}^T, \mathbf{H}_k = \begin{bmatrix} 0 & 1 \end{bmatrix}, \mathbf{C}_k = \begin{bmatrix} 0 \end{bmatrix}. \quad (3.15)$$

Table 3.1: Comparison of SNR value for different methods.

Input signal	SNR by EKF method	SNR by LMS method
Sinusoidal signal in LPF	43.769	32.737
Square wave in LPF	55.994	34.314
Sinusoidal signal in HPF	58.144	26.866
Square wave in HPF	62.650	60.480

The matrices \mathbf{F}_k , \mathbf{B}_k , \mathbf{H}_k and \mathbf{C}_k for RC HPF are obtained by discretizing equations (3.9)-(3.10). They are :-

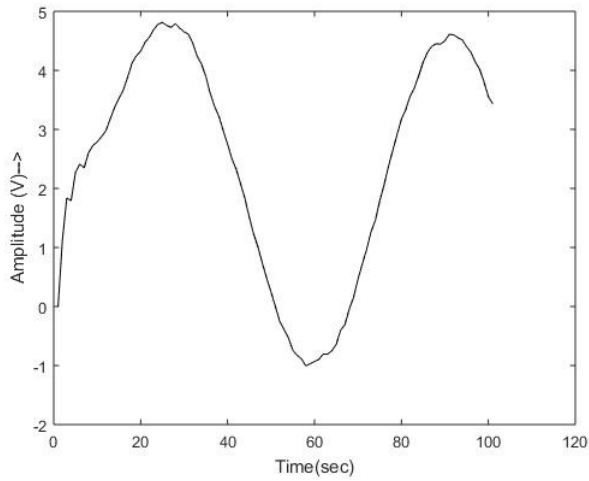
$$\mathbf{F}_k = \begin{bmatrix} 1 - \frac{T_s}{C_1} \left(\frac{1}{R_1} + \frac{1}{R_2} \right) & -\frac{T_s}{R_2 C_1} \\ -\frac{T_s}{R_2 C_2} & 1 - \frac{T_s}{R_2 C_2} \end{bmatrix}, \mathbf{B}_k = \begin{bmatrix} \frac{T_s}{C_1} \left(\frac{1}{R_1} + \frac{1}{R_2} \right) \\ \frac{T_s}{R_2 C_2} \end{bmatrix}, \mathbf{H}_k = [-1 \quad -1]^T, \mathbf{C}_k = [0 \quad 1] \quad (3.16)$$

3.3 Simulation Results using EKF Method

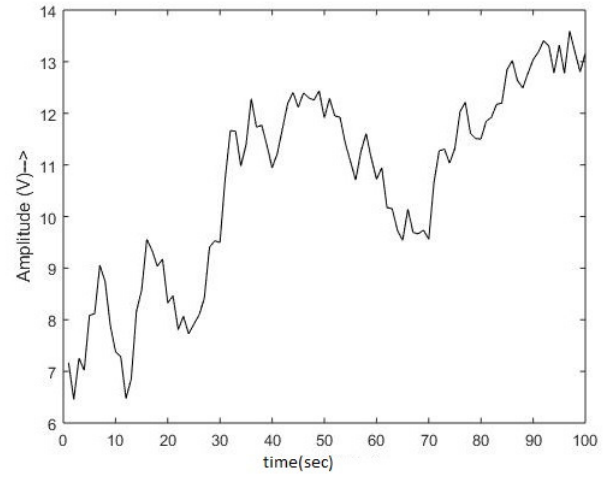
We estimated the output voltage of RC LPF and RC HPF for two different inputs. The applied sinusoidal input contains maximum amplitude of 10 V and frequency 0.01 Hz. The white Gaussian noise of zero mean and 0.5 variance has been used for estimation purpose. The output response of LPF circuit using EKF method (Chapter 1.4.2) and LMS method (Chapter 1.8) is shown in Figure 3.2(a) and 3.2(b) respectively. Figure 3.2(c) and 3.2(d) show output voltage estimation of HPF using EKF and LMS methods respectively for sinusoidal noisy input. Figure 3.3(a) and 3.3(b) show the LPF estimated output voltage for noisy square wave input signal. Similarly, Figure 3.3(c) and 3.3(d) show output voltage estimation of HPF for noisy square wave input signal using EKF and LMS methods respectively. Table 3.1 shows the signal to noise ratio (SNR) in each case. The SNR expression is given as :-

$$SNR = 10 \log_{10} \left[\frac{\sum_{i=1}^n (\hat{y}_i)^2}{\sum_{i=1}^n (\hat{y}_i - y_i)^2} \right] \quad (3.17)$$

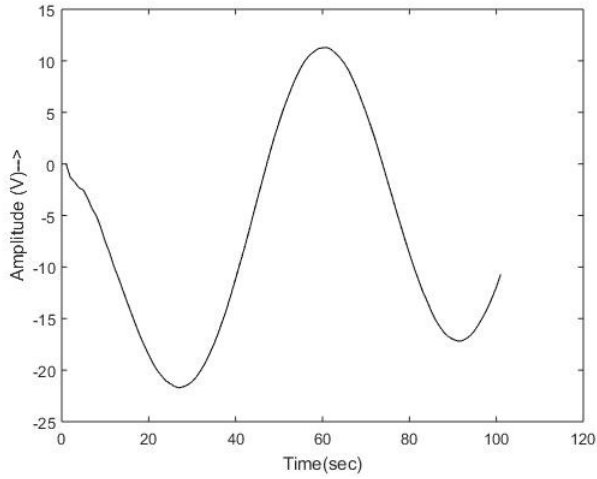
where \hat{y} denotes estimated value, y denotes actual value and n is the number of samples.



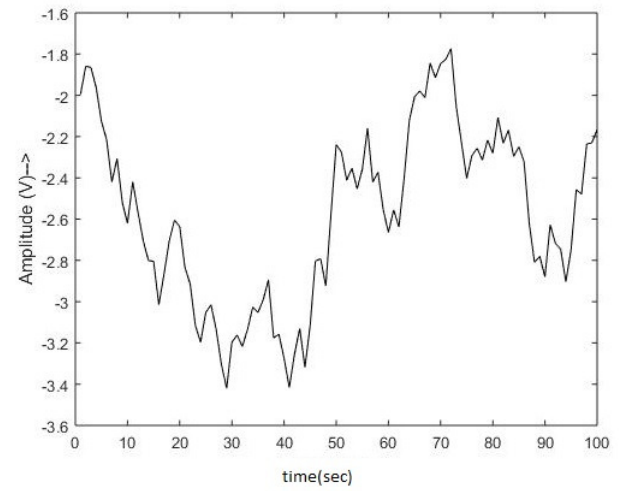
(a) Estimated output voltage of LPF using EKF method.



(b) Estimated output voltage of LPF using LMS method.

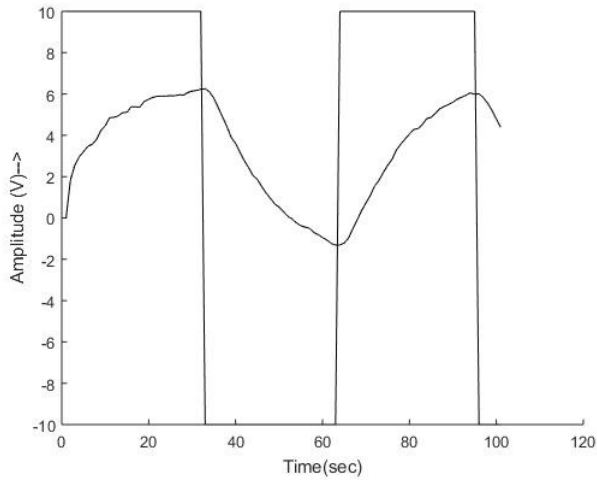


(c) Estimated output voltage of HPF using EKF method.

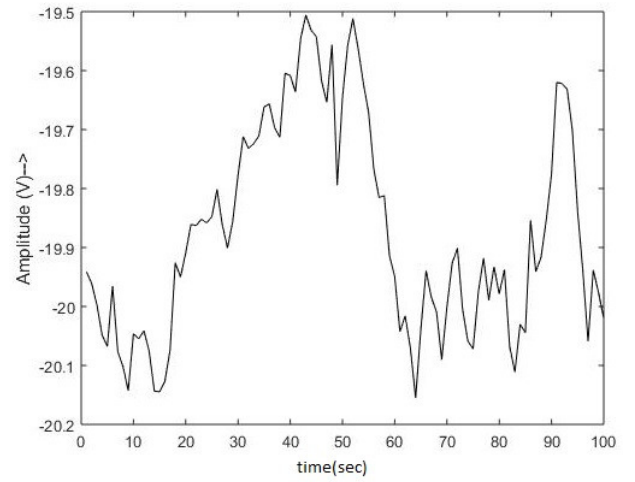


(d) Estimated output voltage of HPF using LMS method.

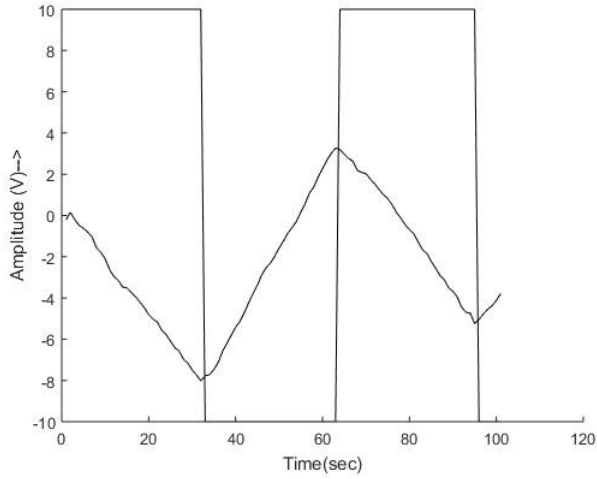
Figure 3.2: Estimated output voltage of RC filter for sinusoidal wave.



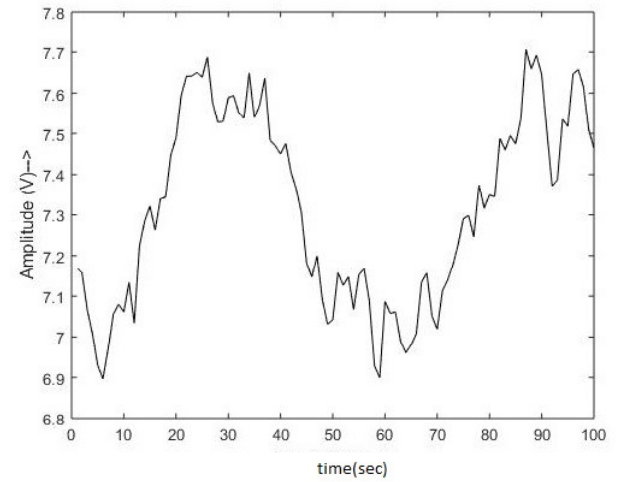
(a) Estimated output voltage of LPF using EKF method.



(b) Estimated output voltage of LPF using LMS method.



(c) Estimated output voltage of HPF using EKF method.



(d) Estimated output voltage of HPF using LMS method.

Figure 3.3: Estimated output voltage of RC filter for square wave.

Table 3.2: Performance of different methods for LPF.

input signal	Parameter	EKF method	UKF method
Noisy input signal with $\mu = 0, \sigma^2 = 0.1$	SNR(dB)	24.44	40.55
	RMSE	0.2842	0.0402
Noisy input signal with $\mu = 0, \sigma^2 = 0.5$	SNR(dB)	11.17	31.56
	RMSE	0.5803	0.0991
Noisy input signal with $\mu = 0, \sigma^2 = 1.0$	SNR(dB)	7.57	23.66
	RMSE	1.4794	1.2746

Table 3.3: Performance of different methods for HPF.

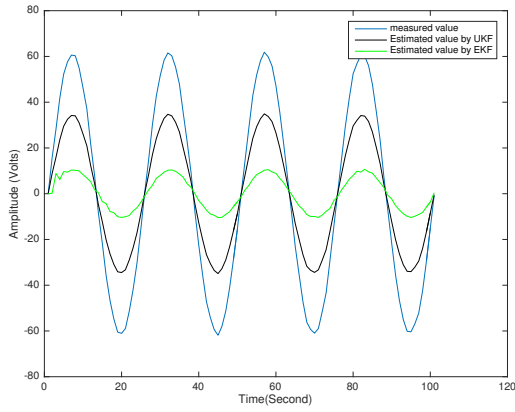
Input signal	Parameter	EKF method	UKF method
Noisy input signal with $\mu = 0, \sigma^2 = 0.1$	SNR(dB)	28.57	40.12
	RMSE	0.1588	0.0457
Noisy input signal with $\mu = 0, \sigma^2 = 0.5$	SNR(dB)	14.46	26.15
	RMSE	1.0521	0.1867
Noisy input signal with $\mu = 0, \sigma^2 = 1.0$	SNR(dB)	8.96	20.99
	RMSE	1.810	0.2175

3.4 Simulation Results using UKF Method

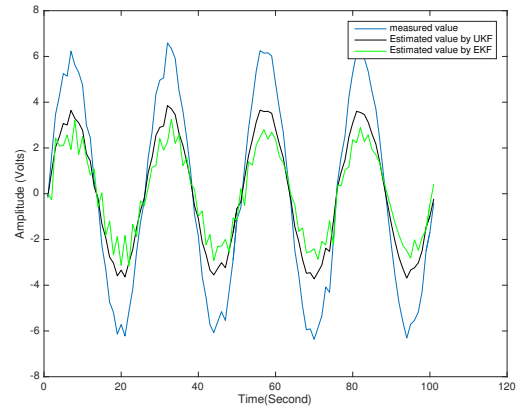
We estimated the output voltage of RC LPF and RC HPF for two different inputs:- (i) noiseless input, and (ii) noisy input. The applied sinusoidal input with maximum amplitude of 10 V and frequency 0.04 Hz. The white Gaussian noise of zero mean and different variances have been used as noisy input for estimation purpose. The PSPICE simulated values have been taken as actual value. The output voltages of LPF and HPF circuits using UKF method (Chapter 1.4.4) and EKF method under different noisy inputs have been shown in Figure 3.4. Figure 3.5 presents the error comparison of EKF and UKF methods for different noise values. Table 3.2 and 3.3 show the comparison of SNR and root mean square error (RMSE) for both circuits using UKF and EKF methods. RMSE is expressed as :-

$$RMSE = \sqrt{\frac{\sum_{i=1}^n (\hat{y}_i - y_i)^2}{n}} \quad (3.18)$$

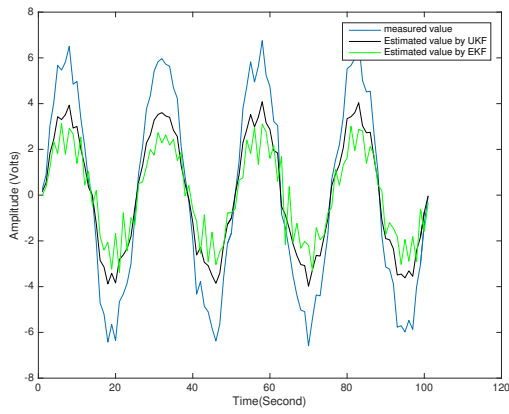
where \hat{y} denotes estimated value, y denotes actual value and n is the number of samples.



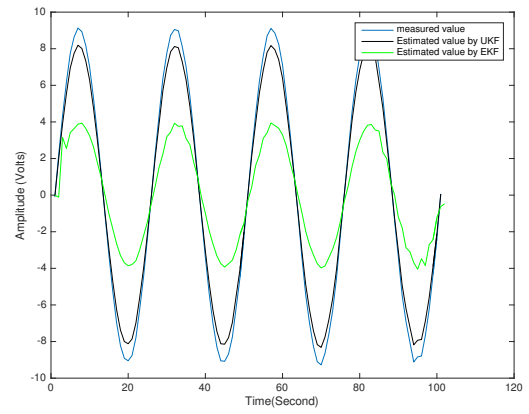
(a)



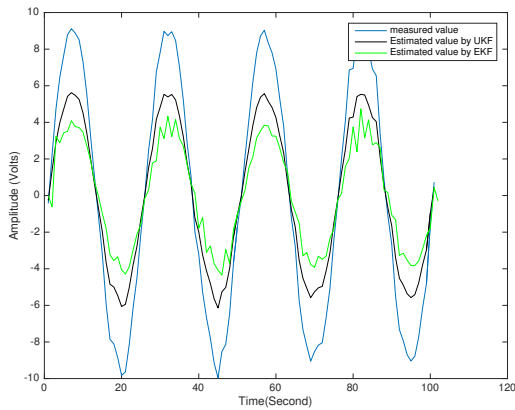
(b)



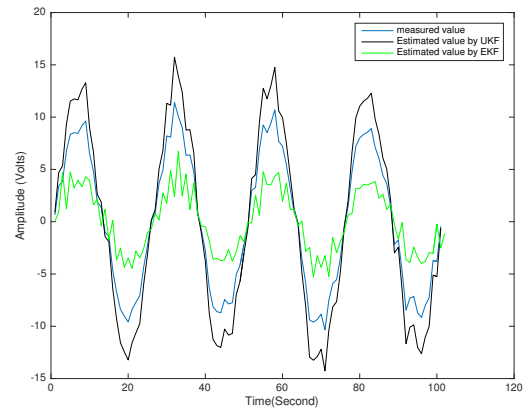
(c)



(d)

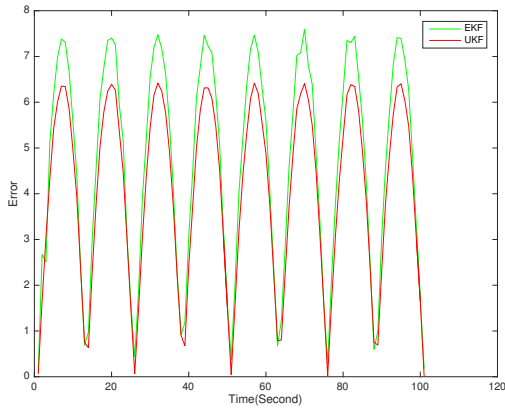


(e)

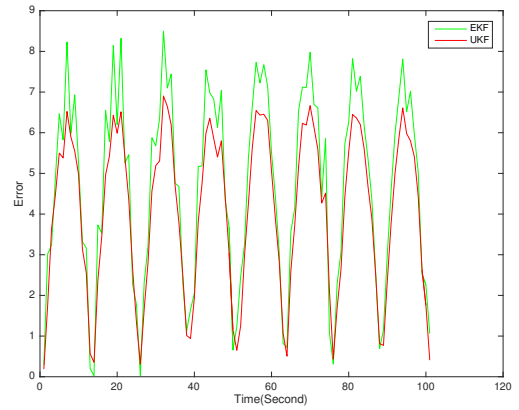


(f)

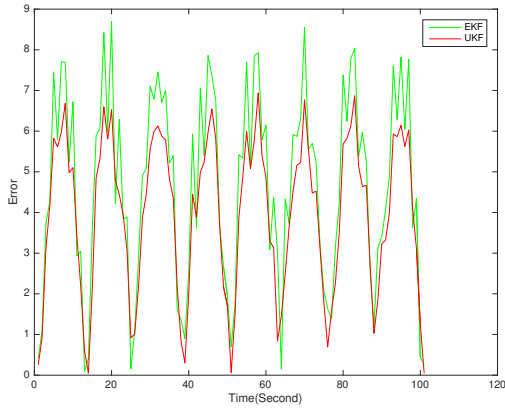
Figure 3.4: Comparison of output voltage estimation of LPF using noisy input with a) $\mu = 0$, $\sigma^2 = 0.1$, b) $\mu = 0$, $\sigma^2 = 0.5$, c) $\mu = 0$, $\sigma^2 = 1.0$, Comparison of output voltage estimation of HPF using noisy input with d) $\mu = 0$, $\sigma^2 = 0.1$, e) $\mu = 0$, $\sigma^2 = 0.5$, f) $\mu = 0$, $\sigma^2 = 1.0$.



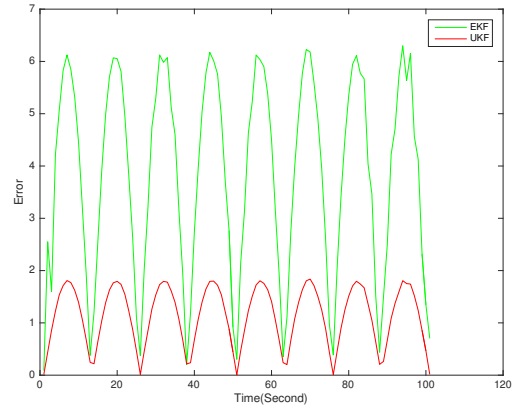
(a)



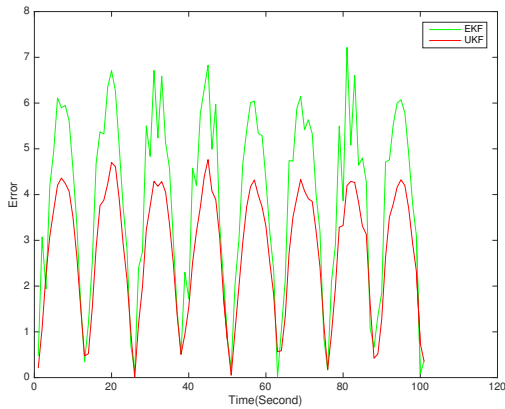
(b)



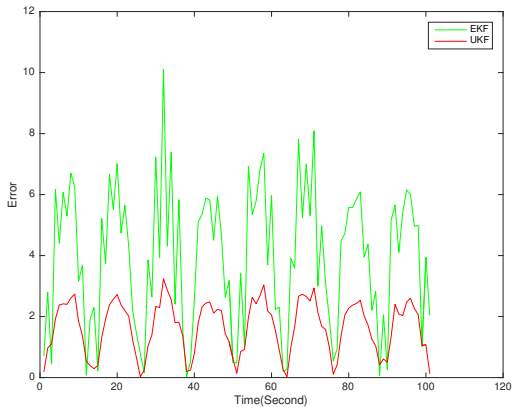
(c)



(d)



(e)



(f)

Figure 3.5: Comparison of estimation error for LPF using noisy input with a) $\mu = 0$, $\sigma^2 = 0.1$, b) $\mu = 0$, $\sigma^2 = 0.5$, c) $\mu = 0$, $\sigma^2 = 1.0$, Comparison of estimation error for HPF using noisy input with d) $\mu = 0$, $\sigma^2 = 0.1$, e) $\mu = 0$, $\sigma^2 = 0.5$, f) $\mu = 0$, $\sigma^2 = 1.0$.

3.5 Conclusions

In this chapter, output voltage of RC LPF and HPF has been estimated using EKF and UKF methods. Results show that though EKF method provide better estimation as compared to LMS method, But UKF methods results are better than EKF method due to smaller linearization error of UKF method. Also, the SNR value of UKF method is better than EKF method. UKF method presents smaller RMSE as compared to EKF method as UKF method is accurate to the third order for any nonlinearity.

Chapter 4

State Estimation of Single-Phase Rectifier Circuit

This chapter ¹ presents the implementation of different versions of KF algorithm on single-phase rectifier circuit for state estimation. For this, the nonlinear system dynamics have been modeled using differential equations. To obtain the state space model of the circuit, Kirchhoff's laws have been used.

In the previous chapter, EKF and UKF methods have been implemented on RC circuits. In this chapter, EKF, IEKF (Chapter 1.4.3) and UKF methods have been implemented on diode circuit.

The Major contributions of the proposed work are :- (i) real-time state estimation of the single-phase rectifier circuit using different versions of KF has been computed. (ii) state-space model of dynamic single-phase rectifier circuit has been obtained using KVL and KCL (iii) input voltage is modeled as the zero mean white noise. (iv) The output results of different versions of KF algorithm have been compared with each other. Simulation results validate the performance of the proposed method.

¹The result of this chapter is based on the following research papers (i) Amit Kumar Gautam and Sudipta Majumdar, "Parameter estimation of diode circuit using extended Kalman filter," World Academy of Science, Engineering and Technology International Journal of Electronics and Communication Engineering, ISSN no. 1307- 6892, vol. 12, no. 9, pp. 605-610, 2018, (ii) Amit Kumar Gautam and Sudipta Majumdar, "Iterated extended Kalman filter based state estimation of diode circuit," in Journal of Physics: Conference Series 2070 (2021) 012092, pp. 1-10, 2021, (iii) Amit Kumar Gautam and Sudipta Majumdar, "State estimation of single-phase rectifier based load using unscented Kalman filter," in 2nd IEEE International Conference on Power Electronics, Intelligent Control and Energy Systems (ICPEICES-2018), pp. 1172-1177, 2018.

Single-phase rectifier circuit has been used in various applications including voltage clamper for ac-dc power conversion [80], as pulse width modulation rectifier [81] and railway electrical traction system [82].

The state space modeling of single-phase full wave rectifier (FWR) circuit has been derived in section 4.1. Section 4.2 presents implementation of EKF method to single-phase FWR circuit. Simulation results of single-phase FWR circuit using EKF, IEKF and UKF methods are presented in sections 4.3, 4.4 and 4.5 respectively.

4.1 State Space Model

Single-phase FWR circuit is shown in Figure 4.1. $v_i(t)$ is the input voltage. The circuit consists of inductor L_s and resistor R_s . The capacitor C is used at the output, which is in parallel with the load resistance R_L . We assumed that D_1 to D_4 are identical diodes with voltage drop equal to v_D . $i_D(t)$ and $v_c(t)$ are the diode current and capacitor voltage respectively. Using the KVL and KCL, we have

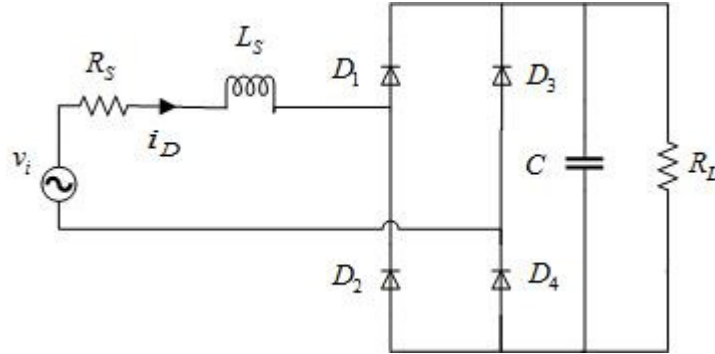


Figure 4.1: Circuit diagram of single-phase FWR.

$$C \frac{d}{dt} v_c(t) + \frac{v_c(t)}{R_L} = i_D(t) \quad (4.1)$$

$$v_i(t) = R_s i_D(t) + L_s \frac{d}{dt} i_D(t) + 2v_D + v_c(t) \quad (4.2)$$

where $i_D(t) = I_0(e^{v_D/V_T} - 1)$. Representing (4.1) and (4.2) in terms of state equations, we have

$$\frac{d}{dt}v_c(t) = -\frac{1}{R_L C}v_c(t) + \frac{1}{C}i_D(t) \quad (4.3)$$

$$\frac{d}{dt}i_D(t) = -\frac{1}{L_S}v_c(t) - \frac{(R_S + 2V_T/I_0)}{L_S}i_D(t) + \frac{V_T}{L_S I_0^2}i_D^2(t) - \frac{1}{L_S}v_i(t) \quad (4.4)$$

Here, V_T and I_0 denote the thermal voltage and reverse saturation current of diode respectively. Representing (4.3) and (4.4) in state space form as :-

$$\frac{d}{dt}\mathbf{x} = \mathbf{F}\mathbf{x} + \mathbf{B}\mathbf{u} \quad (4.5)$$

where \mathbf{x} is the state vector consisting of two states $v_c(t)$ and $i_D(t)$ respectively. The state transition matrix \mathbf{F} and input vector \mathbf{B} are :-

$$\mathbf{F} = \begin{bmatrix} -\frac{1}{R_L C} & \frac{1}{C} \\ -\frac{1}{L_S} & -\frac{(R_S + 2V_T/I_0)}{L_S} + \frac{2V_T^2}{I_0} \end{bmatrix}, \mathbf{B} = \begin{bmatrix} 0 & \frac{1}{L_S} \end{bmatrix}^T \quad (4.6)$$

The state space model is given as :-

$$\frac{d}{dt} \begin{bmatrix} v_c(t) \\ i_D(t) \end{bmatrix} = \begin{bmatrix} -\frac{1}{R_L C} & \frac{1}{C} \\ -\frac{1}{L_S} & -\frac{(R_S + 2V_T/I_0)}{L_S} + \frac{2V_T^2}{I_0} \end{bmatrix} \begin{bmatrix} v_c(t) \\ i_D(t) \end{bmatrix} + \begin{bmatrix} 0 \\ \frac{1}{L_S} \end{bmatrix} v_i(t) \quad (4.7)$$

The measurement model is :-

$$\mathbf{z} = \mathbf{H}\mathbf{x} \quad (4.8)$$

where

$$\mathbf{H} = \begin{bmatrix} 1 & 0 \\ 0 & 1 \end{bmatrix} \quad (4.9)$$

4.2 Implementation of EKF algorithm

The discrete form of equation (4.7) can be obtained using Euler-Maruyama method. Substituting $t = kT_s$. Where $k = 1, 2, 3, \dots$ and T_s is sampling time. In general, the

Table 4.1: Comparison of capacitor voltage (v_C) estimation using different methods.

Input signal	Parameter	LMS method	EKF method
Noiseless	SNR(dB)	0.42	1.07
input	RMSE	1.24	0.86
Noisy input signal with mean 0 and variance 0.1	SNR(dB)	0.40	1.01
	RMSE	1.50	0.96
Noisy input signal with mean 0 and variance 0.5	SNR(dB)	0.35	1.00
	RMSE	2.10	1.01
Noisy input signal with mean 0 and variance 1.0	SNR(dB)	0.26	0.90
	RMSE	2.15	1.02
Noisy input signal with mean 0 and variance 2.0	SNR(dB)	0.10	0.76
	RMSE	3.17	2.42

discrete-time state-space equations can be written as :-

$$\mathbf{x}_{k+1} = \mathbf{F}_k \mathbf{x}_k + \mathbf{B}_k \mathbf{u}_k + \mathbf{G}_k \mathbf{w}_k \quad (4.10)$$

$$\mathbf{z}_k = \mathbf{H}_k \mathbf{x}_k + \mathbf{C}_k \mathbf{u}_k + \mathbf{D}_k \mathbf{v}_k \quad (4.11)$$

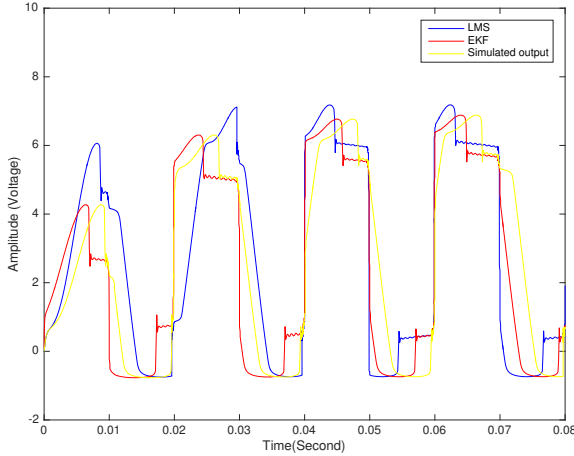
The matrices \mathbf{F}_k , \mathbf{B}_k and \mathbf{H}_k are :-

$$\mathbf{F}_k = \begin{bmatrix} 1 - \frac{T_s}{R_L C} & \frac{T_s}{C} \\ -\frac{T_s}{L_S} & 1 - \frac{T_s(R_S + 2V_T/I_0)}{L_S} + \frac{2V_T^2 T_s}{I_0} \end{bmatrix}, \mathbf{B}_k = \begin{bmatrix} 0 \\ \frac{T_s}{L_S} \end{bmatrix}, \mathbf{H}_k = \begin{bmatrix} 1 & 0 \\ 0 & 1 \end{bmatrix}^T$$

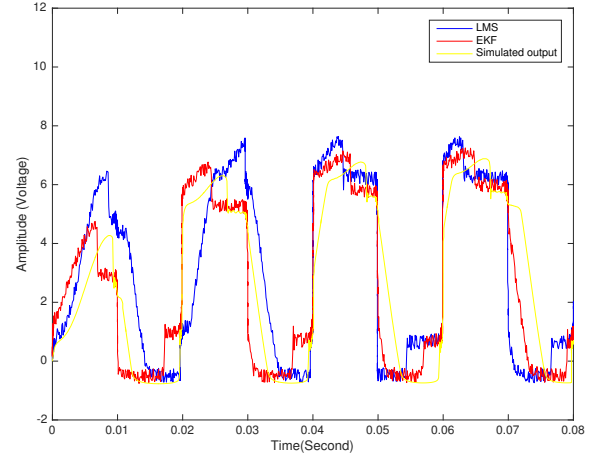
$$\mathbf{C}_k = 0, \mathbf{D}_k = 0. \quad (4.12)$$

4.3 Simulation Results using EKF Method

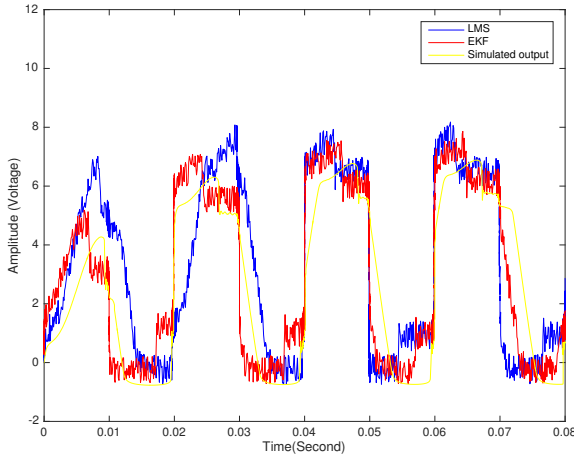
The states of single-phase rectifier circuit have been estimated in MATLAB using EKF method and compared with LMS method. The sinusoidal input of 10 volts and 50 KHz frequency has been used. The system noise and measurement noise are white Gaussian noise of zero mean with 0.5 and 0.1 variances respectively. The PSPICE simulated values have been considered as the actual value. Simulations have been performed using noiseless input signal and noisy input signal respectively. Figure 4.2 to 4.3 show the comparison of estimated capacitor voltage and diode current using EKF and LMS methods with PSPICE simulations. Table 4.1 and Table 4.2 compare the RMSE and SNR(dB) of EKF and LMS methods for capacitor voltage and diode current respectively.



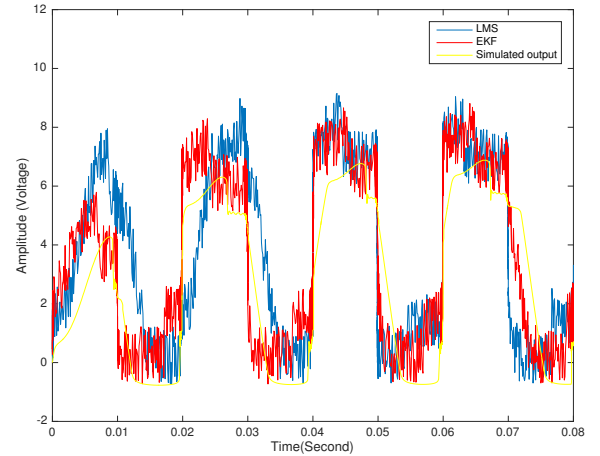
(a)



(b)



(c)

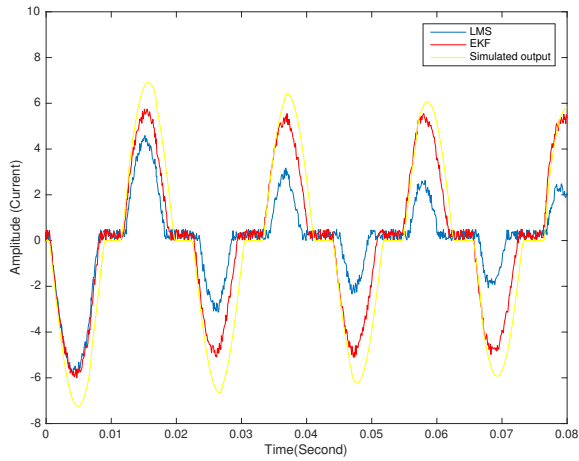


(d)

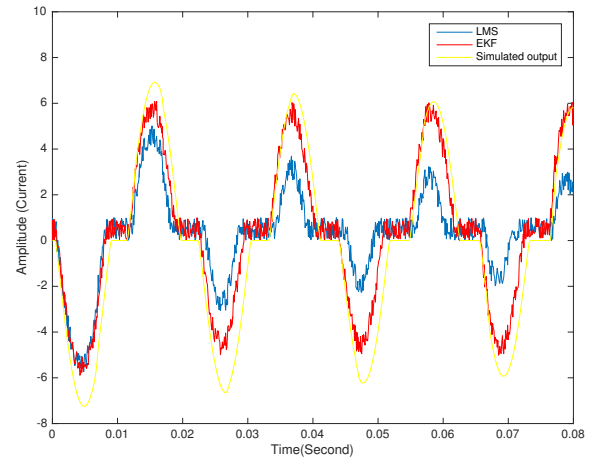
Figure 4.2: Estimated voltage using EKF and LMS methods for noisy signal with a) $\mu = 0$, $\sigma^2 = 0.1$, b) $\mu = 0$, $\sigma^2 = 0.5$, c) $\mu = 0$, $\sigma^2 = 1.0$, d) $\mu = 0$, $\sigma^2 = 2.0$.

Table 4.2: Comparison of diode current (i_D) estimation using different methods.

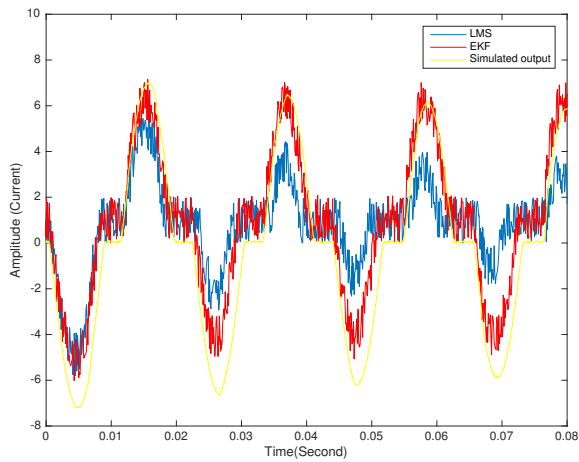
Input signal	Parameter	LMS method	EKF method
Noiseless input	SNR(dB)	0.258	1.290
	RMSE	0.69	0.3359
Noisy input signal with mean 0 and variance 0.1	SNR(dB)	0.20	1.05
	RMSE	1.40	0.66
Noisy input signal with mean 0 and variance 0.5	SNR(dB)	0.16	1.01
	RMSE	2.45	1.56
Noisy input signal with mean 0 and variance 1.0	SNR(dB)	0.10	1.0
	RMSE	2.55	1.82
Noisy input signal with mean 0 and variance 2.0	SNR(dB)	0.054	0.87
	RMSE	2.95	2.56



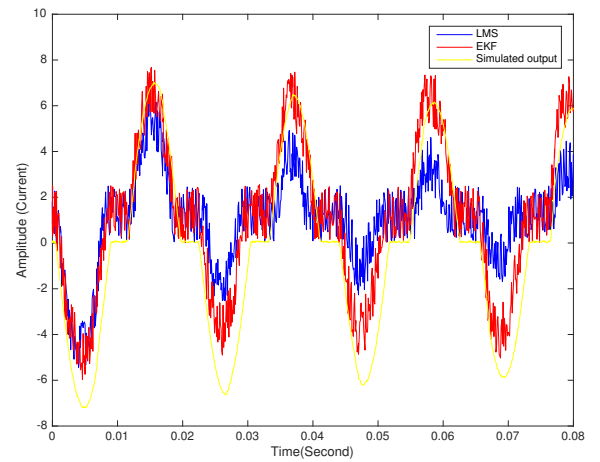
(a)



(b)



(c)



(d)

Figure 4.3: Estimated current using EKF and LMS methods for noisy signal with a) $\mu = 0$, $\sigma^2 = 0.1$, b) $\mu = 0$, $\sigma^2 = 0.5$, c) $\mu = 0$, $\sigma^2 = 1.0$, d) $\mu = 0$, $\sigma^2 = 2.0$.

Table 4.3: Comparison of capacitor voltage (v_C) estimation using different methods.

Input signal	Parameter	IEKF method	EKF method
Noiseless input	SNR(dB)	1.42	1.07
	RMSE	0.24	0.86
Noisy input signal with mean 0 and variance 0.1	SNR(dB)	1.39	1.01
	RMSE	0.50	0.96
Noisy input signal with mean 0 and variance 0.5	SNR(dB)	1.15	1.00
	RMSE	0.89	1.01
Noisy input signal with mean 0 and variance 1.0	SNR(dB)	1.06	0.90
	RMSE	1.10	1.57

4.4 Simulation Results using IEKF Method

The simulations have been performed in MATLAB software. The capacitor voltage and diode current have been estimated using IEKF method and compared with EKF method. A sinusoidal input of 10 volts and frequency 50 Hz has been used at input for simulation purpose. The system and measurement noise are white Gaussian noise with zero mean and variance 0.5 and 0.01 respectively. The thermal voltage (V_T) and reverse saturation current (I_0) are 0.025 volts and 10 amperes respectively. The diode model used for PSPICE simulation is *D1N4002*. The circuit component values are: $R_L = 750$, $R_S = 17.5$, $L_S = 91.9mH$ and $C = 100\mu F$. Figure 4.4 to Figure 4.5 show the comparison of estimated capacitor voltage and diode current using IEKF method with EKF method and PSPICE simulated values. The PSPICE simulated values have been considered as the actual value. The RMSE and SNR(dB) values have been used to evaluate the performance of proposed method. Table 4.3 and 4.4 present the comparison of the estimated parameters using IEKF method with EKF method and PSPICE simulated values. The estimated currents are identically mapped to the transients over the first half period, whereas deviations are noted between the estimated and actual values in succeeding half periods due to change in initial value of the capacitor voltage.

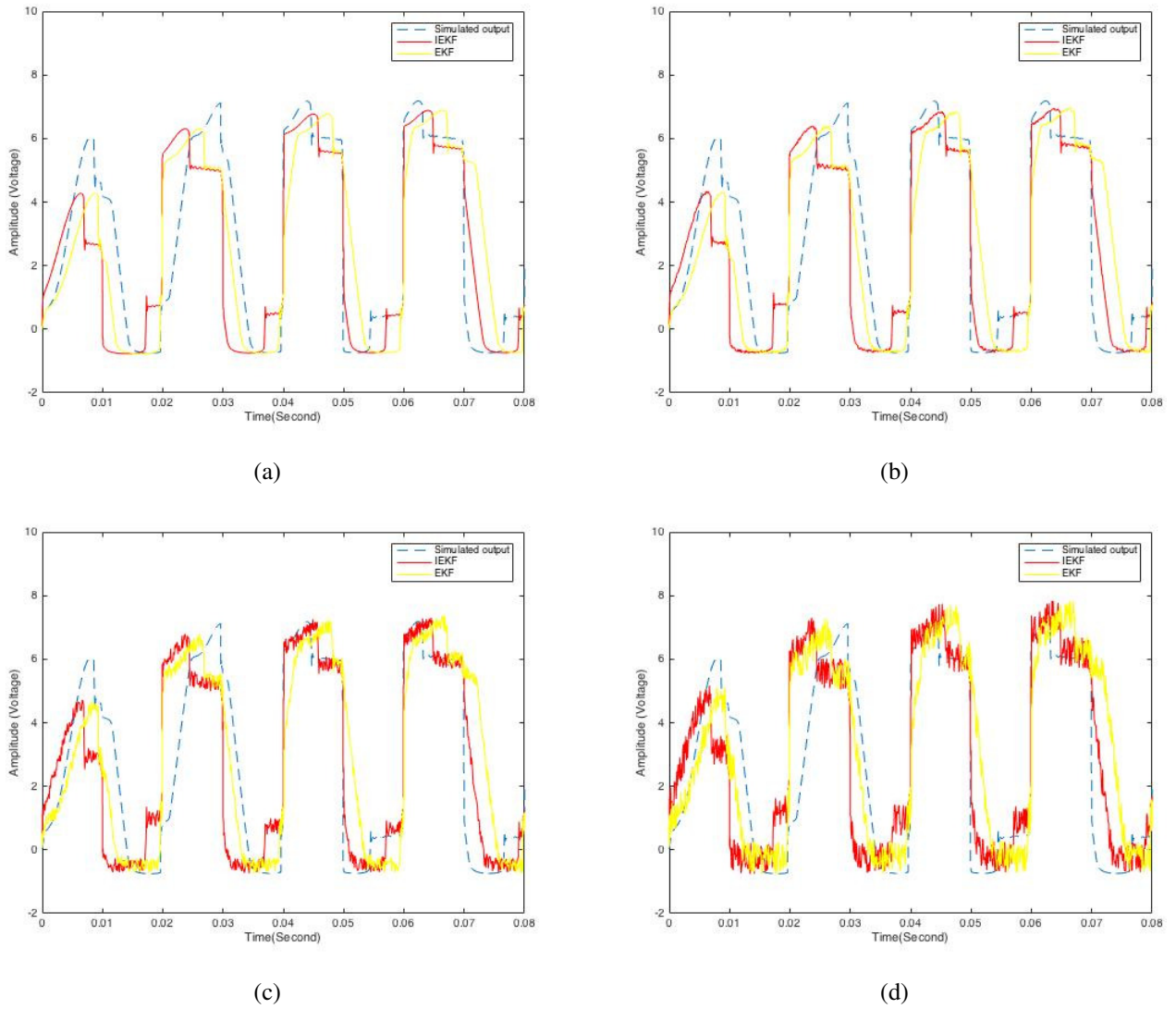
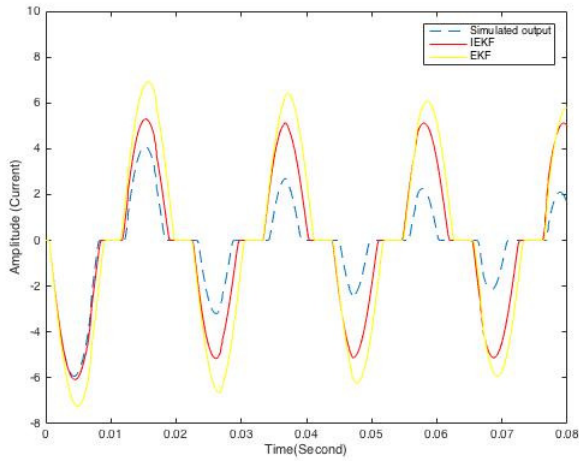


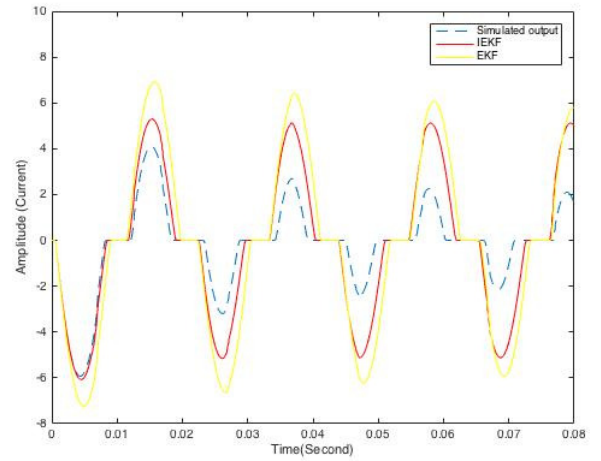
Figure 4.4: Estimated voltage using EKF and IEKF methods for a) noiseless input signal, b) signal with $\mu = 0$, $\sigma^2 = 0.1$, c) signal with $\mu = 0$, $\sigma^2 = 0.5$, d) signal with $\mu = 0$, $\sigma^2 = 1.0$.

Table 4.4: Comparison of diode current (i_D) estimation using different methods.

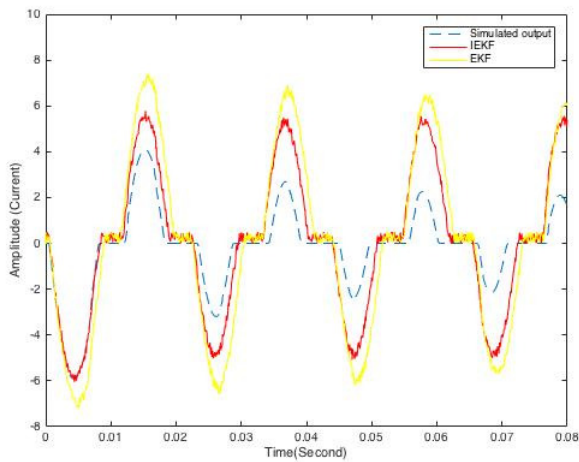
Input signal	Parameter	IEKF method	EKF method
Noiseless input	SNR(dB)	1.55	1.290
	RMSE	0.19	0.336
Noisy input signal with mean 0 and variance 0.1	SNR(dB)	1.20	1.05
	RMSE	0.40	0.66
Noisy input signal with mean 0 and variance 0.5	SNR(dB)	1.16	1.01
	RMSE	0.50	1.56
Noisy input signal with mean 0 and variance 1.0	SNR(dB)	1.10	1.0
	RMSE	0.53	1.82



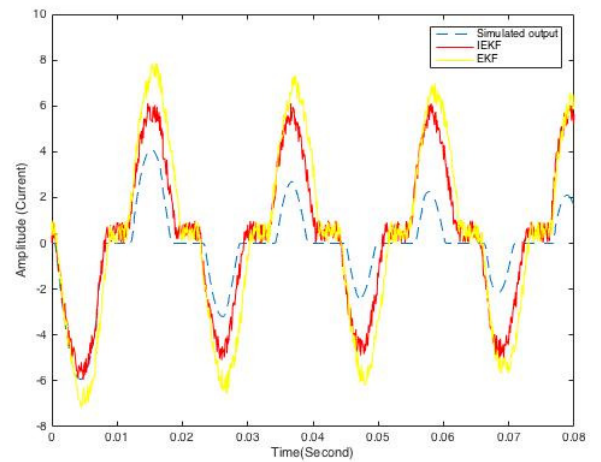
(a)



(b)



(c)



(d)

Figure 4.5: Estimated current using EKF and IEKF methods for a) noiseless input signal, b) signal with $\mu = 0$, $\sigma^2 = 0.1$, c) signal with $\mu = 0$, $\sigma^2 = 0.5$, d) signal with $\mu = 0$, $\sigma^2 = 1.0$.

Table 4.5: Comparison of capacitor voltage (v_C) estimation using different methods.

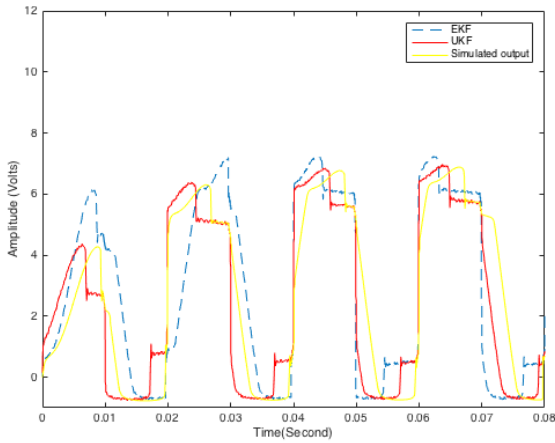
Input signal	Parameter	UKF method	EKF method
Noiseless input	SNR(dB)	2.42	1.07
	RMSE	0.40	0.86
Noisy input signal with mean 0 and variance 0.1	SNR(dB)	2.40	1.01
	RMSE	0.50	0.96
Noisy input signal with mean 0 and variance 0.5	SNR(dB)	1.35	1.00
	RMSE	0.70	1.01
Noisy input signal with mean 0 and variance 1.0	SNR(dB)	1.26	0.90
	RMSE	0.75	1.02

4.5 Simulation Results using UKF

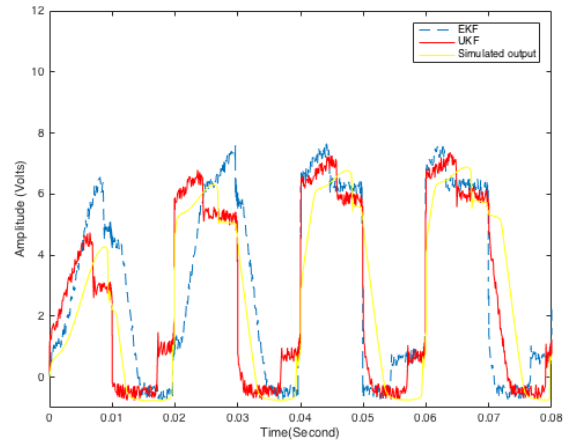
The capacitor voltage and diode current of single-phase rectifier circuit have been estimated for sinusoidal input voltage. The applied sinusoidal input contains maximum amplitude of 10 V and frequency 50 KHz. The white Gaussian noise of zero mean and different variances have been used for estimation purpose. The system noise and measurement noise are white Gaussian noise of zero mean with variance 0.5 and 0.01 respectively. The parameters used for simulations are $R_L = 750$, $R_S = 17.5$, $L_S = 91.9mH$ and $C = 100\mu F$. $D1N4002$ diode model of PSPICE has been used for simulations. The PSPICE simulated values have been considered as the actual value. The capacitor voltage v_C of single-phase rectifier circuit has been estimated using UKF and EKF methods. Figure 4.6 (a) to Figure 4.6 (c) show the capacitor voltage estimation for different noise values. Also, the estimation of diode current i_D using UKF and EKF methods are shown in Figure 4.6 (d) - Figure 4.6 (f). Table 4.5 and Table 4.6 show the comparison of SNR (dB) value and RMSE for UKF and EKF methods.

4.6 Conclusions

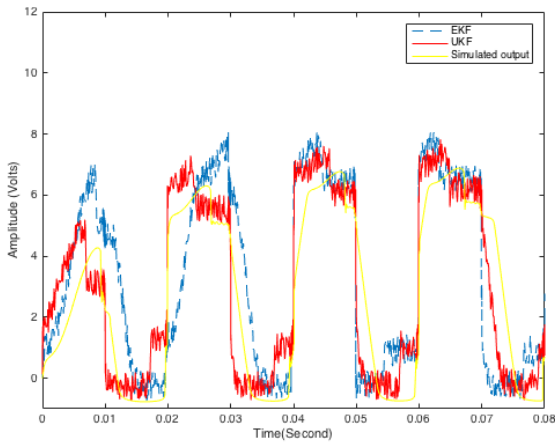
The estimation of parameters of a single-phase rectifier using UKF method is presented in this chapter and compared with LMS, EKF and IEKF methods. Simulation results show the better closeness of estimated values using UKF with PSPICE simulated values as compared to the LMS, EKF and IEKF methods. The SNR value of UKF method is better than LMS, EKF and IEKF methods. Also, RMSE values using UKF



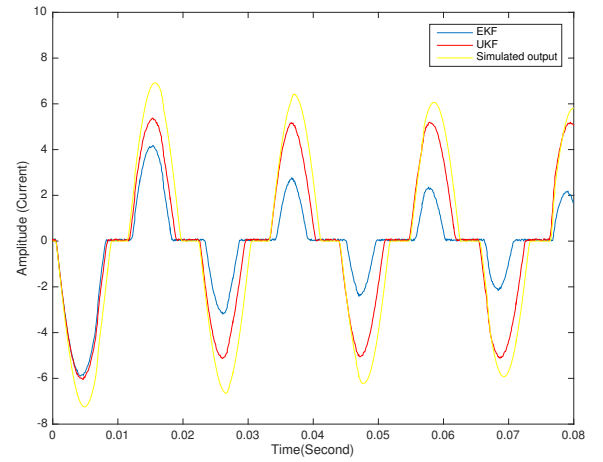
(a) Signal with $\mu = 0, \sigma^2 = 0.1$.



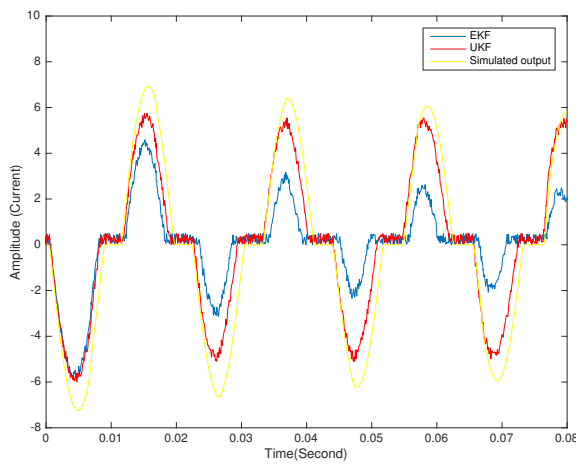
(b) Signal with $\mu = 0, \sigma^2 = 0.5$.



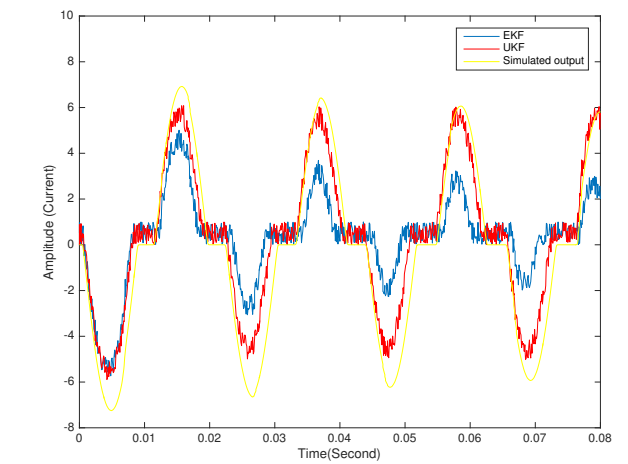
(c) Signal with $\mu = 0, \sigma^2 = 1.0$.



(d) Signal with $\mu = 0, \sigma^2 = 0.1$.



(e) Signal with $\mu = 0, \sigma^2 = 0.5$.



(f) Signal with $\mu = 0, \sigma^2 = 1.0$.

Figure 4.6: Comparison of capacitor voltage and diode current estimation using UKF and EKF methods.

Table 4.6: Comparison of diode current (i_D) estimation using different methods.

Input signal	Parameter	UKF method	EKF method
Noiseless	SNR(dB)	2.50	1.290
input	RMSE	0.10	0.336
Noisy input signal with mean 0 and variance 0.1	SNR(dB)	2.20	1.05
	RMSE	0.40	0.66
Noisy input signal with mean 0 and variance 0.5	SNR(dB)	2.16	1.01
	RMSE	0.45	1.56
Noisy input signal with mean 0 and variance 1.0	SNR(dB)	2.10	1.0
	RMSE	0.55	1.82

method are smaller than LMS, EKF and IEKF methods due to small linearization error of UKF method. Simulation results demonstrate the superiority of the UKF method.

Chapter 5

State Estimation of Transistor Circuit

This chapter ¹ presents the implementation of different versions of KF algorithm on the following circuits for state and parameter estimation:-

(i) CE-based BJT circuit.

(ii) BJT-based DA circuit.

For this, the nonlinear system dynamics have been modeled using Kronecker product. To obtain the state-space model of the circuit, Gummel Poon model, Ebers-Moll model of the BJTs and Kirchhoff's laws have been used.

In the previous chapter, various state estimation filtering has been implemented on diode circuit, whereas in this chapter, these filtering are implemented on BJT circuit. The use of Ebers Moll model and Gummel Poon model to obtain the state space model increases the complexity as compared to the diode circuit. The use of Kronecker product reduces the mathematical complexity of the BJT circuit.

Major contributions of the proposed work are :- (i) real-time state estimation of the analog transistor circuits using different versions of KF has been computed, (ii) state-space model of dynamic analog circuits has been obtained using Ebers-Moll Model and Gummel Poon model with KVL and KCL, (iii) input voltage is modeled as the zero mean white noise, (iv) The output results of different versions of KF algorithm have

¹The result of this chapter is based on the following research papers (i) Amit Kumar Gautam and Sudipta Majumdar, "State estimation of common emitter amplifier using iterated extended Kalman filters," International Journal of Innovative Technology and Exploring Engineering, ISSN no. 2278-3075, vol. 8, no. 9, pp. 1784-1789, 2019, (ii) Amit Kumar Gautam and Sudipta Majumdar, "Kronecker product based modeling of Darlington amplifier and state estimation using unscented Kalman filter," International Journal of Electronics Letters, ISSN no. 2168-1732, 2022.

been compared with each other. Simulation results validate the performance of the proposed method.

CE BJT is an important IC which is useful in different electronic circuits and chip designing applications such as two cascaded common base and CE devices [83], wideband resistive feedback low noise amplifier (LNA) [84], trans impedance amplifier circuit [85], frequency reconfigurable millimeter wave power amplifier (PA) [86], class-F PA [87]. Also, it is useful in dual-vector phase rotator (DVR) to drive a Doherty amplifier in beamformer [88]. Monolithic microwave integrated circuit chips also use the CE BJT circuit [89] and BJT-based trans impedance amplifier is used in optical network link [90].

Darlington amplifier has been used in various applications including broadband high data rate communication systems. The three-stage Darlington feedback amplifier presents better stability than single stage Darlington feedback amplifier. DA circuit has been used in various broadband circuits. Also, it has high speed applications. Beside these, it is also used in low noise amplifier [91], mixer [92], power amplifier [93], distributed amplifier and active baluns [94]. The DA is also used as a benchmark for verification of compact models at mm-wave frequencies [95]. Shukla and Pandey [96] used DA together with Sziklai to model two stage small signal amplifier. Mojab and Mazumder [97] proposed optical Darlington transistor for high power applications. Weng et al. [98] proposed broadband DA using heterojunction bipolar transistor for high speed data communications. Various designs have been proposed for DA. Lee et al. [99] proposed the design of ultra wideband DA. Weng et al. [100] proposed design of DA for microwave broadband applications.

The Kirchhoff's law and the Ebers-Moll model are applied for state modeling of the CE BJT circuit in section 5.1.1. Section 5.1.2 includes the implementation of EKF and IEKF methods to CE amplifier circuit. Section 5.1.3 presents simulation results. Section 5.2.1 formulates state modeling of DA circuit using KCL and Gummel-Poon model. Section 5.2.2 presents implementation of UKF with Kronecker product to DA circuit. Section 5.2.3 presents simulation results.

5.1 State Estimation of CE Amplifier Circuit

5.1.1 State Space Model

Figure 5.1 shows the CE BJT amplifier. It consists of resistors R_C , R_E and R_1 . C_B is mainly used to suppress dc voltage. It also consists of collector capacitor C_C and emitter capacitor C_E . Input u is applied to the base terminal and output v_0 is taken across the load resistor R_L . The dynamic equations for this circuit are obtained using

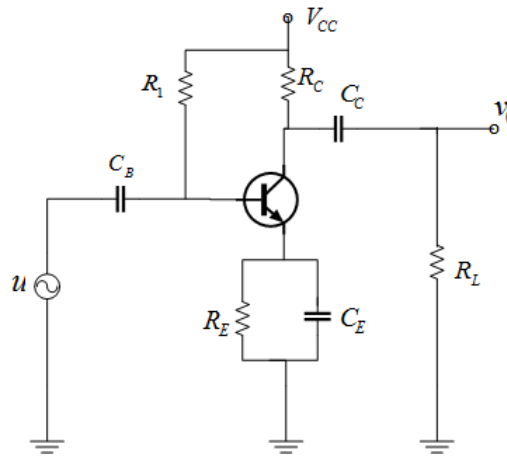


Figure 5.1: Diagram of CE amplifier circuit.

KCL as :-

$$I_E = C_E \frac{d}{dt} v_E + \frac{v_E}{R_E} \quad (5.1)$$

$$I_B = C_B \frac{du}{dt} - C_B \frac{dv_B}{dt} + \frac{V_{CC}}{R_1} - \frac{v_B}{R_1} \quad (5.2)$$

$$C_C \frac{d}{dt} (v_C) - C_C \frac{d}{dt} (v_0) = \frac{v_0}{R_L} \quad (5.3)$$

$$\frac{V_{CC}}{R_C} - \frac{v_C}{R_C} = I_C + \frac{v_0}{R_L} \quad (5.4)$$

where state variables are namely v_E , v_B , v_C and v_0 . In order to obtain the state space equations, the Ebers-Moll model [101] is used. Using Taylor's series expansion, (2.4)

and (2.5) can be expanded as follows :-

$$I_E = K_1 v_E + K_2 v_B + K_3 v_C + K_4 v_E v_E + K_5 v_B v_B + K_6 v_C v_C + K_7 v_B v_E + K_8 v_B v_C \quad (5.5)$$

$$I_C = K_9 v_E + K_{10} v_B + K_{11} v_C + K_{12} v_E v_E + K_{13} v_B v_B + K_{14} v_C v_C + K_{15} v_B v_E + K_{16} v_B v_C \quad (5.6)$$

$$I_B = (K_1 - K_9) v_E + (K_2 - K_{10}) v_B + (K_3 - K_{11}) v_C + (K_4 - K_{12}) v_E v_E + (K_5 - K_{13}) v_B v_B \\ + (K_6 - K_{14}) v_C v_C + (K_7 - K_{15}) v_B v_E + (K_8 - K_{16}) v_B v_C \quad (5.7)$$

where

$$\begin{aligned} K_1 &= \frac{I_{ES}}{V_T}, & K_2 &= -\frac{I_{ES} - \alpha_R I_{CS}}{V_T}, & K_3 &= -\frac{\alpha_R I_{CS}}{V_T}, & K_4 &= -\frac{I_{ES}}{2V_T^2}, \\ K_5 &= -\frac{I_{ES} - \alpha_R I_{CS}}{2V_T^2}, & K_6 &= \frac{\alpha_R I_{CS}}{2V_T^2}, & K_7 &= \frac{I_{ES}}{V_T^2}, & K_8 &= -\frac{\alpha_R I_{CS}}{V_T^2}, \\ K_9 &= \frac{-\alpha_F I_{ES}}{V_T}, & K_{10} &= \frac{\alpha_F I_{ES} - I_{CS}}{V_T}, & K_{11} &= \frac{I_{CS}}{V_T}, & K_{12} &= \frac{\alpha_F I_{ES}}{2V_T^2}, \\ K_{13} &= \frac{\alpha_F I_{ES} - I_{CS}}{2V_T^2}, & K_{14} &= \frac{-I_{CS}}{2V_T^2}, & K_{15} &= \frac{-\alpha_F I_{ES}}{V_T}, & K_{16} &= \frac{I_{CS}}{V_T}. \end{aligned}$$

Substituting (5.5)-(5.7) in (5.1)-(5.4), we get :-

$$\frac{dv_E}{dt} = K_{17} v_E + K_{18} v_B + K_{19} v_C + K_{20} v_E v_E + K_{21} v_B v_B + K_{22} v_C v_C + K_{23} v_B v_E + K_{24} v_B v_C \quad (5.8)$$

$$\frac{dv_B}{dt} = K_{25} v_E + K_{26} v_B + K_{27} v_C + K_{28} v_E v_E + K_{29} v_B v_B + K_{30} v_C v_C + K_{31} v_B v_E + K_{32} v_B v_C + u' \\ + K_{33} V_{CC} \quad (5.9)$$

$$\frac{dv_C}{dt} = K_{34} v_E + K_{35} v_B + K_{36} v_C + K_{37} v_0 + K_{38} v_E v_E + K_{39} v_B v_B + K_{40} v_C v_C + K_{41} v_B v_E + K_{42} v_B v_C \quad (5.10)$$

$$\frac{dv_0}{dt} = K_{34} v_E + K_{35} v_B + K_{36} v_C + K_{43} v_0 + K_{38} v_E v_E + K_{39} v_B v_B + K_{40} v_C v_C + K_{41} v_B v_E + K_{42} v_B v_C \quad (5.11)$$

where $u' = \frac{d}{dt} u$.

$$\begin{aligned} K_{17} &= \frac{1}{C_E} \left(K_1 - \frac{1}{R_E} \right), & K_{18} &= \frac{K_2}{C_E}, & K_{19} &= \frac{K_3}{C_E}, & K_{20} &= \frac{K_4}{C_E}, \\ K_{21} &= \frac{K_5}{C_E}, & K_{22} &= \frac{K_6}{C_E}, & K_{23} &= \frac{K_7}{C_E}, & K_{24} &= \frac{K_8}{C_E}, \\ K_{25} &= \frac{K_9 - K_1}{C_B}, & K_{26} &= \frac{1}{C_B} \left(K_{10} - K_2 + \frac{1}{R_1} \right), & K_{27} &= \frac{K_{11} - K_3}{C_B}, & K_{28} &= \frac{K_{12} - K_4}{C_B}, \\ K_{29} &= \frac{K_{13} - K_5}{C_B}, & K_{30} &= \frac{K_{14} - K_6}{C_B}, & K_{31} &= \frac{K_{15} - K_7}{C_B}, & K_{32} &= \frac{K_{16} - K_8}{C_B}, \\ K_{33} &= \frac{1}{C_B R_1}, & K_{34} &= \frac{-\alpha_F R_L R_C}{C_E Z_E} \left(K_1 - \frac{1}{R_E} \right), & K_{35} &= \frac{-\alpha_F R_L R_C K_2}{C_E Z_E}, & K_{36} &= \frac{-\alpha_F R_L R_C K_3}{C_E Z_E}, \\ K_{37} &= \frac{R_C}{R_L (R_L + R_C)}, & K_{38} &= \frac{-\alpha_F R_L R_C K_4}{C_E Z_E}, & K_{39} &= \frac{-\alpha_F R_L R_C K_5}{C_E Z_E}, & K_{40} &= \frac{-\alpha_F R_L R_C K_6}{C_E Z_E}, \\ K_{41} &= \frac{-\alpha_F R_L R_C K_7}{C_E Z_E}, & K_{42} &= \frac{-\alpha_F R_L R_C K_8}{C_E Z_E}, & K_{43} &= \frac{1}{C_C (R_L + R_C)}. \end{aligned}$$

5.1.2 Implementation of EKF and IEKF

The discrete time state space equations can be written as :-

$$\mathbf{x}_{k+1} = \mathbf{F}_k \mathbf{x}_k + \mathbf{B}_k \mathbf{u}_k + \mathbf{G}_k \mathbf{w}_k \quad (5.12)$$

$$\mathbf{z}_k = \mathbf{H}_k \mathbf{x}_k + \mathbf{C}_k \mathbf{u}_k + \mathbf{D}_k \mathbf{v}_k \quad (5.13)$$

where

$$\mathbf{x}_k = \begin{bmatrix} v_E(k) & v_B(k) & v_C(k) & v_0(k) \end{bmatrix}^T \quad (5.14)$$

$$\mathbf{B}_k = \begin{bmatrix} 0 & 1 & 0 & 0 \end{bmatrix}^T, \mathbf{C}_k = 0, \mathbf{D}_k = 0 \quad (5.15)$$

$$\mathbf{F}_k = \frac{d}{dx} \boldsymbol{\varphi}(\mathbf{x}_k, \mathbf{u}_k) = \begin{bmatrix} F_{11} & F_{12} & F_{13} & F_{14} \\ F_{21} & F_{22} & F_{23} & F_{24} \\ F_{31} & F_{32} & F_{33} & F_{34} \\ F_{41} & F_{42} & F_{43} & F_{44} \end{bmatrix} \quad (5.16)$$

where

$$F_{11} = 1 + K_{17} + K_{20}v_E(k-1),$$

$$F_{12} = K_{18} + K_{21}v_B(k-1) + K_{23}v_E(k-1),$$

$$F_{13} = K_{19} + K_{22}v_C(k-1) + K_{24}v_B(k-1),$$

$$F_{14} = 0,$$

$$F_{21} = K_{25} + K_{28}v_E(k-1),$$

$$F_{22} = 1 + K_{26} + K_{29}v_B(k-1) + K_{31}v_E(k-1),$$

$$F_{23} = K_{27} + K_{30}v_C(k-1) + K_{32}v_B(k-1),$$

$$F_{24} = 0,$$

$$F_{31} = K_{34} + K_{38}v_E(k-1),$$

$$F_{32} = K_{35} + K_{39}v_B(k-1) + K_{41}v_E(k-1),$$

$$F_{33} = 1 + K_{36} + K_{40}v_C(k-1) + K_{42}v_B(k-1),$$

$$F_{34} = K_{37},$$

$$F_{41} = K_{34} + K_{38}v_E(k-1),$$

$$F_{42} = K_{35} + K_{39}v_B(k-1) + K_{41}v_E(k-1),$$

$$F_{43} = K_{36} + K_{40}v_C(k-1) + K_{42}v_B(k-1),$$

$$F_{44} = 1 + K_{43}.$$

The state space model is :-

$$\begin{bmatrix} v_E(k) \\ v_B(k) \\ v_C(k) \\ v_0(k) \end{bmatrix} = \begin{bmatrix} F_{11} & F_{12} & F_{13} & F_{14} \\ F_{21} & F_{22} & F_{23} & F_{24} \\ F_{31} & F_{32} & F_{33} & F_{34} \\ F_{41} & F_{42} & F_{43} & F_{44} \end{bmatrix} \begin{bmatrix} v_E(k-1) \\ v_B(k-1) \\ v_C(k-1) \\ v_0(k-1) \end{bmatrix} + \begin{bmatrix} 0 \\ 1 \\ 0 \\ 0 \end{bmatrix} \mathbf{u}'(k-1) \quad (5.17)$$

The measurement model is :-

$$\mathbf{z}_k = \mathbf{H}_k \mathbf{x}_k \quad (5.18)$$

where

$$\mathbf{H}_k = \frac{d}{d\mathbf{x}} \mathbf{h}(\mathbf{x}_k, \mathbf{u}_k) = \begin{bmatrix} 0 & 0 & 0 & 1 \end{bmatrix} \quad (5.19)$$

The following steps have been used to implement EKF :-

1. **Initialization:** We used the following steps after initializing $\mathbf{C}_w, \mathbf{C}_v, \Sigma_0$ and \mathbf{x}_0 .
2. **State prediction:** Using (5.16), we computed \mathbf{F}_k . (1.14) is used to compute Σ_k .
3. **Measurement update:** To determine K_k, z_k , and Σ_k , \mathbf{H}_k is computed using (5.19).

To implement IEKF algorithm, firstly threshold value ε is set to a small value. Counter i is set to zero. Then, state \mathbf{x} is estimated. The counter i is increased by one. Then, until (1.25) is satisfied, K_k and state update are computed using (1.23) and (1.24) respectively. Finally, covariance error is calculated using (1.27).

5.1.3 Simulation Results

MATLAB software has been used to implement the equations of CE BJT circuit. The following circuit elements and parameter values are used for simulations :- $R_1 = 100K\Omega, R_C = 10K\Omega, R_E = 6K\Omega, R_L = 5K\Omega, C_B = 10\mu F, C_C = 10\mu F, C_E = 10\mu F, \alpha_F = 0.98, \alpha_R = 0.25, I_{ES} = 1 \times 10^{-15}, I_{CS} = 1 \times 10^{-13}, V_T = 0.026V, V_{CC} = 20V$.

Thus, two distinct scenarios: (i) estimation with noiseless input, and (ii) estimation with noisy input have been taken into account. Figure 5.2(a) shows the input sinusoidal wave with a frequency of 10 kHz and a sample step size of 0.1. Then, the output voltage of the CE BJT circuit was estimated with noisy inputs with different variances and zero-mean white Gaussian noise. The initial value of variances for process noise is 0.5 and initial value of standard deviation for measurement noise is 0.01. The SNR value for noisy inputs using EKF and IEKF methods is shown in Table 5.1. The RMS error for both approaches for noisy input is shown in Table 5.2. The estimated output for noiseless input using the IEKF and EKF methods is shown in Figure 5.2 (b). The estimated output for noisy input using the IEKF and EKF methods is shown in Figure 5.2 (c) and compared with simulated values.

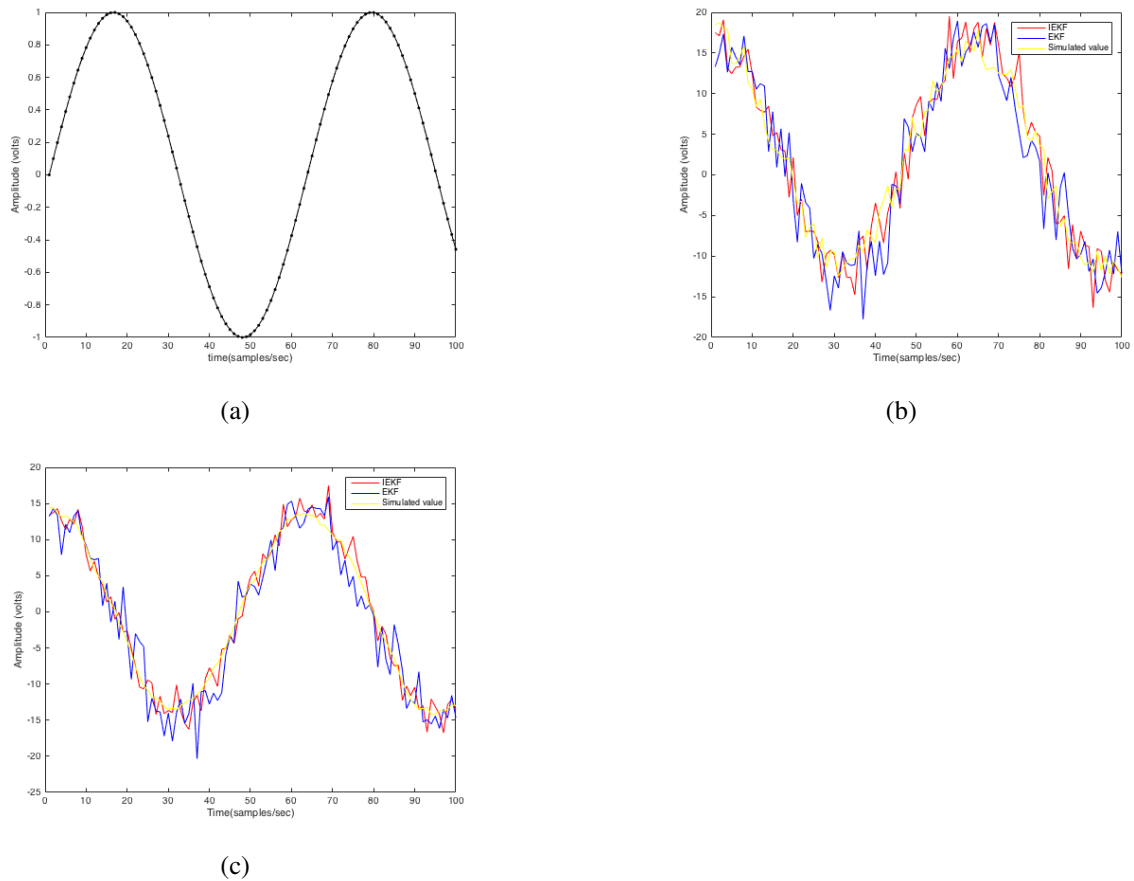


Figure 5.2: a) Input signal, b) Estimated output for the noiseless input using the IEKF and EKF methods with PSPICE simulation, c) Estimated output for the noisy input using the IEKF and EKF methods with PSPICE simulation.

Table 5.1: Comparison of SNR value using EKF and IEKF methods.

Noise Variance (σ^2)	SNR (dB) by EKF	SNR (dB) by IEKF
0.5	33.34	34.86
1	27.82	28.43
5	15.1763	15.68
10	8.51	9.56

Table 5.2: Comparison of parameters using EKF and IEKF methods.

Parameter	EKF	IEKF
Computation Time (Sec.)	4.04	2.28
RMSE(dB)	78.1	73.9

5.1.4 Conclusions

This chapter estimated the output voltage of BJT CE circuit using IEKF method and compares the performance of IEKF with EKF method. MATLAB simulations show that IEKF method gives better SNR as compared to EKF method, as IEKF method reduces the linearization error by considering the measurement during linearization of measurement model.

5.2 State Estimation of DA Circuit using Unscented Kalman Filter

5.2.1 State Space Model

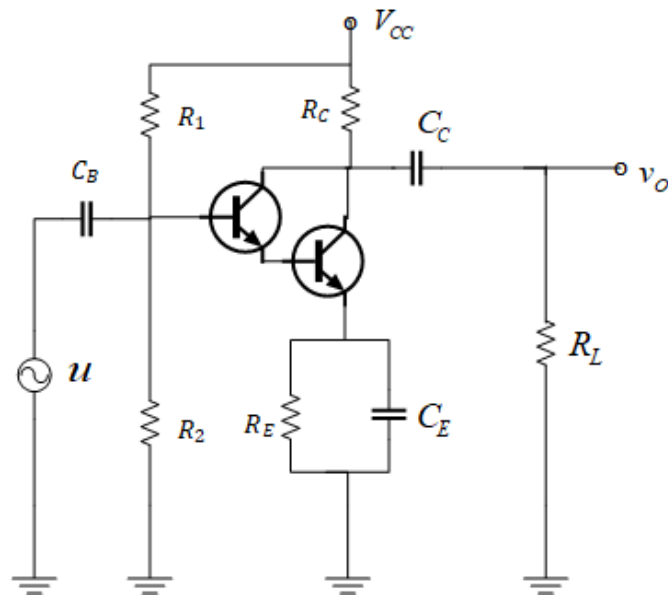


Figure 5.3: Circuit diagram of Darlington pair amplifier.

DA circuit is shown in Figure 5.3. Q_1 and Q_2 are the emitter follower and common emitter transistor respectively. This circuit consists of resistors R_C , R_E , R_1 , R_2 , R_L and capacitors C_B , C_C and C_E respectively. Sinusoidal input u has been applied to the circuit. v_0 denotes the output voltage of the amplifier circuit. Q_1 and Q_2 are identical transistors and operate at the same collector current namely I_C . β is the current gain of each transistor, and then overall gain β_T is calculated as :-

$$\beta_T = \beta^2 \quad (5.20)$$

The equations (5.21)-(5.25) represent the dynamic equations of the DA, which have

been obtained using KVL and KCL.

$$C_B \frac{d}{dt} (v_{B_1} - u) + I_{B_1} + \frac{v_{B_1}}{R_2} + \frac{v_{B_1} - V_{CC}}{R_1} = 0 \quad (5.21)$$

$$I_{E_2} = C_E \frac{d}{dt} v_{E_2} + \frac{v_{E_2}}{R_E} \quad (5.22)$$

$$C_C \frac{d}{dt} (v_C - v_0) = \frac{v_0}{R_L} \quad (5.23)$$

$$I_C = I_{C_1} + I_{C_2} + \frac{v_0}{R_L} \quad (5.24)$$

$$V_{CC} = R_C I_C + V_{C_2 E_2} + Z_E I_{E_2} \quad (5.25)$$

where I_{B_1} , I_{B_2} , I_{C_1} , I_{C_2} , I_{E_1} and I_{E_2} are the base, collector and emitter currents of Q_1 and Q_2 respectively. Z_E denotes the total impedance at the emitter terminal. The emitter voltages of Q_1 and Q_2 are v_{E_1} and v_{E_2} respectively. v_{B_1} , v_C and v_0 are the base voltage of Q_1 , collector voltage and output voltage respectively. The transistor is replaced by Gummel-Poon model. The Gummel-Poon equations are :-

$$I_{BF} = \frac{I_S}{\beta_F} [e^{(qV_{BE}/N_F K T)} - 1] \quad (5.26)$$

$$I_{BR} = \frac{I_S}{\beta_R} [e^{(qV_{BC}/N_R K T)} - 1] \quad (5.27)$$

$$I_{LE} = I_{SE} [e^{(qV_{BE}/N_E K T)} - 1] \quad (5.28)$$

$$I_{LC} = I_{SC} [e^{(qV_{BC}/N_C K T)} - 1] \quad (5.29)$$

$$I_{CT} = I_S [e^{(qV_{BE}/N_F K T)} - e^{(qV_{BC}/N_R K T)}] \quad (5.30)$$

where V_T and I_s denote thermal voltage and saturation current (SC) respectively. N_F and β_F are emission coefficient (EC) and current gain in forward direction, N_R and β_R are EC and current gain in reverse direction, N_E and I_{SE} are EC and SC at base to emitter, N_C and I_{SC} are EC and SC at base to collector. I_C , I_E and I_B are obtained as :-

$$I_C = I_{CT} - I_{LC} - I_{BR} - C_{BC} \frac{d}{dt} v_{BC} \quad (5.31)$$

$$I_E = I_{CT} + I_{LE} + I_{BF} + C_{BE} \frac{d}{dt} v_{BE} \quad (5.32)$$

$$I_B = I_E - I_C \quad (5.33)$$

Substituting (5.26)-(5.30) into (5.31)-(5.33), we obtain I_C , I_E and I_B as :-

$$I_C = K_1 v_B + K_2 v_E + K_3 v_C + K_4 v_B v_B + K_5 v_C v_C + K_6 v_E v_E + K_7 v_B v_C + K_8 v_B v_E - C_{BC} \frac{d}{dt} v_{BC} \quad (5.34)$$

$$I_E = K_9 v_B + K_{10} v_E + K_{11} v_C + K_{12} v_B v_B + K_{13} v_C v_C + K_{14} v_E v_E + K_{15} v_B v_C + K_{16} v_B v_E + C_{BE} \frac{d}{dt} v_{BE} \quad (5.35)$$

$$I_B = (K_9 - K_1) v_B + (K_{10} - K_2) v_E + (K_{11} - K_3) v_C + (K_{12} - K_4) v_B v_B + (K_{13} - K_5) v_C v_C \\ + (K_{14} - K_6) v_E v_E + (K_{15} - K_7) v_B v_C + (K_{16} - K_8) v_B v_E + C_{BE} \frac{d}{dt} v_{BE} - C_{BC} \frac{d}{dt} v_{BC} \quad (5.36)$$

where

$$\begin{aligned} K_1 &= \frac{I_S}{V_T} \left\{ \frac{1}{N_F} - \frac{1}{N_R} \left(1 + \frac{1}{\beta_R} \right) \right\} - \frac{I_{SC}}{N_C V_T}, & K_2 &= \frac{-I_S}{N_F V_T}, \\ K_3 &= \frac{I_S}{V_T} \left\{ \frac{1}{N_R} \left(1 + \frac{1}{\beta_R} \right) \right\} + \frac{I_{SC}}{V_T N_C}, & K_4 &= \frac{I_S}{2V_T^2} \left\{ \frac{1}{N_F^2} - \frac{1}{N_R^2} \left(1 + \frac{1}{\beta_R} \right) \right\} - \frac{I_{SC}}{2V_T^2 N_C^2}, \\ K_5 &= \frac{-1}{2V_T^2} \left\{ \frac{I_{SC}}{N_C^2} + \frac{I_S}{N_R^2} \left(1 + \frac{1}{\beta_R} \right) \right\}, & K_6 &= \frac{I_S}{2N_F^2 V_T^2}, \\ K_7 &= \frac{1}{V_T^2} \left\{ \frac{I_{SC}}{N_C^2} + \frac{I_S}{N_R^2} \left(1 + \frac{1}{\beta_R} \right) \right\}, & K_8 &= \frac{-I_S}{N_F^2 V_T^2}, \\ K_9 &= \frac{1}{V_T} \left\{ \frac{I_{SE}}{N_E} + \frac{I_S}{N_F} \left(1 + \frac{1}{\beta_F} \right) - \frac{I_S}{N_R} \right\}, & K_{10} &= \frac{-1}{V_T} \left\{ \frac{I_S}{N_F} \left(1 + \frac{1}{\beta_F} \right) + \frac{I_{SE}}{N_E} \right\}, \\ K_{11} &= \frac{I_S}{N_R V_T}, & K_{12} &= \frac{1}{2V_T^2} \left[\frac{I_{SE}}{N_E^2} + I_S \left\{ \frac{1}{N_F^2} \left(1 + \frac{1}{\beta_R} \right) - \frac{1}{N_R^2} \right\} \right], \\ K_{13} &= \frac{-I_S}{2N_R^2 V_T^2}, & K_{14} &= \frac{1}{2V_T^2} \left\{ \frac{I_{SE}}{N_E^2} + \frac{I_S}{N_F^2} \left(1 + \frac{1}{\beta_F} \right) \right\}, \\ K_{15} &= \frac{I_S}{N_R^2 V_T^2}, & K_{16} &= \frac{-1}{V_T^2} \left[\frac{I_{SE}}{N_E^2} + I_S \left\{ \frac{1}{N_F^2} \left(-1 + \frac{1}{2\beta_F} \right) \right\} \right] \end{aligned}$$

Now, input can be modeled as Ornstein-Uhlenbeck process considering both the Brownian process and white Gaussian noise as :-

$$\frac{du}{dt} = -\gamma u + \sigma_j \rho_j N_j(t) \quad (5.37)$$

$$du(t) = -\gamma u dt + \sigma_j \rho_j dB_j(t) \quad (5.38)$$

where γ , σ_j and ρ_j are positive constants. $N_j(t)$ denotes white Gaussian noise with $\mathcal{N}(0, 1)$. $B_j(t)$ denotes Brownian motion process. Substituting (5.34) - (5.36) into (5.21)

- (5.25), we obtain the following equations :-

$$\begin{aligned} dv_{E_1} = & K_{17}v_{E_1}dt + K_{18}v_{E_2}dt + K_{19}v_Cdt + K_{20}v_{E_1}v_{E_1}dt + K_{21}v_{E_2}v_{E_2}dt + K_{22}v_Cv_Cdt \\ & + K_{23}v_{E_1}v_Cdt + K_{24}v_{E_1}v_{E_2}dt \end{aligned} \quad (5.39)$$

$$\begin{aligned} dv_{E_2} = & K_{25}v_{E_1}dt + K_{26}v_{E_2}dt + K_{27}v_Cdt + K_{28}v_{E_1}v_{E_1}dt + K_{29}v_{E_2}v_{E_2}dt + K_{30}v_Cv_Cdt \\ & + K_{31}v_{E_1}v_Cdt + K_{32}v_{E_1}v_{E_2}dt \end{aligned} \quad (5.40)$$

$$\begin{aligned} dv_{B_1} = & K_{33}v_{E_1}dt + K_{34}v_{E_2}dt + K_{35}v_{B_1}dt + K_{36}v_Cdt + K_{37}v_0dt + K_{38}v_{E_1}v_{E_1}dt \\ & + K_{39}v_{E_2}v_{E_2}dt + K_{40}v_Cv_Cdt + K_{41}v_{B_1}v_{B_1}dt + K_{42}v_{E_1}v_Cdt + K_{43}v_{E_1}v_{E_2}dt \\ & + K_{44}v_{B_1}v_Cdt + K_{45}v_{B_1}v_{E_1}dt + K_{46}[-\gamma u + \sigma_1 \rho_1 B_1(t)] + K_{47}V_{CC}dt \end{aligned} \quad (5.41)$$

$$\begin{aligned} dv_C = & K_{48}v_{E_1}dt + K_{49}v_{E_2}dt + K_{50}v_{B_1}dt + K_{51}v_Cdt + K_{52}v_0K_{53}v_{E_1}v_{E_1}dt \\ & + K_{54}v_{E_2}v_{E_2}dt + K_{55}v_Cv_Cdt + K_{56}v_{B_1}v_{B_1}dt + K_{57}v_{E_1}v_Cdt + K_{58}v_{E_1}v_{E_2}dt \\ & + K_{59}v_{B_1}v_Cdt + K_{60}v_{B_1}v_{E_1}dt + K_{61}[-\gamma u + \sigma_2 \rho_2 B_2(t)] + K_{62}V_{CC}dt \end{aligned} \quad (5.42)$$

$$\begin{aligned} dv_0 = & K_{48}v_{E_1}dt + K_{49}v_{E_2}dt + K_{50}v_{B_1}dt + K_{51}v_Cdt + K_{63}v_0dt + K_{53}v_{E_1}v_{E_1}dt \\ & + K_{54}v_{E_2}v_{E_2}dt + K_{55}v_Cv_Cdt + K_{56}v_{B_1}v_{B_1}dt + K_{57}v_{E_1}v_Cdt + K_{58}v_{E_1}v_{E_2}dt \\ & + K_{59}v_{B_1}v_Cdt + K_{60}v_{B_1}v_{E_1}dt + K_{61}[-\gamma u + \sigma_3 \rho_3 B_3(t)] + K_{62}V_{CC}dt \end{aligned} \quad (5.43)$$

where

$$\begin{aligned} K_{17} &= \frac{K_9}{C_E} \left(1 - \frac{C_{BE}}{C_{BC}} \right), & K_{18} &= \frac{1}{C_E} \left\{ K_{10} - \frac{1}{R_E} - \frac{C_{BE}}{C_{BC}} \left(-1 + \frac{1}{Z_E} \right) \right\}, \\ K_{19} &= \frac{K_{11}}{C_E} \left(1 - \frac{C_{BE}}{C_{BC}} \right), & K_{20} &= \frac{K_{12}}{C_E} \left(1 - \frac{C_{BE}}{C_{BC}} \right), \\ K_{21} &= \frac{K_{14}}{C_E} \left(1 - \frac{C_{BE}}{C_{BC}} \right), & K_{22} &= \frac{K_{13}}{C_E} \left(1 - \frac{C_{BE}}{C_{BC}} \right), \\ K_{23} &= \frac{K_{15}}{C_E} \left(1 - \frac{C_{BE}}{C_{BC}} \right), & K_{24} &= \frac{K_{16}}{C_E} \left(1 - \frac{C_{BE}}{C_{BC}} \right), \\ K_{25} &= \frac{-K_9}{C_E} \frac{C_{BE}}{C_{BC}}, & K_{26} &= \frac{K_{10}}{C_E} - \frac{1}{C_E R_E} + \frac{1}{C_{BC}} \left(-K_{10} + \frac{1}{Z_E} \right) \left(1 + \frac{C_{BE}}{C_E} \right), \\ K_{27} &= \frac{K_{11}}{C_E} - \frac{1}{C_{BC}} \left(1 + \frac{C_{BE}}{C_E} \right), & K_{28} &= K_{12} \left\{ \frac{1}{C_E} - \frac{1}{C_{BC}} \left(1 + \frac{C_{BE}}{C_E} \right) \right\}, \\ K_{29} &= \frac{K_{14}}{C_E} \left(1 - \frac{C_E + C_{BE}}{C_{BC}} \right), & K_{30} &= \frac{K_{13}}{C_E} \left(1 - \frac{C_E + C_{BE}}{C_{BC}} \right), \\ K_{31} &= \frac{K_{15}}{C_E} \left(1 - \frac{C_E + C_{BE}}{C_{BC}} \right), & K_{32} &= \frac{K_{16}}{C_E} \left(1 - \frac{C_E + C_{BE}}{C_{BC}} \right), \\ K_{33} &= \frac{K_1 + 3K_2 - 2K_{10} + K_{17}(2C_{BE} - C_{BC})}{2(C_B + C_{BE}) - C_{BC}}, & K_{34} &= \frac{K_2 + K_{18}(2C_{BE} - C_{BC})}{2(C_B + C_{BE}) - C_{BC}}, \\ K_{35} &= \frac{3K_1 - 2 \left(K_9 + \frac{R_1 R_2}{R_1 + R_2} \right)}{2(C_B + C_{BE}) - C_{BC}}, & K_{36} &= \frac{4K_3 - 2K_{11} + \frac{1}{R_C} + K_{19}(2C_{BE} - C_{BC})}{2(C_B + C_{BE}) - C_{BC}}, \\ K_{37} &= \frac{1}{R_L \{ 2(C_B + C_{BE}) - C_{BC} \}}, & K_{38} &= \frac{K_4 + 3K_6 - 2K_{14} + K_{20}(2C_{BE} - C_{BC})}{2(C_B + C_{BE}) - C_{BC}}, \\ K_{39} &= \frac{K_{21} \left(2C_{BE} - \frac{1}{C_{BC}} \right)}{2(C_B + C_{BE}) - C_{BC}}, & K_{40} &= \frac{2C_{BE}K_3 + 4K_5 - 2K_{13} - K_{22}C_{BC}}{2(C_B + C_{BE}) - C_{BC}}, \\ K_{41} &= \frac{3K_4 - 2K_{12}}{2(C_B + C_{BE}) - C_{BC}}, & K_{42} &= \frac{K_7 + K_{23}(2C_{BE} - C_{BC})}{2(C_B + C_{BE}) - C_{BC}}, \\ K_{43} &= \frac{K_8 + K_{24}(2C_{BE} - C_{BC})}{2(C_B + C_{BE}) - C_{BC}}, & K_{44} &= \frac{3K_7 - 2K_{15}}{2(C_B + C_{BE}) - C_{BC}}, \\ K_{45} &= \frac{3K_8 - 2K_{16}}{2(C_B + C_{BE}) - C_{BC}}, & K_{46} &= \frac{2C_B}{2(C_B + C_{BE}) - C_{BC}}, \end{aligned}$$

$$\begin{aligned}
K_{47} &= \frac{2}{R_L\{2(C_B+C_{BE})-C_{BC}\}}, & K_{48} &= \frac{K_2-K_{10}+K_{17}C_{BE}-(C_B+C_{BE}-C_{BC})(-K_{17}+\frac{K_1+K_2}{C_{BC}})}{2(C_B+C_{BE})-C_{BC}}, \\
K_{49} &= \frac{K_{18}C_{BE}-(C_B+C_{BE}-C_{BC})(-K_{18}+\frac{K_2}{C_{BC}})}{2(C_B+C_{BE})-C_{BC}}, & K_{50} &= \frac{K_1\left\{1-\frac{1}{C_{BC}}(C_B+C_{BE}-C_{BC})\right\}-K_9-\frac{R_1R_2}{R_1+R_2}}{2(C_B+C_{BE})-C_{BC}}, \\
K_{51} &= \frac{K_3-K_{11}+K_{19}C_{BE}-(C_B+C_{BE}-C_{BC})\left(-K_{19}+\frac{2K_3+\frac{1}{R_C}}{C_{BC}}\right)}{2(C_B+C_{BE})-C_{BC}}, & K_{52} &= \frac{(C_B+C_{BE}-C_{BC})}{R_L C_{BC}\{2(C_B+C_{BE})-C_{BC}\}}, \\
K_{53} &= \frac{K_6-K_{14}+K_{20}C_{BE}-(C_B+C_{BE}-C_{BC})\left(-K_{20}+\frac{2K_6+K_4}{C_{BC}}\right)}{2(C_B+C_{BE})-C_{BC}}, & K_{54} &= \frac{K_{21}(C_B+2C_{BE}-C_{BC})}{2(C_B+C_{BE})-C_{BC}}, \\
K_{55} &= \frac{-K_{13}+K_{22}(1+C_{BE})}{2(C_B+C_{BE})-C_{BC}}, & K_{56} &= \frac{K_4\left\{1-\frac{1}{C_{BC}}(C_B+C_{BE}-C_{BC})\right\}-K_{12}}{2(C_B+C_{BE})-C_{BC}}, \\
K_{57} &= \frac{K_{23}C_{BE}+(C_B+C_{BE}-C_{BC})(K_{23}-\frac{K_7}{C_{BC}})}{2(C_B+C_{BE})-C_{BC}}, & K_{58} &= \frac{K_{24}C_{BE}+(C_B+C_{BE}-C_{BC})(K_{24}-\frac{K_8}{C_{BC}})}{2(C_B+C_{BE})-C_{BC}}, \\
K_{59} &= \frac{K_7\left\{1-\frac{1}{C_{BC}}(C_B+C_{BE}-C_{BC})\right\}-K_{15}}{2(C_B+C_{BE})-C_{BC}}, & K_{60} &= \frac{K_8\left\{1-\frac{1}{C_{BC}}(C_B+C_{BE}-C_{BC})\right\}-K_{16}}{2(C_B+C_{BE})-C_{BC}}, \\
K_{61} &= \frac{C_B}{2(C_B+C_{BE})-C_{BC}}, & K_{62} &= \frac{1}{R_L\{2(C_B+C_{BE})-C_{BC}\}}, \\
K_{63} &= \frac{1}{R_L\{2(C_B+C_{BE})-C_{BC}\}}\left\{\frac{-1}{C_C}+\frac{(C_B+C_{BE}-C_{BC})}{C_{BC}}\right\}.
\end{aligned}$$

5.2.2 Implementation of UKF

Representing (5.39)-(5.43) as state space model in terms of Kronecker product, we have

$$\begin{aligned}
d\mathbf{x}(t) &= F^1\mathbf{x}(t) + F^2[\mathbf{x}(t) \otimes \mathbf{x}(t)] + F^3\mathbf{u}(t) + F^4[\mathbf{x}(t) \otimes \mathbf{u}(t)] + F^5d\mathbf{B}(t) \\
&\quad + F^6[\mathbf{x}(t) \otimes d\mathbf{B}(t)] + F^7\mathbf{V}_{cc}
\end{aligned} \tag{5.44}$$

where \otimes denotes the Kronecker product. State vector $\mathbf{x}(t)$ is formed as :-

$$\mathbf{x}(t) = \begin{bmatrix} v_{E_1}(t) & v_{E_2}(t) & v_{B_1}(t) & v_C(t) & v_0(t) \end{bmatrix}^T \tag{5.45}$$

where

$$F^1 = \begin{bmatrix} K_{17} & K_{18} & 0 & K_{19} & 0 \\ K_{25} & K_{26} & 0 & K_{27} & 0 \\ K_{33} & K_{34} & K_{35} & K_{36} & K_{37} \\ K_{48} & K_{49} & K_{50} & K_{51} & K_{52} \\ K_{48} & K_{49} & K_{50} & K_{51} & K_{63} \end{bmatrix},$$

$$\begin{aligned}
F^2 &= \begin{bmatrix} K_{20} & K_{24} & 0 & K_{23} & 0 & 0 & K_{21} & 0 & 0 & 0 & 0 & 0 & 0 \\ K_{28} & K_{32} & 0 & K_{31} & 0 & 0 & K_{29} & 0 & 0 & 0 & 0 & 0 & 0 \\ K_{38} & K_{43} & 0 & K_{42} & 0 & 0 & K_{39} & 0 & 0 & 0 & K_{45} & 0 & K_{41} & K_{44} \\ K_{53} & K_{58} & 0 & K_{57} & 0 & 0 & K_{54} & 0 & 0 & 0 & K_{66} & 0 & K_{56} & K_{59} \\ K_{53} & K_{58} & 0 & K_{57} & 0 & 0 & K_{54} & 0 & 0 & 0 & K_{60} & 0 & K_{56} & K_{59} \end{bmatrix}, \\
F^3 &= \begin{bmatrix} 0 & 0 & -\gamma K_{46} & -\gamma K_{61} & -\gamma K_{61} \end{bmatrix}^T, F^4 = 0, \\
F^5 &= \begin{bmatrix} 0 \\ 0 \\ \rho_1 \sigma_1 \\ \rho_2 \sigma_2 \\ \rho_3 \sigma_3 \end{bmatrix}, F^6 = 0, F^7 = \begin{bmatrix} 0 & 0 & K_{47} & K_{62} & K_{62} \end{bmatrix}^T, \\
dB(t) &= \begin{bmatrix} dB_1(t) & dB_2(t) & dB_3(t) & dB_4(t) & dB_5(t) \end{bmatrix}^T.
\end{aligned}$$

Measurement model is :-

$$dz(t) = H\mathbf{x}(t) + \sigma_v d\mathbf{C}_v \quad (5.46)$$

where

$$H = \begin{bmatrix} 1 & 0 & 0 & 0 & 0 \\ 0 & 1 & 0 & 0 & 0 \\ 0 & 0 & 1 & 0 & 0 \\ 0 & 0 & 0 & 1 & 0 \\ 0 & 0 & 0 & 0 & 1 \end{bmatrix}$$

In discrete time, (5.44) is represented as :-

$$\mathbf{x}_{k+1} = F_k^1 \mathbf{x}_k + F_k^2 [\mathbf{x}_k \otimes \mathbf{x}_k] + F_k^3 \mathbf{u}_k + F_k^4 [\mathbf{x}_k \otimes \mathbf{u}_k] + F_k^5 B_k + F_k^6 [\mathbf{x}_k \otimes B_k] + F_k^7 V_{cc} \quad (5.47)$$

where

$$\mathbf{x}_k = \begin{bmatrix} v_{E_1,k} & v_{E_2,k} & v_{B_1,k} & v_{C,k} & v_{0,k} \end{bmatrix}^T$$

$$\begin{aligned}
F_k^1 &= \frac{d}{d\mathbf{x}_k} f(\mathbf{x}_k, \mathbf{u}_k) = \begin{bmatrix} 1 + T_s K_{17} & T_s K_{18} & 0 & T_s K_{19} & 0 \\ T_s K_{25} & 1 + T_s K_{26} & 0 & T_s K_{27} & 0 \\ T_s K_{33} & T_s K_{34} & 1 + T_s K_{35} & T_s K_{36} & T_s K_{37} \\ T_s K_{48} & T_s K_{49} & T_s K_{50} & 1 + T_s T_s K_{51} & T_s K_{52} \\ T_s K_{48} & T_s K_{49} & T_s K_{50} & K_{51} & 1 + T_s K_{63} \end{bmatrix}, \\
F_k^2 &= \begin{bmatrix} T_s K_{20} & T_s K_{24} & 0 & T_s K_{23} & 0 & 0 & T_s K_{21} & 0 & 0 & 0 & 0 & 0 & 0 \\ T_s K_{28} & T_s K_{32} & 0 & T_s K_{31} & 0 & 0 & T_s K_{29} & 0 & 0 & 0 & 0 & 0 & 0 \\ T_s K_{38} & T_s K_{43} & 0 & T_s K_{42} & 0 & 0 & T_s K_{39} & 0 & 0 & 0 & T_s K_{45} & 0 & T_s K_{41} & T_s K_{44} \\ T_s K_{53} & T_s K_{58} & 0 & T_s K_{57} & 0 & 0 & T_s K_{54} & 0 & 0 & 0 & T_s K_{66} & 0 & T_s K_{56} & T_s K_{59} \\ T_s K_{53} & T_s K_{58} & 0 & T_s K_{57} & 0 & 0 & T_s K_{54} & 0 & 0 & 0 & K_{60} & 0 & T_s K_{56} & T_s K_{59} \end{bmatrix}, \\
F_k^3 &= \begin{bmatrix} 0 & 0 & -\gamma T_s K_{46} & -\gamma T_s K_{61} & -\gamma T_s K_{61} \end{bmatrix}^T, F_k^4 = 0, \\
F_k^5 &= \begin{bmatrix} 0 \\ 0 \\ T_s \rho_1 \sigma_1 \\ T_s \rho_2 \sigma_2 \\ T_s \rho_3 \sigma_3 \end{bmatrix}, F_k^6 = 0, \\
F_k^7 &= \begin{bmatrix} 0 & 0 & T_s K_{47} & T_s K_{62} & T_s K_{62} \end{bmatrix}^T, \\
\mathbf{B}_k &= \frac{d}{d\mathbf{u}_k} \varphi(\mathbf{x}_k, \mathbf{u}_k) = \begin{bmatrix} 0 & 0 & T_s K_{46} & T_s K_{61} & T_s K_{61} \end{bmatrix}^T.
\end{aligned}$$

where T_s is the sampling time. The measurement model is :-

$$\mathbf{z}_k = H_k \mathbf{x}_k \quad (5.48)$$

where

$$H_k = \frac{d}{d\mathbf{x}_k} h(\mathbf{x}_k, \mathbf{u}_k) = \begin{bmatrix} 1 & 0 & 0 & 0 & 0 \\ 0 & 1 & 0 & 0 & 0 \\ 0 & 0 & 1 & 0 & 0 \\ 0 & 0 & 0 & 1 & 0 \\ 0 & 0 & 0 & 0 & 1 \end{bmatrix}$$

5.2.3 Simulation Results

For PSPICE simulations, we used NPN DA transistor (Q2N2222). The derived equations (5.47) and (5.48) have been implemented in MATLAB software. For simulation,

following values have been used :-

$$\begin{array}{ll}
 R_1 = 22K\Omega, & R_2 = 5K\Omega, \\
 R_C = 1K\Omega, & R_E = 0.1K\Omega, \\
 R_L = 10\Omega, & C_C = 22\mu F, \\
 C_B = 22\mu F, & C_E = 11\mu F, \\
 q = 1 \times 10^{-19}, & k = 1.38 \times 10^{-23}, \\
 T = 300k, & I_S = 4.11 \times 10^{-15}, \\
 I_{SE} = 1.8 \times 10^{-15}, & I_{SC} = 0, \\
 N_C = 4.064, & N_E = 3.43 \\
 C_{bc} = 8.83 \times 10^{-13}, & C_{be} = 5.46 \times 10^{-13}, \\
 N_f = 1, & N_r = 1, \\
 \beta_f = 416.64, & \beta_r = 0.711, \\
 \beta = 2, & V_{CC} = 20.
 \end{array}$$

We estimated the output voltage of EKF, IEKF and UKF methods for the sinusoidal input signal with a maximum amplitude of 1 mV and frequency 1 KHz. The white Gaussian noise of zero mean and different variances have been used for estimation purposes. The output voltages of amplifier circuit have been estimated using EKF, IEKF and UKF methods for different noisy inputs as shown in Figure 5.4. Tables 5.3 and 5.4 show the comparison of SNR (dB) and RMSE for amplifier circuit using EKF, IEKF and UKF methods. Tables 5.5, 5.6 and 5.7 show the computational complexity of EKF, IEKF and UKF methods respectively for a single iteration. It shows that UKF method has less complexity than EKF and IEKF methods. We use the following dimensions for various parameters :-

$$\mathbf{x}_k \in \mathbb{R}^{n \times 1}, \mathbf{F}_k \in \mathbb{R}^{n \times n}, \mathbf{u}_k \in \mathbb{R}^{1 \times p}, \Sigma_k \in \mathbb{R}^{n \times n}, \mathbf{C}_{w,k} \in \mathbb{R}^{n \times n}, \mathbf{H}_k \in \mathbb{R}^{d \times n} \text{ and } \mathbf{z}_k \in \mathbb{R}^{d \times n}.$$

The identification of the parameters for covariance matrices $\mathbf{C}_{w,k}$ and $\mathbf{C}_{v,k}$ are important aspect of a good estimation. But, due to the complexity in choosing the optimum value of $\mathbf{C}_{w,k}$ and $\mathbf{C}_{v,k}$, many methods have been proposed in literature. We used typical trial and error method [102]. The advantage of using this method is that it is simple to be accomplished. Table 5.8 shows different $\mathbf{C}_{w,k}$ and $\mathbf{C}_{v,k}$ values with their corresponding MSE value obtained by trial and error method. We used covariances of system noise $\mathbf{C}_{w,k} = \text{diag}[0.001, 0.001, 0.001, 0.001, 0.001]$ and covariance of measurement

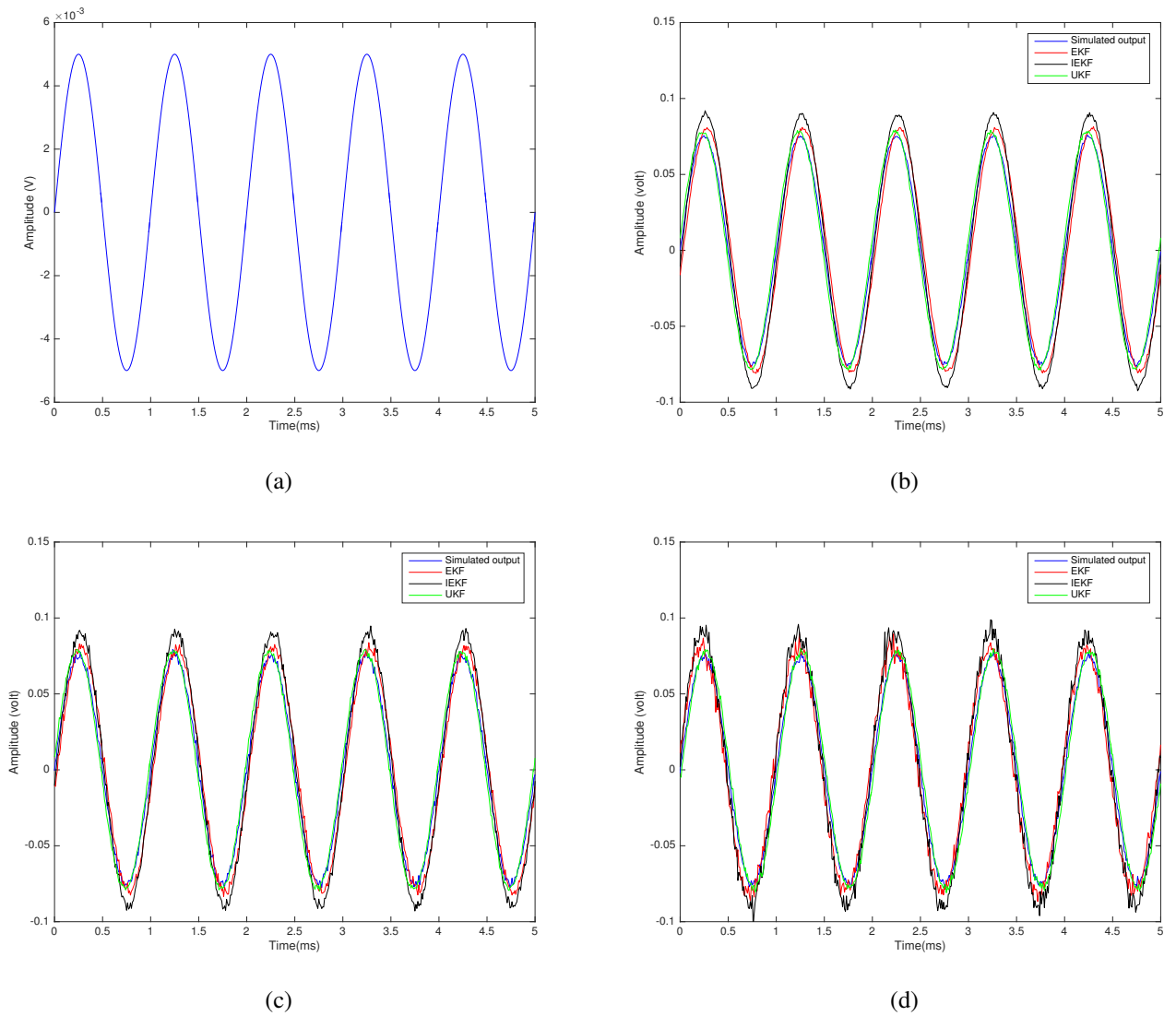


Figure 5.4: a) Input sinusoidal voltage. Comparison of output voltage estimation of DA using EKF, IEKF and UKF methods for noisy input with b) $\mu = 0$, $\sigma^2 = 0.1$, c) $\mu = 0$, $\sigma^2 = 0.5$, d) $\mu = 0$, $\sigma^2 = 1.0$.

noise $C_{v,k} = 0.1$ which corresponds to minimum MSE.

5.2.4 Conclusions

The voltage estimation of a DA using UKF method is presented in this chapter, and the results have been compared with EKF and IEKF methods. Simulation results using UKF method show the better closeness of estimated output voltage with actual simulated values as compared to the EKF and IEKF methods. UKF method presents a smaller MSE value as compared to EKF and IEKF methods as UKF method is accurate to the third order for any nonlinearity.

Table 5.3: Comparison of SNR (dB) of DA for different methods.

S.No.	Noisy signal with Gaussian noise	Input Frequency (Hz)	EKF method	IEKF method	UKF method
1	$\mu = 0, \sigma^2 = 0.1$	20	101.600	103.250	116.140
		200	101.620	103.750	116.409
		2000	101.645	104.125	116.456
2	$\mu = 0, \sigma^2 = 0.5$	20	87.851	90.460	106.960
		200	87.832	90.490	107.060
		2000	88.150	92.460	107.960
3	$\mu = 0, \sigma^2 = 1.0$	20	83.021	85.250	98.120
		200	84.350	85.500	98.512
		2000	84.990	86.250	99.120

Table 5.4: RMSE of output voltage estimation using EKF, IEKF and UKF methods.

S.No.	Noisy signal with Gaussian noise	Input Frequency (Hz)	EKF method	IEKF method	UKF method
1	$\mu = 0$ $\sigma^2 = 0.1$	20	0.610	0.561	0.390
		200	0.620	0.570	0.399
		2000	0.635	0.579	0.401
2	$\mu = 0$ $\sigma^2 = 0.5$	20	0.640	0.592	0.410
		200	0.645	0.599	0.421
		2000	0.652	0.605	0.429
3	$\mu = 0$ $\sigma^2 = 1.0$	20	0.672	0.608	0.422
		200	0.679	0.618	0.452
		2000	0.690	0.650	0.459

Table 5.5: Computational complexity for EKF method.

Equation number	Number of multiplication
(1.13)	$n^2 + np$
(1.14)	$2n^3$
(1.16)	$2n^2d + 3nd^2$
(1.17)	$2n^2d$
(1.18)	$n^2d + 2n^3$
Total no. of multiplication	$4n^3 + n^2 + 5n^2d + 3nd^2 + np \approx \mathbf{O}(4n^3)$

Table 5.6: Computational complexity for IEKF method.

Equation number	Number of multiplication
(1.13)	$n^2 + np$
(1.14)	$2n^3$
(1.23)	$2n^2d + 3nd^2$
(1.24)	$5nd^2 + 2d^2$
(1.25)	$n^2d + 2n^3$
Total no. of multiplication	$4n^3 + n^2 + 3n^2d + 3nd^2 + 2d^2 + 5nd + np \approx \mathbf{O}(4n^3)$

Table 5.7: Computational complexity for UKF method.

Equation number	Number of multiplication
(1.30)	$n^2 + np$
(1.32)	$4n^2$
(1.33)	$4nd$
(1.34)	nd
(1.36)	$4d^2$
(1.37)	nd^2
(1.38)	$2nd$
(1.39)	$n^2d + nd^2$
Total no. of multiplication	$5n^2 + n^2d + 2nd^2 + 4d^2 + 7nd + np \approx \mathbf{O}(5n^2)$

Table 5.8: Comparison of MSE with different values of $C_{w,k}$ and $C_{v,k}$ using trial and error method.

S.No.	Values of $C_{w,k}$ and $C_{v,k}$	MSE	Remarks
1.	$C_{w,k} = 1e^{-6}$ and $C_{v,k} = 1e^{-2}$	17.156	Very poor
2.	$C_{w,k} = 1e^{-7}$ and $C_{v,k} = 1e^{-3}$	22.876	Very poor
3.	$C_{w,k} = 1e^{-4}$ and $C_{v,k} = 1e^{-1}$	3.9870	Poor
4.	$C_{w,k} = 1e^{-3}$ and $C_{v,k} = 1e^{-2}$	0.3648	Good
5.	$C_{w,k} = 1e^{-3}$ and $C_{v,k} = 1e^{-1}$	0.2438	Very Good

Chapter 6

State Estimation and Parameter Estimation of Transmission Line

This Chapter ¹ presents the implementation of KF (Chapter 1.4.1), EKF and UKF methods on NTL for state and parameter estimation. For this, state-space model of the NTL circuit has been derived. As Telegrapher's equations used for modeling the NTL are a function of space and time, the Fourier series expansion of the voltage and current have been used to obtain the time-dependent equations. Further, Kronecker product has been used for representation of Fourier unitary transform. The measurements have been obtained by solving the eigenvector problem. The frequency-domain analysis is used to obtain the state-space equations. For this, the four distributed parameters of the line are expanded in Fourier series.

Till now versions of KF method have been implemented on lumped circuits. Now, these algorithms are implemented on distributed circuits.

Major contribution of this work is :- (i) state space model for NTL has been obtained by including Fourier series expansion of state and Gaussian noise vectors in the SDE, (ii) Clarke transformation matrix has been utilized for phase to sequence transformation which allows to represent the three-phase transmission line into fully transposed

¹The result of this chapter is based on the following research papers (i) Amit Kumar Gautam, Sudipta Majumdar and Harish Parthasarathy, "State and parameter estimation of non-uniform transmission line using Kronecker product based modeling," IEEE Transactions on Power Delivery, ISSN no.1937-4208, 2022.(ii) Amit Kumar Gautam and Sudipta Majumdar, "Application of stochastic filter to three-phase nonuniform transmission lines," International Journal of Electronics, ISSN no. 1362-3060, 2023.

transmission line, (iii) measurement model for current and voltage vectors at a finite set of spatial points along the line is expressed in terms of the spatial Fourier series coefficients. Also, the frequency domain analysis is used to obtain the eigenvalue and eigenvector for measurement model, (iv) The voltage and current of NTL are expanded in Fourier series to obtain the sparse matrix formulation using Kronecker product. Kronecker product representation of discrete unitary transforms results in computer efficient implementation. (v) This work implements the analysis of non-linearity effect in transmission line using perturbation theory. For this, the nonlinearity of the transmission line is included by perturbing the voltage and current of the line. (vi) Finally, KF, EKF and UKF algorithms have been used for state and parameter estimation respectively which requires the measurement model. The measurement model involves the current and voltage Fourier series coefficients. The measurements have been obtained by forming the eigenvalue problem.

In literature, various methods have been proposed for state estimation of power system. In [103], Ghiasi *et al.* proposed one node method for voltage and current estimation at the intermediate points of a lossy transmission line. It uses the Bergeron model of a transmission line. This method has the advantage of using parameters at one end of the transmission line which needs less computation time, less input data, and less memory than other methods. In [104], Fan *et al.* used an ensemble KF for fault location on transmission lines. The advantage of this method is its easy implementation. Also, the foreknowledge of fault type or fault location is not required. In [105], Rakpenthai *et al.* presented a nonlinear optimization based weighted least squares method that uses constrained nonlinear optimization. The method uses the bus voltage phasors and temperature of transmission line conductor for state estimation purpose. In [106], Malhara *et al.* proposed a least squares based state estimation for transmission line using various parameters to prevent malicious attacks. In [107], Liu *et al.* used dynamic state estimation for protection of series compensated transmission lines. The method used the dynamic model of protection zone. It has the advantage of faster detection of internal faults as compared to the legacy protection function. In [108], a least squares based state estimation of transmission line equation is proposed to estimate the conductor sag levels to generate the warning signal. In [109], Liu *et al.* proposed protection of mutually coupled transmission lines that uses dynamic state estimation based protection (EBP) algorithm and performed numerical experiments on various scenarios. In [110], Liu *et al.* proposed dynamic

state estimation for fault location of transmission line that works on the sample values and uses the dynamic model. The method provides the higher accuracy than traditional methods. In [111], Liu *et al.* proposed the fault location of non-homogeneous transmission line using state estimation. The unconstrained weighted least square method is used for estimation by formulating the method of the non-homogeneous transmission line with fault. In [112], Yang *et al.* used unscented information filtering (UIF) method for state estimation of power networks. As the UIF is a nonlinear state estimation method, it achieves better accuracy than centralized UIF, maximum a posteriori (MAP) and the local UIF estimator. In [113], Li *et al.* proposed fully distributed state estimation using weighted least square method and graph theory for estimation of power system. The method has better performance than the traditional methods. In [114], Mohammed *et al.* used a modified reiterated Kalman filter for state estimation of power system that can handle the lost and delayed measurements. In [115], Alhelou *et al.* used dynamic state estimation for decentralized load frequency control. The method has the advantage of high accuracy, efficiency and easy implementation.

In [116], Dobakhshari *et al.* proposed closed-form and non-iterative solution for Supervisory Control And Data Acquisition (SCADA) based state estimation. The method has the advantage of fast implementation and low computation burden.

Various methods have been used in the literature for parameter estimation of transmission lines. Ritzmann *et al.* [117] proposed the impedance estimation method for transmission lines by assuming linearly changing parameters for short periods. The method presents better accuracy as compared to other methods. [118] presented a technique for estimation of electrical parameter of transmission line. The method uses synchronized sampled data. This method has the ability to obtain the steady state values of voltage and current of the transmission line as a function of time and line logic. Also, it has the ability to overcome practical obstacles during estimation. Tolic *et al.* [119] presented a method for determining the transmission losses in which, probability density estimation is done using the nonlinear least squares method. Yang *et al.* [120] proposed a method for conditional failure rate of transmission line. In [121], Asprou *et al.* proposed a method to estimate the erroneous transmission line parameters that are stored in database of power system control centre. The main advantage is that it needs only one phasor measurement units. In [122], Wang *et al.* presented least squares estimation based single line parameters estimation method to estimate the actual transmission line parameters. The method presents

very small estimation errors. In [123], Sima *et al.* proposed an analytic method for estimating the lightning performance of transmission lines. This takes smaller computation time as compared to the traditional method. In [124], Sivanagaraju *et al.* proposed transmission line parameter estimation using hybrid measurements from phasor measurements and used for differential protection of the transmission lines. In [125], Halligan *et al.* presented a method to estimate the maximum crosstalk in transmission line. In [126], Ren *et al.* used state estimation and parameters tracking iteratively along with static parameter estimation to estimate the parameters of overhead transmission lines. The method is able to track the transmission line parameter for different conditions. They used state and parameter estimation of three-phase untransposed transmission line. For this, they used weighted-least-square (WLS) method for static state estimation and KF method for parameter estimation. We used KF and EKF for state and parameter estimation of single-phase transmission line.

The State space model of NTL circuit has been derived in Section 6.1.1. Section 6.1.2 describes the frequency domain analysis of NTL to obtain a measurement vector. Section 6.1.3 presents state and parameter estimation for transmission line circuit. Simulation results are presented in Section 6.1.4. Section 6.2.1 presents the mathematical modeling of three phase NTL circuit. Section 6.2.2 describes modeling of transposed and untransposed NTL. the frequency domain analysis of the parameter estimation of three-phase NTL is presented in section 6.2.3. Section 6.2.4 includes state and parameter estimation of NTL circuit. Section 6.2.5 presents simulation results.

6.1 State Estimation and Parameter Estimation of Single-Phase nonuniform Transmission Line

6.1.1 State Space Model

This section presents the state space analysis of NTL. An equivalent circuit of a transmission line has been shown in Figure 6.1. The four fundamental parameters of the nonuniform distribution line are namely, resistance $R(z)$, inductance $L(z)$, capacitance $C(z)$ and conductance $G(z)$ per unit length d . The line voltage $v(t, z)$ and line current $i(t, z)$ at any point on the NTL is represented by both space and time dependent

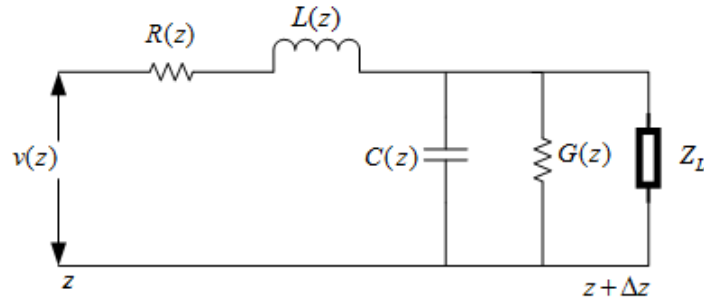


Figure 6.1: Circuit diagram of a nonuniform transmission line.

partial differential equations (Telegrapher's equation) as :-

$$\frac{d}{dz}v(t, z) + R(z)i(t, z) + L(z)\frac{d}{dt}i(t, z) = w_v(t, z) \quad (6.1)$$

$$\frac{d}{dz}i(t, z) + G(z)v(t, z) + C(z)\frac{d}{dt}v(t, z) = w_i(t, z) \quad (6.2)$$

where $R(z) = R(z|\theta)$, $L(z) = L(z|\theta)$, $C(z) = C(z|\theta)$ and $G(z) = G(z|\theta)$ are NTL parameters.

They can be assumed as :-

$$R(z) = R(z|\theta) = \sum_{m=1}^p \theta[m]R_m(z) \quad (6.3)$$

$$L(z) = L(z|\theta) = \sum_{m=1}^p \theta[m]L_m(z) \quad (6.4)$$

$$C(z) = C(z|\theta) = \sum_{m=1}^p \theta[m]C_m(z) \quad (6.5)$$

$$G(z) = G(z|\theta) = \sum_{m=1}^p \theta[m]G_m(z) \quad (6.6)$$

$w_v(t, z)$ and $w_i(t, z)$ are zero mean exponential correlation process. Also, consider the voltage $v(t, z)$, current $i(t, z)$, $w_v(t, z)$ and $w_i(t, z)$ vectors of transmission line in terms of

spatial Fourier series as :-

$$v(t, z) = \sum_n v_n(t) \exp\left(\frac{j2\pi n z}{d}\right) \quad (6.7)$$

$$i(t, z) = \sum_n i_n(t) \exp\left(\frac{j2\pi n z}{d}\right) \quad (6.8)$$

$$w_v(t, z) = \sum_n w_{v,n}(t) \exp\left(\frac{j2\pi n z}{d}\right) \quad (6.9)$$

$$w_i(t, z) = \sum_n w_{i,n}(t) \exp\left(\frac{j2\pi n z}{d}\right) \quad (6.10)$$

where d is the total length of the transmission line. $v_n(t)$, $i_n(t)$, $w_{v,n}(t)$ and $w_{i,n}(t)$ are the Fourier coefficients with respect to time t . (6.7)-(6.10) can also be expressed in their matrix form as :-

$$\mathbf{V}(z) = \sum_N v(n) \mathbf{W}_N^{nz} \quad (6.11)$$

$$\mathbf{I}(z) = \sum_N i(n) \mathbf{W}_N^{nz} \quad (6.12)$$

$$\mathbf{W}_v(z) = \sum_N w_v(n) \mathbf{W}_N^{nz} \quad (6.13)$$

$$\mathbf{W}_i(z) = \sum_N w_i(n) \mathbf{W}_N^{nz} \quad (6.14)$$

where $\mathbf{V}(z)$, $\mathbf{I}(z)$, $\mathbf{W}_v(z)$, $\mathbf{W}_i(z)$ are N point DFT at $k = 0, \dots, (N-1)$. Weight matrix (\mathbf{W}_N) is simply defined as :-

$$\mathbf{W}_N = e^{j2\pi/N} = \begin{bmatrix} \mathbf{W}_N^0 & \mathbf{W}_N^0 & \mathbf{W}_N^0 & \dots & \mathbf{W}_N^0 \\ \mathbf{W}_N^0 & \mathbf{W}_N^1 & \mathbf{W}_N^2 & \dots & \mathbf{W}_N^{N-1} \\ \vdots & \vdots & \vdots & \dots & \vdots \\ \vdots & \vdots & \vdots & \dots & \vdots \\ \mathbf{W}_N^0 & \mathbf{W}_N^{N-1} & \mathbf{W}_N^{2N-1} & \dots & \mathbf{W}_N^{(N-1)^2} \end{bmatrix} \quad (6.15)$$

This Weight matrix (\mathbf{W}_N) can be represented by sparse matrix factorization using Kronecker product [127] as :-

$$\mathbf{W}_N = \left\{ \mathbf{B} \right\}_{N/2} \otimes \mathbf{W}_{N/2}, \mathbf{W}_1 = 1 \quad (6.16)$$

where N is a power of two, and $\left\{ \mathbf{B} \right\}_{N/2}$ has $N/2$ matrices in the set, with the i^{th} matrix $i = 0$ to $(N/2 - 1)$ given by

$$\mathbf{B}_i = \left\{ \begin{array}{ll} \begin{bmatrix} 1 & 1 \\ 1 & j \end{bmatrix}, & i = 1 \\ \begin{bmatrix} 1 & 1 \\ 1 & -1 \end{bmatrix}, & \text{otherwise} \end{array} \right\}$$

For example, if we choose $N = 8$, then \mathbf{W}_8 can be expressed as:-

$$\mathbf{W}_8 = \{\mathbf{B}\}_4 \otimes \{\mathbf{B}\}_2 \otimes \mathbf{W}_2 \quad (6.17)$$

where

$$\{\mathbf{B}\}_4 = \begin{bmatrix} \begin{bmatrix} 1 & 1 \\ 1 & -1 \end{bmatrix} & & & \\ & \begin{bmatrix} 1 & -j \\ 1 & j \end{bmatrix} & & \\ & & \begin{bmatrix} 1 & 1 \\ 1 & -1 \end{bmatrix} & \\ & & & \begin{bmatrix} 1 & 1 \\ 1 & -1 \end{bmatrix} \end{bmatrix}, \quad \{\mathbf{B}\}_2 = \begin{bmatrix} \mathbf{I}_2 \otimes \begin{bmatrix} 1 & 1 \\ 1 & -1 \end{bmatrix} & \\ & \mathbf{I}_2 \otimes \begin{bmatrix} 1 & -j \\ 1 & j \end{bmatrix} \end{bmatrix},$$

and $\mathbf{W}_2 = \mathbf{I}_4 \otimes \begin{bmatrix} 1 & 1 \\ 1 & -1 \end{bmatrix}$. Therefore, (6.11)-(6.14) are rearranged as:-

$$\mathbf{V}(z) = \sum_N v(n) \times \{\mathbf{B}\}_{N/2} \otimes \mathbf{W}_{N/2} \quad (6.18)$$

$$\mathbf{I}(z) = \sum_N i(n) \times \{\mathbf{B}\}_{N/2} \otimes \mathbf{W}_{N/2} \quad (6.19)$$

$$\mathbf{W}_v(z) = \sum_N w_v(n) \times \{\mathbf{B}\}_{N/2} \otimes \mathbf{W}_{N/2} \quad (6.20)$$

$$\mathbf{W}_i(z) = \sum_N w_i(n) \times \{\mathbf{B}\}_{N/2} \otimes \mathbf{W}_{N/2} \quad (6.21)$$

From (6.3)-(6.6), the value of $R_m(z)$, $L_m(z)$, $C_m(z)$ and $G_m(z)$ can be expressed in terms of spatial Fourier series in z with period d as:-

$$R_m(z) = \sum_n R_m[n] \exp\left(\frac{j2\pi n z}{d}\right) \quad (6.22)$$

$$L_m(z) = \sum_n L_m[n] \exp\left(\frac{j2\pi n z}{d}\right) \quad (6.23)$$

$$C_m(z) = \sum_n C_m[n] \exp\left(\frac{j2\pi n z}{d}\right) \quad (6.24)$$

$$G_m(z) = \sum_n G_m[n] \exp\left(\frac{j2\pi n z}{d}\right) \quad (6.25)$$

where the coefficients $R_m[n]$, $L_m[n]$, $C_m[n]$ and $G_m[n]$ are represented in finite form. (6.26)-(6.29) are truncated their Fourier series from $m = 1$ to $m = P$ as :-

$$R[n|\theta] = R[n] = \sum_{m=1}^P \theta[m]R_m[n] \quad (6.26)$$

$$L[n|\theta] = L[n] = \sum_{m=1}^P \theta[m]L_m[n] \quad (6.27)$$

$$C[n|\theta] = C[n] = \sum_{m=1}^P \theta[m]C_m[n] \quad (6.28)$$

$$G[n|\theta] = G[n] = \sum_{m=1}^P \theta[m]G_m[n] \quad (6.29)$$

Substituting (6.3)-(6.10) along with (6.22)-(6.29) into (6.1)-(6.2) and equating both sides coefficients, we have

$$\sum_m R[n-m|\theta]i_m(t) + \sum_m L[n-m|\theta]i'_m(t) + \frac{j2\pi n}{d}v_n(t) = w_{v,n}(t) \quad (6.30)$$

$$\sum_m G[n-m|\theta]v_m(t) + \sum_m C[n-m|\theta]v'_m(t) + \frac{j2\pi n}{d}i_n(t) = w_{i,n}(t) \quad (6.31)$$

where $i'_m(t) = \frac{d}{dt}i_m(t)$ and $v'_m(t) = \frac{d}{dt}v_m(t)$. $v_n(t)$, $i_n(t)$, $w_{v,n}(t)$ and $w_{i,n}(t)$ are defined in their Fourier series vectors of samples size $2N + 1$ as :-

$$\left(\left(v_{(n)}(t) \right) \right)_{-N}^{+N} = \mathbf{v}(t) \quad (6.32)$$

$$\left(\left(i_{(n)}(t) \right) \right)_{-N}^{+N} = \mathbf{i}(t) \quad (6.33)$$

$$\left(\left(w_{(v,n)}(t) \right) \right)_{-N}^{+N} = \mathbf{w}_v(t) \quad (6.34)$$

$$\left(\left(w_{(i,n)}(t) \right) \right)_{-N}^{+N} = \mathbf{w}_i(t) \quad (6.35)$$

Also, the line parameters are expressed in terms of Fourier series matrices as follows

:-

$$\left(\left(R[n-m|\theta] \right) \right)_{-N \leq n, l \leq N} = \mathbf{R}(\theta) = \sum_{m=1}^p \theta[m] \mathbf{R}_m \quad (6.36)$$

$$\left(\left(L[n-m|\theta] \right) \right)_{-N \leq n, l \leq N} = \mathbf{L}(\theta) = \sum_{m=1}^p \theta[m] \mathbf{L}_m \quad (6.37)$$

$$\left(\left(C[n-m|\theta] \right) \right)_{-N \leq n, l \leq N} = \mathbf{C}(\theta) = \sum_{m=1}^p \theta[m] \mathbf{C}_m \quad (6.38)$$

$$\left(\left(G[n-m|\theta] \right) \right)_{-N \leq n, l \leq N} = \mathbf{G}(\theta) = \sum_{m=1}^p \theta[m] \mathbf{G}_m \quad (6.39)$$

where

$$\mathbf{R}_m = \left(\left(R[n-l] \right) \right)_{-N \leq n, l \leq N}, \mathbf{L}_m = \left(\left(L[n-l] \right) \right)_{-N \leq n, l \leq N}$$

$$\mathbf{C}_m = \left(\left(C[n-l] \right) \right)_{-N \leq n, l \leq N}, \mathbf{G}_m = \left(\left(G[n-l] \right) \right)_{-N \leq n, l \leq N}$$

Substituting (6.32)-(6.35) along with (6.36)-(6.39) into (6.30)-(6.31), we get

$$\mathbf{R}[\theta] \mathbf{i}(t) + \mathbf{L}[\theta] \mathbf{i}'(t) + j \mathbf{D} \mathbf{v}(t) = \mathbf{w}_v(t) \quad (6.40)$$

$$\mathbf{G}[\theta] \mathbf{v}(t) + \mathbf{C}[\theta] \mathbf{v}'(t) + j \mathbf{D} \mathbf{i}(t) = \mathbf{w}_i(t) \quad (6.41)$$

where $\mathbf{D} = \text{diag} \left[\frac{2\pi n}{d}; -N \leq n \leq N \right]$. Rearranging (6.40)-(6.41) to find their state space model, we get

$$\frac{d}{dt} \begin{bmatrix} \mathbf{v}(t) \\ \mathbf{i}(t) \end{bmatrix} = - \begin{bmatrix} \mathbf{C}[\theta]^{-1} \mathbf{G}[\theta] & j \mathbf{D} \\ j \mathbf{D} & \mathbf{L}[\theta]^{-1} \mathbf{R}[\theta] \end{bmatrix} \begin{bmatrix} \mathbf{v}(t) \\ \mathbf{i}(t) \end{bmatrix} + \begin{bmatrix} \mathbf{C}[\theta]^{-1} & 0 \\ 0 & \mathbf{L}[\theta]^{-1} \end{bmatrix} \begin{bmatrix} \mathbf{w}_i(t) \\ \mathbf{w}_v(t) \end{bmatrix} \quad (6.42)$$

where state vector matrix denoted by $\xi(t)$ is represented as :-

$$\begin{bmatrix} \mathbf{v}(t) \\ \mathbf{i}(t) \end{bmatrix} = \xi(t) = \xi_R(t) + j \xi_I(t) \quad (6.43)$$

Here, $\xi_R(t)$ and $\xi_I(t)$ denote real and imaginary terms respectively.

State transition matrix $\mathbf{F}(\theta)$ obtained from (6.42) is defined in real and imaginary

terms as :-

$$- \begin{bmatrix} \mathbf{C}[\theta]^{-1} \mathbf{G}[\theta] & j \mathbf{D} \\ j \mathbf{D} & \mathbf{L}[\theta]^{-1} \mathbf{R}[\theta] \end{bmatrix} = \mathbf{F}_R(\theta) + j \mathbf{F}_I(\theta) \quad (6.44)$$

Also, processes noise matrix is

$$\begin{bmatrix} \mathbf{C}[\theta]^{-1} & \mathbf{0} \\ \mathbf{0} & \mathbf{L}[\theta]^{-1} \end{bmatrix} = \mathbf{P}_R(\theta) + j \mathbf{P}_I(\theta) \quad (6.45)$$

$$\begin{bmatrix} \mathbf{w}_i(t) \\ \mathbf{w}_v(t) \end{bmatrix} = \mathbf{w}(t) = \mathbf{w}_R(t) + j \mathbf{w}_I(t) \quad (6.46)$$

Substituting (6.43)-(6.46) into (6.42), the line equation is

$$(\xi'_R(t) + j \xi'_I(t)) = (\mathbf{F}_R(\theta) + j \mathbf{F}_I(\theta))(\xi_R(t) + j \xi_I(t)) + (\mathbf{P}_R(\theta) + j \mathbf{P}_I(\theta))(\mathbf{w}_R(t) + j \mathbf{w}_I(t)) \quad (6.47)$$

Seperating into real and imaginary parts, we get

$$\xi'_R(t) = \mathbf{F}_R(\theta) \xi_R(t) - \mathbf{F}_I(\theta) \xi_I(t) + \mathbf{P}_R(\theta) \mathbf{w}_R(t) - \mathbf{P}_I(\theta) \mathbf{w}_I(t) \quad (6.48)$$

$$\xi'_I(t) = \mathbf{F}_R(\theta) \xi_I(t) + \mathbf{F}_I(\theta) \xi_R(t) + \mathbf{P}_R(\theta) \mathbf{w}_I(t) + \mathbf{P}_I(\theta) \mathbf{w}_R(t) \quad (6.49)$$

Rearranging into matrix notation, we get

$$\frac{d}{dt} \begin{bmatrix} \xi_R(t) \\ \xi_I(t) \end{bmatrix} = \begin{bmatrix} \mathbf{F}_R[\theta] & -\mathbf{F}_I[\theta] \\ \mathbf{F}_I[\theta] & \mathbf{F}_R[\theta] \end{bmatrix} \begin{bmatrix} \xi_R(t) \\ \xi_I(t) \end{bmatrix} + \begin{bmatrix} \mathbf{P}_R[\theta] & -\mathbf{P}_I[\theta] \\ \mathbf{P}_I[\theta] & \mathbf{P}_R[\theta] \end{bmatrix} \begin{bmatrix} \mathbf{w}_R(t) \\ \mathbf{w}_I(t) \end{bmatrix} \quad (6.50)$$

where $\frac{d}{dt} \theta(t) = \varepsilon_{\theta(t)}$ The parameter vector to be estimated must are added in (6.43) to obtain the augmented matrix as :-

$$\boldsymbol{\eta}(t) = \left[\xi_R(t), \xi_I(t), \theta(t) \right]^T \quad (6.51)$$

Therefore, the combined augmented state space model is :-

$$\frac{d}{dt} \begin{bmatrix} \xi_R(t) \\ \xi_I(t) \\ \theta(t) \end{bmatrix} = \begin{bmatrix} \mathbf{F}_R[\theta] & -\mathbf{F}_I[\theta] & \mathbf{0} \\ \mathbf{F}_I[\theta] & \mathbf{F}_R[\theta] & \mathbf{0} \\ \mathbf{0} & \mathbf{0} & \mathbf{I} \end{bmatrix} \begin{bmatrix} \xi_R(t) \\ \xi_I(t) \\ \theta(t) \end{bmatrix} + \begin{bmatrix} \mathbf{P}_R[\theta] & -\mathbf{P}_I[\theta] & \mathbf{0} \\ \mathbf{P}_I[\theta] & \mathbf{P}_R[\theta] & \mathbf{0} \\ \mathbf{0} & \mathbf{0} & \mathbf{I} \end{bmatrix} \begin{bmatrix} \mathbf{w}_R(t) \\ \mathbf{w}_I(t) \\ \varepsilon_{\theta(t)} \end{bmatrix} \quad (6.52)$$

where I is the unitary matrix of sample size $2N + 1$. For EKF implementation in (6.52), we must calculate the Jacobian matrix. Therefore, we differentiate $\mathbf{F}_R(\theta)$, $\mathbf{F}_I(\theta)$, $\mathbf{P}_R(\theta)$, $\mathbf{P}_I(\theta)$ w.r.t. θ . These expressions are derived as follows :-

$$\frac{d}{d\theta(m)}(\mathbf{F}_R(\theta) + j\mathbf{F}_I(\theta)) = - \begin{bmatrix} \frac{d}{d\theta(m)} \mathbf{C}[\theta]^{-1} \mathbf{G}[\theta] & \mathbf{0} \\ \mathbf{0} & \frac{d}{d\theta(m)} \mathbf{L}[\theta]^{-1} \mathbf{R}[\theta] \end{bmatrix} \quad (6.53)$$

$$\frac{d}{d\theta(m)} \mathbf{C}[\theta]^{-1} \mathbf{G}[\theta] = - \mathbf{C}[\theta]^{-1} \frac{d}{d\theta(m)} \mathbf{C}[\theta] \mathbf{C}[\theta]^{-1} \mathbf{G}[\theta] + \mathbf{C}[\theta]^{-1} \frac{d}{d\theta(m)} \mathbf{G}[\theta] \quad (6.54)$$

$$= - \mathbf{C}[\theta]^{-1} \mathbf{C}_m \mathbf{C}[\theta]^{-1} \mathbf{G}[\theta] + \mathbf{C}[\theta]^{-1} \mathbf{G}_m \quad (6.55)$$

similarly,

$$\frac{d}{d\theta(m)} \mathbf{L}[\theta]^{-1} \mathbf{R}[\theta] = - \mathbf{L}[\theta]^{-1} \frac{d}{d\theta(m)} \mathbf{L}[\theta] \mathbf{L}[\theta]^{-1} \mathbf{R}[\theta] + \mathbf{L}[\theta]^{-1} \frac{d}{d\theta(m)} \mathbf{R}[\theta] \quad (6.56)$$

$$= - \mathbf{L}[\theta]^{-1} \mathbf{L}_m \mathbf{L}[\theta]^{-1} \mathbf{R}[\theta] + \mathbf{L}[\theta]^{-1} \mathbf{R}_m \quad (6.57)$$

Considering the equations of the form

$$d\xi(t) = \mathbf{F}(t, \xi(t), \theta(t))dt + \mathbf{G}(t, \xi(t), \theta(t))d\mathbf{B}(t) \quad (6.58)$$

$$d\theta(t) = d\varepsilon_{\theta(t)} \quad (6.59)$$

and the measurement equation is of the form

$$d\mathbf{z}(t) = \mathbf{h}(t, \xi(t))dt + d\mathbf{v}(t) \quad (6.60)$$

In fact, the state equations are linear in $\xi(t)$ and hence can be expressed as :-

$$d\xi(t) = \mathbf{F}(t, \theta(t))\xi(t)dt + \mathbf{G}(t, \theta(t))d\mathbf{B}(t) \quad (6.61)$$

$$d\theta(t) = d\varepsilon_{\theta(t)} \quad (6.62)$$

and the measurement equations are also linear in $\xi(t)$ and hence can be expressed as :-

$$d\mathbf{z}(t) = \mathbf{H}\xi(t)dt + d\mathbf{v}(t) \quad (6.63)$$

Equivalently, in the discretized form,

$$\xi_{n+1} = (\mathbf{I} + \Delta \mathbf{F}_n(\theta_n))\xi_n + \mathbf{G}_n(\theta_n)\mathbf{w}_{n+1} \quad (6.64)$$

$$\theta_{n+1} = \theta_n + \varepsilon_{n+1} \quad (6.65)$$

$$\mathbf{z}_n = \mathbf{H}\xi_n + \mathbf{v}_n \quad (6.66)$$

Thus if the parameter $\theta_n = \theta$ are known, we would require a simple KF to estimate the state as :-

$$\hat{\xi}_{n|n} = \mathbb{E}(\xi_n | \mathbf{z}_k, k \leq n) \quad (6.67)$$

$$\hat{\xi}_{n+1|n} = \mathbb{E}(\xi_{n+1} | \mathbf{z}_k, k \leq n) \quad (6.68)$$

If however, θ is unknown, then we must use the EKF in the following form :-

$$\begin{bmatrix} \hat{\xi}_{n+1|n} \\ \hat{\theta}_{n+1|n} \end{bmatrix} = \begin{bmatrix} (\mathbf{I} + \Delta \mathbf{F}_n(\hat{\theta}_{n|n}))\hat{\xi}_{n|n} \\ \hat{\theta}_{n|n} \end{bmatrix} \quad (6.69)$$

$$\begin{bmatrix} \hat{\xi}_{n+1|n+1} \\ \hat{\theta}_{n+1|n+1} \end{bmatrix} = \begin{bmatrix} \hat{\xi}_{n+1|n} \\ \hat{\theta}_{n+1|n} \end{bmatrix} + \mathbf{K}_{n+1}(\mathbf{z}_{n+1} - \mathbf{H}\hat{\xi}_{n+1|n}) \quad (6.70)$$

$$\mathbf{P}_{n+1|n} = \mathbf{A}\mathbf{P}_{n|n}\mathbf{A}^T + \mathbf{G}_n(\hat{\theta}_{n|n})\Theta\mathbf{G}_n(\hat{\theta}_{n|n})^T \quad (6.71)$$

$$\mathbf{P}_{n+1|n+1} = (\mathbf{I} - \mathbf{K}_{n+1}\mathbf{H})\mathbf{P}_{n+1|n}(\mathbf{I} - \mathbf{K}_{n+1}\mathbf{H})^T + \mathbf{K}_{n+1}\mathbf{R}_v\mathbf{K}_{n+1}^T \quad (6.72)$$

where

$$\mathbf{K}_{n+1} = \mathbf{P}_{n+1|n}\mathbf{H}^T(\mathbf{R}_v + \mathbf{H}\mathbf{P}_{n+1|n}\mathbf{H}^T)^{-1} \quad (6.73)$$

$$\mathbf{A} = \begin{bmatrix} \mathbf{I}_d + \Delta \mathbf{F}_n(\hat{\theta}_{n|n}) & \Delta \mathbf{F}'_n(\hat{\theta}_{n|n})(\mathbf{I} \otimes \hat{\xi}_{n|n}) \\ \mathbf{0} & \mathbf{I}_p \end{bmatrix} \quad (6.74)$$

The use of state estimation for measurement techniques in real system is as follows :- Suppose a transmission line is not operating satisfactorily owing to noise. For example, it may cause the voltage supply coming from the mains to fluctuate a great deal. Then we require to introduce control terms along the line. Since we do not have direct access to the line voltage/current but only to its real EKF estimate, we can design a feedback controller that computes the error between the desired state $\hat{\xi}_d(t)$ (i.e. the desire line voltage and current with $\hat{\xi}(t)$) and its true EKF estimate $\hat{\xi}(t)$ into the line dynamics. Such a feedback control will result in modified state dynamics of the form

$$d\xi(t) = \mathbf{F}(t, \theta(t))\xi(t)dt + \mathbf{G}(t, \theta(t))d\mathbf{B}(t) + \mathbf{K}_c(\xi_d(t) - \hat{\xi}(t)) \quad (6.75)$$

or equivalently in the discrete-time domain, we have :-

$$\xi_{n+1} = (\mathbf{I} + \Delta \mathbf{F}_n(\theta))\xi_n + \mathbf{G}_n(\theta)\mathbf{w}_{n+1} + \mathbf{K}_c(n)(\xi_{dn} - \hat{\xi}_{n|n}) \quad (6.76)$$

The feedback control coefficient $\mathbf{K}_c(n)$ is adaptively or on a block processing basis controller to minimize $\mathbb{E}\|\xi_{d(n+1)} - \xi_{n+1}\|^2$. For example, the noiseless dynamics of ξ_{dn} is $\hat{\xi}_{d(n+1)} = (\mathbf{I} + \Delta \mathbf{F}_n(\theta))\xi_{dn}$ and hence,

$$\xi_{d(n+1)} - \xi_{n+1} = (\mathbf{I} + \Delta \mathbf{F}_n(\theta))(\xi_{dn} - \xi_n) - \mathbf{G}_n(\theta)\mathbf{w}_{n+1} - \mathbf{K}_c(n)(\xi_{dn} - \hat{\xi}_{n|n}) \quad (6.77)$$

where

$$\hat{\xi}_{n+1|n+1} = (\mathbf{I} + \Delta \mathbf{F}_n(\theta))\hat{\xi}_{n|n} + \mathbf{K}(n+1)(\mathbf{H}\xi_{n+1} + \mathbf{v}_{n+1} - \mathbf{H}(\mathbf{I} + \Delta \mathbf{F}_n(\theta))\hat{\xi}_{n|n}) \quad (6.78)$$

$$\begin{aligned} &= (\mathbf{I} + \Delta \mathbf{F}_n(\theta))\hat{\xi}_{n|n} + \mathbf{K}(n+1)(\mathbf{H}((\mathbf{I} + \Delta \mathbf{F}_n(\theta))\xi_n + \mathbf{G}_n(\theta)\mathbf{w}_{n+1} + \mathbf{v}_{n+1}) \\ &\quad - \mathbf{H}(\mathbf{I} + \Delta \mathbf{F}_n(\theta))\hat{\xi}_{n|n}) \end{aligned} \quad (6.79)$$

$$\begin{aligned} &= (\mathbf{I} + \Delta \mathbf{F}_n(\theta))\hat{\xi}_{n|n} + \mathbf{K}(n+1)\mathbf{H}(\mathbf{I} + \Delta \mathbf{F}_n(\theta))(\xi_n - \hat{\xi}_{n|n}) \\ &\quad + \mathbf{K}(n+1)\mathbf{G}_n(\theta)\mathbf{w}_{n+1} + \mathbf{K}(n+1)\mathbf{v}_{n+1} \end{aligned} \quad (6.80)$$

Thus

$$\begin{aligned} \xi_{d(n+1)} - \hat{\xi}_{n+1|n+1} &= (\mathbf{I} + \Delta \mathbf{F}_n(\theta))(\xi_{dn} - \hat{\xi}_{n|n}) - \mathbf{K}(n+1)\mathbf{H}(\mathbf{I} + \Delta \mathbf{F}_n(\theta))(\xi_n - \hat{\xi}_{n|n}) \\ &\quad - \mathbf{K}(n+1)\mathbf{G}_n(\theta)\mathbf{w}_{n+1} - \mathbf{K}(n+1)\mathbf{v}_{n+1} \end{aligned} \quad (6.81)$$

From these two coupled linear stochastic difference equations (Chapter 1.6) for the two kind of error, trajectory tracker error $(\xi_{dn} - \xi_n)$ and state estimation error $(\xi_{dn} - \hat{\xi}_{n|n})$, we can in principle compute $\sum_n \mathbb{E}\|(\xi_{dn} - \xi_n)\|^2$ and $\sum_n \mathbb{E}\|(\xi_{dn} - \hat{\xi}_{n|n})\|^2$ and choose the feedback controller coefficient $\mathbf{K}_c(n)$ to minimize some weighted combination in these two error energies.

The measurement model consists of measuring the line voltage and current at the spatial points z_1, \dots, z_m . so that this model becomes

$$d\xi_{v,n}(t) = v(t, z_n)dt + dw_{v,n}(t), \quad n = 1, 2, \dots, m \quad (6.82)$$

$$d\xi_{i,n}(t) = i(t, z_n)dt + dw_{i,n}(t), \quad n = 1, 2, \dots, m \quad (6.83)$$

Now noting that $v(t, z_n)$ and $i(t, z_n)$ can be expressed as linear combinations of the

Fourier series components of the line voltage and current, i.e.

$$v(t, z_n) = \sum_n v_n(t) \exp(j2\pi n z_n / d), \quad n = 1, 2, \dots, m \quad (6.84)$$

$$i(t, z_n) = \sum_n i_n(t) \exp(j2\pi n z_n / d), \quad n = 1, 2, \dots, m \quad (6.85)$$

We can separate this into real and imaginary components and then express the measurement model in vector form as :-

$$d\mathbf{z}(t) = (\mathbf{H}_1 \xi_R(t) + \mathbf{H}_2 \xi_I(t)) dt + \mathbf{v}(t) = \mathbf{H} \boldsymbol{\eta}(t) dt + d\mathbf{v}(t) \quad (6.86)$$

where $\mathbf{z}(t) = [\xi_{v,1}(t), \dots, \xi_{v,m}(t), \xi_{i,1}(t), \dots, \xi_{i,m}(t)]^T$ is a $2m \times 1$ real vector.

$$\mathbf{H} = [\mathbf{H}_1, \mathbf{H}_2, \mathbf{0}] \quad (6.87)$$

where the non-zero matrix elements of $\mathbf{H}_1, \mathbf{H}_2$ are $\cos(2\pi n \xi_n / d), \sin(2\pi n \xi_n / d)$. Recall that $\boldsymbol{\eta}(t)$ is the extended state vector $[\xi_R(t)^T, \xi_I(t)^T, \boldsymbol{\theta}(t)^T]^T$ with $\xi_R(t)$ being built out of the real parts of the Fourier series components $v_n(t), i_n(t)$ of the line voltage and current and $\xi_I(t)$ being built out of their imaginary parts.

6.1.2 Modeling of NTL using Frequency Domain Analysis

The line voltage $V(\omega, z)$ and current $I(\omega, z)$ are the Fourier transform of $v(t, z)$ and current $i(t, z)$ and can be expanded into an infinite set of spatial harmonics [128] as follows :-

$$V(\omega, z) = \sum_n e^{-\gamma(\omega)z} \times V_n(\omega) \times e^{j2\pi n z / d} \quad (6.88)$$

$$I(\omega, z) = \sum_n e^{-\gamma(\omega)z} \times I_n(\omega) \times e^{j2\pi n z / d} \quad (6.89)$$

where $\gamma(\omega)$ is propagation constant as :-

$$\gamma(\omega) = \sqrt{[R(\omega, z) + j\omega L(\omega, z)][G(\omega, z) + j\omega C(\omega, z)]} \quad (6.90)$$

(6.1)-(6.2) can be expressed in frequency domain using Fourier transform as :-

$$-\frac{d}{dz}V(\omega, z) = [R(z) + j\omega L(z)]I(\omega, z) + W_v(\omega, z) \quad (6.91)$$

$$-\frac{d}{dz}I(\omega, z) = [G(z) + j\omega C(z)]V(\omega, z) + W_i(\omega, z) \quad (6.92)$$

where

$$Z(z) = Z(z|\theta) = R(z|\theta) + j\omega L(z|\theta) = \sum_n Z_n(\omega|\theta)e^{j2\pi n z/d}$$

$$Z_n(\omega|\theta) = R_n(\theta) + j\omega L_n(\theta).$$

Similarly,

$$Y(z) = Y(z|\theta) = G(z|\theta) + j\omega C(z|\theta) = \sum_n Y_n(\omega|\theta)e^{j2\pi n z/d}$$

$$Y_n(\omega|\theta) = G_n(\theta) + j\omega C_n(\theta).$$

Substituting the Fourier series expansion of the distributed parameters (6.3)-(6.6) along with (6.88) and (6.89) into (6.91) and (6.92). By equating the coefficients of both sides, we get :-

$$\left(\gamma(\omega) - j\frac{2\pi n}{d}\right)V_n(\omega) = \sum_k Z_{n-k}(\omega|\theta)I_k(\omega) + W_{v,n}(\omega) \quad (6.93)$$

$$\left(\gamma(\omega) - j\frac{2\pi n}{d}\right)I_n(\omega) = \sum_k Y_{n-k}(\omega|\theta)V_k(\omega) + W_{i,n}(\omega) \quad (6.94)$$

Here, $V_n(\omega)$, $I_n(\omega)$, $Z_{n-k}(\omega|\theta)$ and $Y_{n-k}(\omega|\theta)$ are periodic with total samples $2N + 1$. Now, perturbation theory is implemented to voltage ($V_n(\omega)$) and current ($I_n(\omega)$) to account the nonlinearity of the transmission line. Expanding the line voltage and current by adding σ as a perturbation parameter, we have :-

$$V_n(\omega) = V_n^{(0)}(\omega) + \sigma V_n^{(1)}(\omega) + \sigma^2 V_n^{(2)}(\omega) + \dots \quad (6.95)$$

$$I_n(\omega) = I_n^{(0)}(\omega) + \sigma I_n^{(1)}(\omega) + \sigma^2 I_n^{(2)}(\omega) + \dots \quad (6.96)$$

where $V_n^{(0)}(\omega)$ and $I_n^{(0)}(\omega)$ are the line voltage and current with $\sigma = 0$ respectively, i.e. linear terms, whereas $\sigma V_n^{(1)}(\omega)$ and $\sigma I_n^{(1)}(\omega)$ respectively represent the perturbation of voltage and current caused by non-linearity. Substituting (6.95) and (6.96) into (6.93)

and (6.94) and equating the coefficients of σ^0 and σ^1 terms, we have

$$(\gamma(\omega)\mathbf{I} - j\mathbf{D}) \mathbf{V}^{(0)}(\omega) = \mathbf{Z}(\omega|\theta) \mathbf{I}^{(0)}(\omega) \quad (6.97)$$

$$(\gamma(\omega)\mathbf{I} - j\mathbf{D}) \mathbf{I}^{(0)}(\omega) = \mathbf{Y}(\omega|\theta) \mathbf{V}^{(0)}(\omega) \quad (6.98)$$

Now, the voltage and current Fourier series vectors and the line impedance and admittance Fourier series matrices are defined as :-

$$\mathbf{V}(\omega) = \left(\left(V(\omega) \right) \right)_{-N}^{+N} \quad (6.99)$$

$$\mathbf{I}(\omega) = \left(\left(I(\omega) \right) \right)_{-N}^{+N} \quad (6.100)$$

$$\mathbf{Z}(\omega|\theta) = \left(\left(Z_{n-k}(\omega|\theta) \right) \right)_{-N}^{+N} \quad (6.101)$$

$$\mathbf{Y}(\omega|\theta) = \left(\left(Y_{n-k}(\omega|\theta) \right) \right)_{-N}^{+N} \quad (6.102)$$

(6.97) and (6.98) can further be organized in the form of a matrix eigenvalue problem for the propagation constant $\gamma(\omega)$ (eigenvalue) and voltage-current Fourier series vector (eigenvector) which is used as measurement vector during the estimation process in KF and EKF method. In matrix form, these equations can be written as :-

$$\begin{bmatrix} j\mathbf{D} - \gamma(\omega) & \mathbf{Z}(\omega|\theta) \\ \mathbf{Y}(\omega|\theta) & j\mathbf{D} - \gamma(\omega) \end{bmatrix} \otimes I_n \times \begin{bmatrix} \mathbf{V}(\omega) \\ \mathbf{I}(\omega) \end{bmatrix} = 0 \quad (6.103)$$

For simulations, measurements have been done using (6.103).

6.1.3 State and Parameter Estimation for Transmission Line Circuit

To implement the state estimation technique for NTL, the state-space model in (6.42) needs to be discretized. The first-order exponential method is used to discretize the model. The discrete model of the NTL is given in (6.104) and (6.105).

$$\mathbf{x}_{n+1} = \mathbf{F}_n \mathbf{x}_n + \mathbf{B}_n \mathbf{u}_n + \mathbf{G}_n \mathbf{w}_n \quad (6.104)$$

$$\mathbf{z}_n = \mathbf{H}_n \mathbf{x}_n + \mathbf{v}_n \quad (6.105)$$

where

$$\mathbf{F}_n = \begin{bmatrix} 1 - T_s \mathbf{C}[\theta]^{-1} \mathbf{G}[\theta] & -jT_s \mathbf{D} \\ -jT_s \mathbf{D} & 1 - T_s \mathbf{L}[\theta]^{-1} \mathbf{R}[\theta] \end{bmatrix}, \mathbf{B}_n = [1, 1]^T,$$

$$\mathbf{G}_n = \begin{bmatrix} \mathbf{C}[\theta]^{-1} & \mathbf{0} \\ \mathbf{0} & \mathbf{L}[\theta]^{-1} \end{bmatrix}, \mathbf{H}_n = \begin{bmatrix} 1 & 0 \\ 0 & 1 \end{bmatrix}.$$

\mathbf{x}_n denote the state vector as $\mathbf{x}_n = [V_n, I_n]^T$. Here \mathbf{u}_n is the input vector. \mathbf{w}_n and \mathbf{v}_n are zero mean Gaussian noise in the state vector with covariance matrix \mathbf{Q}_n and in the measurement vector with covariance matrix \mathbf{R}_n , respectively. The state model is written as :-

$$\begin{bmatrix} \mathbf{V}_{n+1} \\ \mathbf{I}_{n+1} \end{bmatrix} = \begin{bmatrix} 1 - T_s \mathbf{C}[\theta]^{-1} \mathbf{G}[\theta] & -jT_s \mathbf{D} \\ -jT_s \mathbf{D} & 1 - T_s \mathbf{L}[\theta]^{-1} \mathbf{R}[\theta] \end{bmatrix} \begin{bmatrix} \mathbf{V}_n \\ \mathbf{I}_n \end{bmatrix} + \begin{bmatrix} \mathbf{C}[\theta]^{-1} & \mathbf{0} \\ \mathbf{0} & \mathbf{L}[\theta]^{-1} \end{bmatrix} \begin{bmatrix} \mathbf{w}_{i,n} \\ \mathbf{w}_{v,n} \end{bmatrix} \quad (6.106)$$

$$\mathbf{z}_n = \begin{bmatrix} 1 & 0 \\ 0 & 1 \end{bmatrix} \begin{bmatrix} \mathbf{V}_n \\ \mathbf{I}_n \end{bmatrix} + \begin{bmatrix} \mathbf{v}_{1n} \\ \mathbf{v}_{2n} \end{bmatrix} \quad (6.107)$$

where T_s is the sampling time. \mathbf{v}_{1n} and \mathbf{v}_{2n} are the measurement vector of line voltage and line current respectively. As the equation (6.106) is a linear estimation problem, KF has been used to estimate line voltage and line current. A fourth-order parameter vector $\theta_n = [R_n, L_n, C_n, G_n]^T$ is defined for parameter identification. The parameters to be estimated must be added in (6.106) to obtain the augmented matrix as :-

$$\mathbf{x}_n^a = [\mathbf{x}_n^T, \theta_n^T]^T \quad (6.108)$$

The augmented state model is :-

$$\mathbf{x}_{n+1}^a = \mathbf{F}_n^a \mathbf{x}_n^a + \mathbf{B}_n^a \mathbf{u}_n + \mathbf{G}_n^a \mathbf{w}_n^a \quad (6.109)$$

$$\mathbf{z}_n^a = \mathbf{H}_n^a \mathbf{x}_n^a + \mathbf{v}_n^a \quad (6.110)$$

where

$$\mathbf{x}_n^a = \left[V_n, I_n, R_n, L_n, C_n, G_n \right]^T, \mathbf{B}_n^a = \left[1, 1, 0, 0, 0, 0 \right]^T,$$

$$\mathbf{G}_n^a = \begin{bmatrix} \mathbf{C}[\theta]^{-1} & \mathbf{0} & 0 & 0 & 0 & 0 \\ \mathbf{0} & \mathbf{L}[\theta]^{-1} & 0 & 0 & 0 & 0 \\ 0 & 0 & 0 & 0 & 0 & 0 \\ 0 & 0 & 0 & 0 & 0 & 0 \\ 0 & 0 & 0 & 0 & 0 & 0 \\ 0 & 0 & 0 & 0 & 0 & 0 \end{bmatrix}, \mathbf{w}_n^a = \begin{bmatrix} \mathbf{w}_x^T \\ \mathbf{w}_\theta^T \end{bmatrix}.$$

Now, \mathbf{F}_n^a is nonlinear function of \mathbf{x}_n and θ_n . Therefore, EKF can be used to linearize \mathbf{F}_n matrix using Jacobian transform as :-

$$\mathbf{F}_n^a = \begin{bmatrix} \frac{df_1}{dx_1} & \frac{df_1}{dx_2} & \frac{df_1}{d\theta_1} & \frac{df_1}{d\theta_2} & \frac{df_1}{d\theta_3} & \frac{df_1}{d\theta_4} \\ \frac{df_2}{dx_1} & \frac{df_2}{dx_2} & \frac{df_2}{d\theta_1} & \frac{df_2}{d\theta_2} & \frac{df_2}{d\theta_3} & \frac{df_2}{d\theta_4} \\ \frac{df_3}{dx_1} & \frac{df_3}{dx_2} & \frac{df_3}{d\theta_1} & \frac{df_3}{d\theta_2} & \frac{df_3}{d\theta_3} & \frac{df_3}{d\theta_4} \\ \frac{df_4}{dx_1} & \frac{df_4}{dx_2} & \frac{df_4}{d\theta_1} & \frac{df_4}{d\theta_2} & \frac{df_4}{d\theta_3} & \frac{df_4}{d\theta_4} \\ \frac{df_5}{dx_1} & \frac{df_5}{dx_2} & \frac{df_5}{d\theta_1} & \frac{df_5}{d\theta_2} & \frac{df_5}{d\theta_3} & \frac{df_5}{d\theta_4} \\ \frac{df_6}{dx_1} & \frac{df_6}{dx_2} & \frac{df_6}{d\theta_1} & \frac{df_6}{d\theta_2} & \frac{df_6}{d\theta_3} & \frac{d\phi_6}{d\theta_4} \end{bmatrix} \quad (6.111)$$

$$\mathbf{F}_n^a = \begin{bmatrix} 1+T_s(\mathbf{C}[\theta]^{-1}\mathbf{G}_m - \mathbf{C}[\theta]^{-1}\mathbf{C}_m\mathbf{C}[\theta]^{-1}\mathbf{G}[\theta]) & 0 & 0 & 0 & 0 & 0 \\ 0 & 1+T_s(\mathbf{L}[\theta]^{-1}\mathbf{R}_m - \mathbf{L}[\theta]^{-1}\mathbf{L}_m\mathbf{L}[\theta]^{-1}\mathbf{R}[\theta]) & 0 & 0 & 0 & 0 \\ 0 & 0 & 0 & 0 & 0 & 0 \\ 0 & 0 & 0 & 0 & 0 & 0 \\ 0 & 0 & 0 & 0 & 0 & 0 \\ 0 & 0 & 0 & 0 & 0 & 1 \end{bmatrix} \quad (6.112)$$

$$\mathbf{H}_n^a = \begin{bmatrix} 1 & 0 & 0 & 0 & 0 & 0 \\ 0 & 1 & 0 & 0 & 0 & 0 \end{bmatrix} \quad (6.113)$$

$$\mathbf{v}_n^a = \left[\mathbf{v}_x^T, \mathbf{v}_\theta^T \right]^T \quad (6.114)$$

6.1.4 Simulation Results

MATLAB software has been used for simulation of derived equations. As compared to the other line losses, the power loss insulation resistance is small, so conductance G can be neglected. The objective is to estimate line resistance R , reactance X and susceptance B based on measurements up to time n . The per unit (p.u.) parameters values used for simulations are: $R_0 = 1.92 \Omega/\text{Km}$, $X_0 = 39.168 \Omega/\text{Km}$, $B_0 = 1.65 \times 10^{-3} \text{S}/\text{Km}$ and $d = 1000$. The line voltage of NTL is estimated using KF and RLS [129] methods (Chapter 1.9) for a 500 kV, 50 Hz transmission line. The white Gaussian

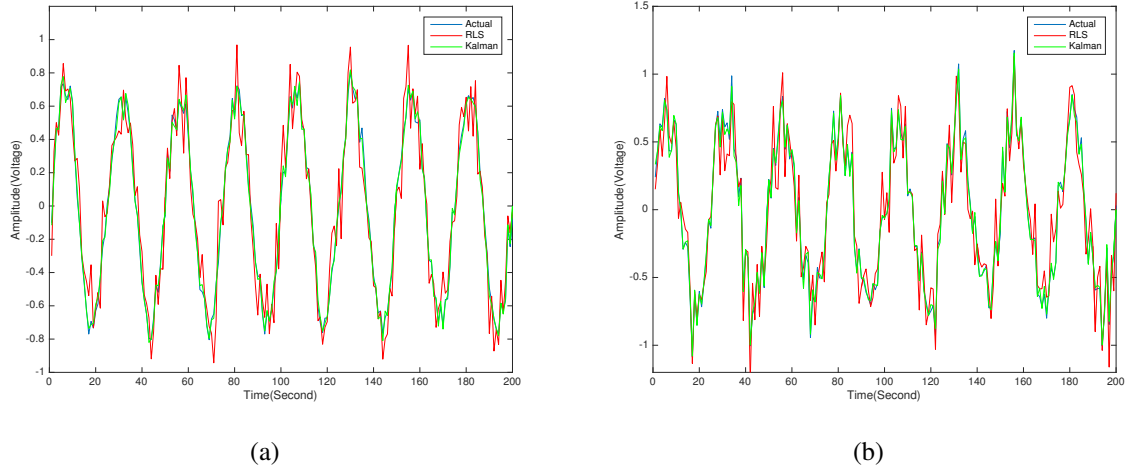


Figure 6.2: Voltage estimation using KF and RLS methods with Gaussian noise input, (a) $\mu=0$, $\sigma^2 = 0.1$, (b) $\mu=0$, $\sigma^2 = 0.5$.

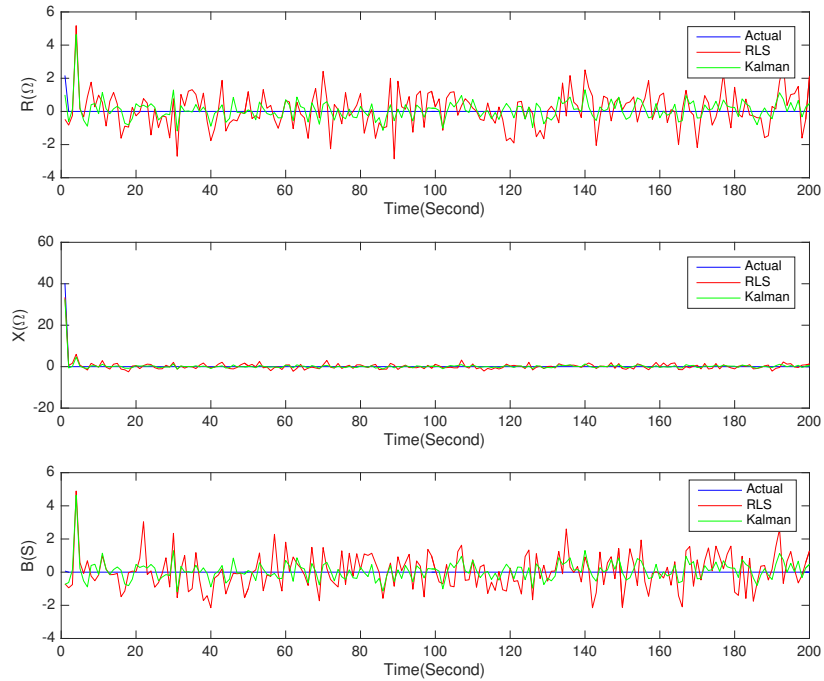
Table 6.1: Comparison of RMSE for R, X, B using RLS and EKF methods.

S. No.	Gaussian noise at input source	Parameter	RMSE using RLS method	RMSE using EKF method
1	$\mu = 0$ $\sigma^2 = 0.0$	$R(\Omega)$	0.5730	0.3775
		$X(\Omega)$	0.6108	0.3803
		$B(S)$	0.5898	0.3780
2	$\mu = 0$ $\sigma^2 = 0.01$	$R(\Omega)$	0.6031	0.3853
		$X(\Omega)$	0.6347	0.3920
		$B(S)$	0.5970	0.3849
3	$\mu = 0$ $\sigma^2 = 0.1$	$R(\Omega)$	0.6155	0.3902
		$X(\Omega)$	0.6778	0.4052
		$B(S)$	0.6678	0.4602
4	$\mu = 0$ $\sigma^2 = 0.5$	$R(\Omega)$	0.7166	0.4287
		$X(\Omega)$	0.7058	0.4135
		$B(S)$	0.7785	0.5091

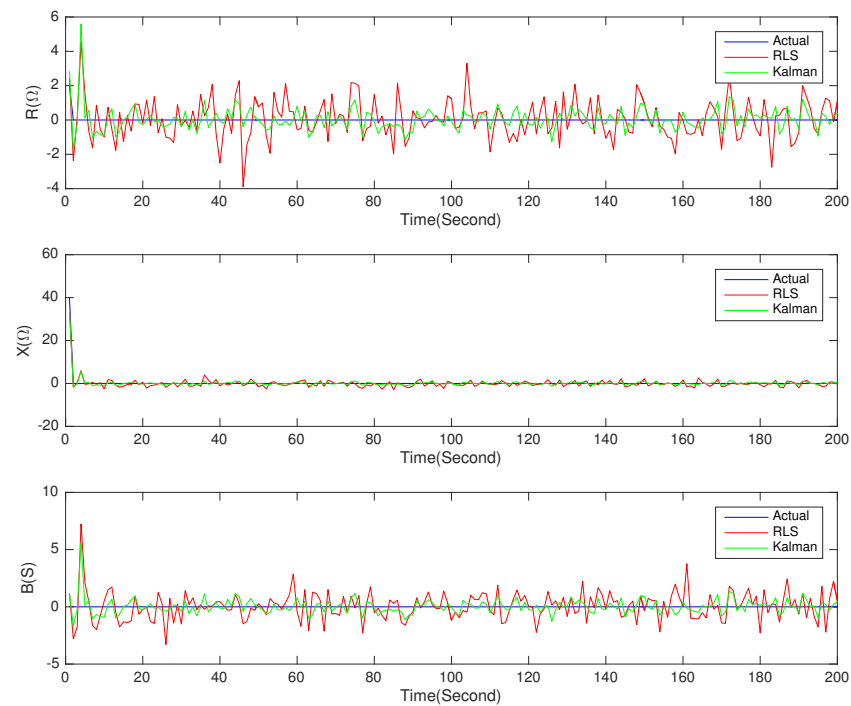
noise of zero mean and different variances have been used for estimation. The process noise and measurement noise used are white Gaussian noise with zero mean and variances 0.001 and 0.1 respectively. The line voltages of NTL circuit have been estimated using KF and RLS methods for different noisy inputs are shown in Figure 6.2. Estimated values have been compared with theoretical value obtained by solving the eigenvalue problem given in equation (6.103). Further, we estimate the distributed parameters of the line. Figure 6.3 shows the estimation of different parameters.

Remarks

1. True EKF is only a suboptimal estimator based on second order truncated Taylor



(a)



(b)

Figure 6.3: Parameters estimation using EKF and RLS methods with Gaussian noise input, (a) $\mu=0, \sigma^2=0.1$, (b) $\mu=0, \sigma^2=0.5$.

Table 6.2: Comparison of standard deviation of parameter errors (σ_e) for R, X, B using RLS and EKF methods.

S. No.	Gaussian noise at input source	Parameter	σ_e using RLS method	σ_e using EKF method
1	$\mu = 0$ $\sigma^2 = 0.0$	R(Ω)	0.832	0.177
		X(Ω)	0.041	0.013
		B(S)	0.788	0.178
2	$\mu = 0$ $\sigma^2 = 0.01$	R(Ω)	1.102	0.255
		X(Ω)	0.090	0.013
		B(S)	0.990	0.250
3	$\mu = 0$ $\sigma^2 = 0.1$	R(Ω)	1.201	0.356
		X(Ω)	0.803	0.045
		B(S)	1.102	0.530
4	$\mu = 0$ $\sigma^2 = 0.5$	R (Ω)	1.504	0.482
		X(Ω)	1.995	0.090
		B (S)	2.503	0.804

Table 6.3: Comparison of SNR (dB) and RMSE for line voltage (v) estimation using KF and RLS methods.

Gaussian noise at input source with $\mu=0$	SNR using KF method	SNR using RLS method	RMSE using KF method	RMSE using RLS method
$\sigma^2 = 0$	41.080	36.975	0.6831	0.7259
$\sigma^2 = 0.1$	40.505	35.858	0.7239	0.9598
$\sigma^2 = 0.5$	37.508	35.192	0.8712	1.0128
$\sigma^2 = 1.0$	33.877	32.687	0.9549	1.2139

expression but when a very large number of random effects contribute to the dynamics, for example, a very large number of Brownian motions in different Fourier bins mode, then the signals by the central limit theorem are the approximately Gaussian and further, when the noise variance is small and the signals are passed through nonlinearly then the output signals equal approximately non-random quantity plus small Gaussian fluctuations *i.e.*

$$\mathbf{f}(x(t)) \ll \mathbf{f}(\mathbb{E}x(t) + \delta x(t)) \simeq \mathbf{f}(\mathbb{E}x(t)) + \mathbf{f}'(\mathbb{E}x(t))\delta x(t) \quad (6.115)$$

So that $\mathbf{f}(x(t))$ can be treated as being approximately Gaussian as the EKF method represents a good approximation of the KF method which has good convergence results.

2. State and measurement model equations are:-

$$\mathbf{x}_{n+1} = \mathbf{f}(\mathbf{x}_n) + \mathbf{w}_{n+1} \quad , \mathbf{x}_n \in \mathbb{R}^{d \times 1} \quad (6.116)$$

$$\mathbf{z}_n = \mathbf{h}(\mathbf{x}_n) + \mathbf{v}_n \quad (6.117)$$

Consider the EKF

$$\hat{\mathbf{x}}_{n+1|n} = \mathbf{f}(\hat{\mathbf{x}}_{n|n}) \quad (6.118)$$

$$\hat{\mathbf{x}}_{n+1|n+1} = \hat{\mathbf{x}}_{n+1|n} + \mathbf{K}_{n+1}(\mathbf{z}_{n+1} - \mathbf{h}(\hat{\mathbf{x}}_{n+1|n})) \quad (6.119)$$

$$= \mathbf{f}(\hat{\mathbf{x}}_{n|n}) + \mathbf{K}_{n+1}(\mathbf{h}(\mathbf{x}_{n+1}) - \mathbf{h}(\hat{\mathbf{x}}_{n+1|n}) + \mathbf{v}_{n+1}) \quad (6.120)$$

$$= \mathbf{f}(\hat{\mathbf{x}}_{n|n}) + \mathbf{K}_{n+1}(\mathbf{h}(\hat{\mathbf{x}}_{n+1|n} + \mathbf{e}_{n+1|n}) - \mathbf{h}(\hat{\mathbf{x}}_{n+1|n}) + \mathbf{v}_{n+1}) \quad (6.121)$$

$$\simeq \mathbf{f}(\hat{\mathbf{x}}_{n|n}) + \mathbf{K}_{n+1}(\mathbf{h}'(\mathbf{x}_{n+1|n})\mathbf{e}_{n+1|n} + \mathbf{v}_{n+1}) \quad (6.122)$$

$$\mathbf{e}_{n+1|n} = \mathbf{x}_{n+1} - \hat{\mathbf{x}}_{n+1|n} \simeq \mathbf{f}(\mathbf{x}_n) + \mathbf{w}_{n+1} - \mathbf{f}(\hat{\mathbf{x}}_{n|n}) \quad (6.123)$$

So

$$\mathbf{e}_{n+1|n+1} = \mathbf{x}_{n+1} - \hat{\mathbf{x}}_{n+1|n+1} \quad (6.124)$$

$$= \mathbf{f}(\hat{\mathbf{x}}_{n|n} + \mathbf{e}_{n|n}) + \mathbf{w}_{n+1} - \hat{\mathbf{x}}_{n+1|n+1} \quad (6.125)$$

$$\simeq \mathbf{f}'(\hat{\mathbf{x}}_{n|n})\mathbf{e}_{n|n} + \mathbf{w}_{n+1} - \mathbf{K}_{n+1}(\mathbf{h}'(\mathbf{f}(\hat{\mathbf{x}}_{n|n}))) (\mathbf{f}'(\hat{\mathbf{x}}_{n|n})\mathbf{e}_{n|n} + \mathbf{w}_{n+1}) + \mathbf{v}_{n+1} \quad (6.126)$$

or

$$\begin{aligned} \mathbf{e}_{n+1|n+1} &\approx \mathbf{f}'(\hat{\mathbf{x}}_{n|n}) - \mathbf{K}_{n+1} \mathbf{h}'(\mathbf{f}(\hat{\mathbf{x}}_{n|n})) \mathbf{f}'(\hat{\mathbf{x}}_{n|n}) \mathbf{e}_{n|n} \\ &+ (\mathbf{I} - \mathbf{K}_{n+1} \mathbf{h}'(\mathbf{f}(\hat{\mathbf{x}}_{n|n}))) \mathbf{w}_{n+1} - \mathbf{K}_{n+1} \mathbf{v}_{n+1} \end{aligned} \quad (6.127)$$

Suppose the nominal value of the state estimator $\hat{\mathbf{x}}_{n|n}$ is $\hat{\mathbf{x}}_0$ and the error covariance matrices $\mathbf{P}_{n+1|n}$ and $\mathbf{P}_{n|n}$ have converged to some constant values to the $\mathbf{K}_{n+1} \rightarrow \mathbf{K}_0$, Then the above recursion can be cast in the form (with $\mathbf{e}_n = \mathbf{e}_{n|n}$) :-

$$\mathbf{e}_{n+1} \approx (\mathbf{I} - \mathbf{K}_0 \mathbf{h}'(\mathbf{f}(\hat{\mathbf{x}}_0))) \mathbf{f}'(\hat{\mathbf{x}}_0) \mathbf{e}_n + (\mathbf{I} - \mathbf{K}_0 \mathbf{h}'(\mathbf{f}(\hat{\mathbf{x}}_0))) \mathbf{w}_{n+1} - \mathbf{K}_0 \mathbf{v}_{n+1} \quad (6.128)$$

It is clear that $\mathbf{e}_n \rightarrow 0$ approximately if the maximum magnitude eigenvalue of the matrix $(\mathbf{I} - \mathbf{K}_0 \mathbf{h}'(\mathbf{f}(\hat{\mathbf{x}}_0))) \mathbf{f}'(\hat{\mathbf{x}}_0)$ is smaller than unity. We have ensured this during our simulations by taking nominal values of $\hat{\mathbf{x}}_0$. The maximum magnitude eigenvalue of a matrix \mathbf{A} is also called its spectral radius and is given by $\rho(\mathbf{A}) = \lim_{n \rightarrow \infty} \|\mathbf{A}^n\|^{1/n} \leq \|\mathbf{A}\|$ where $\|\cdot\|$ denotes spectral norm. Hence, we can ensure stability of the EKF by forcing $\|(\mathbf{I} - \mathbf{K}_0 \mathbf{h}'(\mathbf{f}(\hat{\mathbf{x}}_0))) \mathbf{f}'(\hat{\mathbf{x}}_0)\| < 1$. This can be achieved by changing the Kalman gain matrix \mathbf{K}_0 slightly. This may equivalently be achieved by estimating the error \mathbf{e}_n (using a desire state) and giving a negative error feedback $(-\mathbf{K}_c \mathbf{e}_n)$ into the EKF method so that the dynamics of \mathbf{e}_n becomes (in the absence of noise):-

$$\mathbf{e}_{n+1} = (\mathbf{I} - \mathbf{K}_0 \mathbf{h}'(\mathbf{f}(\hat{\mathbf{x}}_0))) \mathbf{f}'(\hat{\mathbf{x}}_0) \mathbf{e}_n - \mathbf{K}_c \mathbf{e}_n \quad (6.129)$$

with the feedback control matrix \mathbf{K}_c being chosen so that $\rho((\mathbf{I} - \mathbf{K}_0 \mathbf{h}'(\mathbf{f}(\hat{\mathbf{x}}_0))) \mathbf{f}'(\hat{\mathbf{x}}_0) - \mathbf{K}_c) < 1$. Further denoting

$$\mathbf{A} = (\mathbf{I} - \mathbf{K}_0 \mathbf{h}'(\mathbf{f}(\hat{\mathbf{x}}_0))) \mathbf{f}'(\hat{\mathbf{x}}_0) - \mathbf{K}_c \quad (6.130)$$

$$\mathbf{B}_1 = \mathbf{I} - \mathbf{K}_0 \mathbf{h}'(\mathbf{f}(\hat{\mathbf{x}}_0)) \quad (6.131)$$

$$\mathbf{B}_2 = -\mathbf{K}_0 \quad (6.132)$$

We can write the estimation error evolution equation in the presence of noise as

$$\mathbf{e}_{n+1} = \mathbf{A} \mathbf{e}_n + \mathbf{B}_1 \mathbf{w}_{n+1} + \mathbf{B}_2 \mathbf{v}_{n+1} \quad (6.133)$$

which gives to noise contribution to \mathbf{e}_n as

$$\mathbf{e}_n = \sum_{k=0}^{n-1} \mathbf{A}^{n-k-1} (\mathbf{B}_1 \mathbf{w}_{k+1} + \mathbf{B}_2 \mathbf{v}_{k+1}) \quad (6.134)$$

which has variance of

$$\mathbb{E}[\|\mathbf{e}_n\|^2] = \sum_{k=0}^{n-1} \text{Tr}[\mathbf{A}^{n-k-1} (\mathbf{B}_1 \mathbf{Q} \mathbf{B}_1^T + \mathbf{B}_2 \mathbf{R} \mathbf{B}_2^T) \mathbf{A}^{T(n-k-1)}] \quad (6.135)$$

which is bounded above by

$$d \sum_{k=0}^{n-1} \|\mathbf{A}\|^{2(n-k-1)} \|\mathbf{B}_1 \mathbf{Q} \mathbf{B}_1^T + \mathbf{B}_2 \mathbf{R} \mathbf{B}_2^T\| = d \left[\frac{1 - \|\mathbf{A}\|^{2n}}{1 - \|\mathbf{A}\|^2} \right] \|\mathbf{B}_1 \mathbf{Q} \mathbf{B}_1^T + \mathbf{B}_2 \mathbf{R} \mathbf{B}_2^T\| \quad (6.136)$$

are assuming stability so that $\|\mathbf{A}\| < 1$, we get

$$\lim_{n \rightarrow \infty} \mathbb{E}[\|\mathbf{e}_n\|^2] \leq \frac{d}{1 - \|\mathbf{A}\|^2} \|\mathbf{B}_1 \mathbf{Q} \mathbf{B}_1^T + \mathbf{B}_2 \mathbf{R} \mathbf{B}_2^T\| \quad (6.137)$$

3. Our estimation shows that the upper bound is very small as compared to $\|\hat{\mathbf{x}}_{n|n}\|^2$ so that noise does not significantly affect the convergence.
4. Inductance of the line is less prone to noise than the R, G values for the following reason. The line equation in the frequency domain is

$$\frac{d}{dz} V(\omega, z) = -(R + j\omega L)I(\omega, z) + W_v(\omega, z) \quad (6.138)$$

Owing to the factor of w in the numerator and w^2 in the denominator in the expression for \hat{L} , it is clear that if we operate at high frequencies, \hat{L} will have a smaller variance related to L^2 , as compared to that of \hat{R} relative to R . Specially, substituting for $V'(\omega, z)$ is the expression for \hat{R}, \hat{L} gives

$$\hat{R} = \left[\frac{\sum \text{Re}[\overline{I(\omega, z)}] ((R + j\omega L)I(\omega, z) + E_v(\omega, z))}{\sum |I(\omega, z)|^2} \right] \quad (6.139)$$

$$= R + \left[\frac{\sum |I(\omega, z)|^2 \text{Re}[\overline{I(\omega, z)}] E_v(\omega, z)}{\sum |I(\omega, z)|^2} \right] \quad (6.140)$$

$$\hat{L} = \left[\frac{\sum \omega \text{Im}[\overline{I(\omega, z)}] ((R + j\omega L)I(\omega, z) + E_v(\omega, z))}{\sum \omega^2 |I(\omega, z)|^2} \right] \quad (6.141)$$

equivalently

$$\sum_{\omega, z} \text{Re}[\overline{I(\omega, z)} V'(\omega, z)] = \hat{R} \sum_{\omega, z} |I(\omega, z)|^2 \quad (6.142)$$

and

$$\sum_{\omega, z} \omega \text{Im}[\overline{I(\omega, z)} V'(\omega, z)] = \hat{L} \sum_{\omega, z} \omega^2 |I(\omega, z)|^2 \quad (6.143)$$

$$\hat{R} = \left[\frac{\sum_{\omega, z} \text{Re}[\overline{I(\omega, z)} V'(\omega, z)]}{\sum_{\omega, z} |I(\omega, z)|^2} \right] \quad (6.144)$$

$$\hat{L} = \left[\frac{\sum_{\omega, z} \omega \text{Im}[\overline{I(\omega, z)} V'(\omega, z)]}{\sum_{\omega, z} \omega^2 |I(\omega, z)|^2} \right] \quad (6.145)$$

$$= L + \left[\frac{\sum \omega \text{Im}[\overline{I(\omega, z)} E_v(\omega, z)]}{\sum \omega^2 |I(\omega, z)|^2} \right] \quad (6.146)$$

So,

$$\text{Var}(\hat{R} - R) \approx \sigma_{E_v}^2 / \sum |I(\omega, z)|^2 \quad (6.147)$$

$$\text{Var}(\hat{L} - L) \approx \sigma_{E_v}^2 / \sum \omega^2 |I(\omega, z)|^2 \quad (6.148)$$

where $E_v(\omega, z)$ is white noise with

$$\mathbb{E}[E_v(\omega, z) \overline{E_v(\omega', z')}] = \sigma_{E_v}^2 \delta_{\omega\omega'} \delta_{zz'} \quad (6.149)$$

Thus,

$$\frac{\text{Var}(\hat{R} - R)}{R^2} \ll \frac{\text{Var}(\hat{L} - L)}{L^2} \quad (6.150)$$

when ω varies over high frequencies for which $\omega L \gg R$.

6.1.5 Conclusions

In this chapter, KF and EKF methods have been applied for state and parameter estimation of non-uniform transmission line. For this, stochastic based state equations are derived using Telegrapher's equation for transmission line. Measurement equation is formed and measurements for estimation purpose have been obtained by solving the eigenvalue problem. Sparse matrix factorization using Kronecker product for Fourier unitary transform ease the mathematical implementation by providing compact representation. The state and parameters estimated using KF and EKF methods have been compared with RLS method. As the process noise and measurement noise are taken into account by KF and EKF

methods, they present better estimation than RLS method.

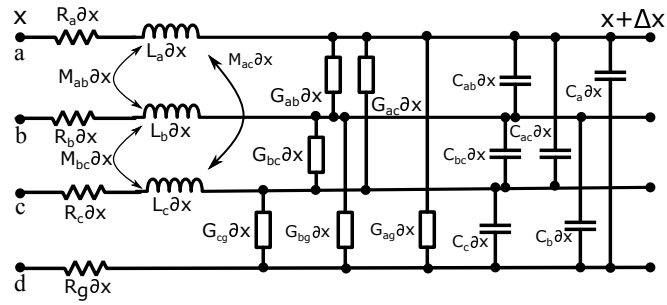


Figure 6.4: Circuit diagram of a three-phase transmission line.

6.2 State Estimation and Parameter Estimation of Three-Phase Transmission Line

6.2.1 Modeling of Three-Phase Transmission Line

A three-phase transmission line model is represented by a 3×3 matrix by assuming that ground has zero potential. An equivalent circuit of three-phase NTL is shown in Fig. 6.4. This circuit has been expressed in the form of differential equations using partial derivatives of phase voltages and phase currents. Segment x and $x + \Delta x$ are considered as sending-end and receiving-end terminal respectively. v_a, v_b, v_c are the phase voltages and i_a, i_b, i_c are the phase current respectively. Note that, phase voltage and current are the function of both time t and distance x . (6.151)-(6.156) are obtained by applying KCL in the circuit. They are :-

$$\frac{\partial}{\partial x} v_a + L_a(x) i'_a + M_{ab}(x) i'_b + M_{ac}(x) i'_c + R_a(x) i_a + R_g(x) (i_a + i_b + i_c) = w_{v_a} \quad (6.151)$$

$$\frac{\partial}{\partial x} v_b + L_b(x) i'_b + M_{ba}(x) i'_a + M_{bc}(x) i'_c + R_b(x) i_b + R_g(x) (i_a + i_b + i_c) = w_{v_b} \quad (6.152)$$

$$\frac{\partial}{\partial x} v_c + L_c(x) i'_c + M_{ca}(x) i'_a + M_{cb}(x) i'_b + R_c(x) i_c + R_g(x) (i_a + i_b + i_c) = w_{v_c} \quad (6.153)$$

$$\begin{aligned} & \frac{\partial}{\partial x} i_a + C_a(x) v'_a + C_{ab}(x) (v'_a - v'_b) + C_{ac}(x) (v'_a - v'_c) + G_{ag}(x) v_a \\ & + G_{ab}(x) (v_a - v_b) + G_{ac}(x) (v_a - v_c) = w_{i_a} \end{aligned} \quad (6.154)$$

$$\begin{aligned} & \frac{\partial}{\partial x} i_b + C_b(x) v'_b + C_{ba}(x) (v'_b - v'_a) + C_{bc}(x) (v'_b - v'_c) + G_{bg}(x) v_b \\ & + G_{ba}(x) (v_b - v_a) + G_{bc}(x) (v_b - v_c) = w_{i_b} \end{aligned} \quad (6.155)$$

$$\begin{aligned} & \frac{\partial}{\partial x} i_c + C_c(x) v'_c + C_{ca}(x) (v'_c - v'_a) + C_{cb}(x) (v'_c - v'_b) + G_{cg}(x) v_c \\ & + G_{ca}(x) (v_c - v_a) + G_{cb}(x) (v_c - v_b) = w_{i_c} \end{aligned} \quad (6.156)$$

where symbol ' represents the derivative *w.r.t.* time *t*. $R_j(x)$, $L_j(x)$ and $C_j(x)$ are resistance, self inductance and self capacitance of phase j respectively ($\forall j = a, b, c$). $M_{jk}(x)$ and $C_{jk}(x)$ are mutual inductance and mutual capacitance between phase j and k respectively ($\forall j, k = a, b, c$). Assuming that the absolute value of mutual inductance and mutual capacitance among phases a, b, c are equal. $G_{jk}(x)$ denotes conductance among phases a, b, c and ground g . $R_g(x)$ denotes resistance of ground.

Representing the phase impedance (Z_{abc}) and phase admittance (Y_{abc}) of a three-phase NTL as:-

$$Z_{abc} = \begin{bmatrix} Z_a & Z_{ab} & Z_{ac} \\ Z_{ab} & Z_b & Z_{bc} \\ Z_{ac} & Z_{bc} & Z_c \end{bmatrix}, Y_{abc} = j \begin{bmatrix} B_a & B_{ab} & B_{ac} \\ B_{ab} & B_b & B_{bc} \\ B_{ac} & B_{bc} & B_c \end{bmatrix} \quad (6.157)$$

where the off-diagonal terms represent the mutual impedance among the phases ab, ba, bc, cb, ac and ca . The phase impedance matrix (Ω/km) and admittance matrix (Ω^{-1}/km) has the following form :-

$$Z_j = R_j + jX_j \quad (6.158)$$

$$Y_j = jB_j \quad (6.159)$$

where $j = a, b, c, ab, bc, ac$. We neglect G_j term because it has small impact on the types of studies that use the model.

6.2.2 Modeling of Transposed/Untransposed Transmission Line

The model in the previous section can be used to represent either transposed or untransposed TL. Positive sequence quantities are used to represent transposed line. The phase quantities are converted into sequence quantities for this purpose. A zero-sequence currents and voltages are expressed as :-

$$i_0 = \frac{1}{3}(i_a + i_b + i_c) \quad (6.160)$$

$$v_0 = \frac{1}{3}(v_a + v_b + v_c) \quad (6.161)$$

Using (6.160)-(6.161) and (6.151)-(6.156) we obtain :-

$$\frac{\partial}{\partial x} v_a + (L_a(x) - M_{ab}(x))i'_a + 3M_{ab}(x)i'_0 + R_a(x)i_a + 3R_g(x)i_0 = w_{v_a} \quad (6.162)$$

$$\frac{\partial}{\partial x} v_b + (L_b(x) - M_{bc}(x))i'_b + 3M_{bc}(x)i'_0 + R_b(x)i_b + 3R_g(x)i_0 = w_{v_b} \quad (6.163)$$

$$\frac{\partial}{\partial x} v_c + (L_c(x) - M_{ca}(x))i'_c + 3M_{ca}(x)i'_0 + R_c(x)i_c + 3R_g(x)i_0 = w_{v_c} \quad (6.164)$$

$$\frac{\partial}{\partial x} i_a + C_a(x)v'_a + 3C_{ab}(x)(v'_a - v'_0) + G_{ag}(x)v_a + 3G_{ab}(x)(v_a - v_0) = w_{i_a} \quad (6.165)$$

$$\frac{\partial}{\partial x} i_b + C_b(x)v'_b + 3C_{bc}(x)(v'_b - v'_0) + G_{bg}(x)v_b + 3G_{ab}(x)(v_b - v_0) = w_{i_b} \quad (6.166)$$

$$\frac{\partial}{\partial x} i_c + C_c(x)v'_c + 3C_{ca}(x)(v'_c - v'_0) + G_{cg}(x)v_c + 3G_{ca}(x)(v_c - v_0) = w_{i_c} \quad (6.167)$$

Voltages and currents in the equation (6.162)-(6.167) are the function of line length x and time t , and their analysis is complicated due to presence of mutual effects among phase conductors and ground. Linear transformation of three-phase system into three independent single-phase circuit allows for removing these mutual effects. In order to de-couple phase quantities, a suitable transformation called Clarke transformation [130] is used to convert the phase quantities into sequence quantities. Clarke transformation matrix gives the relations between phase values with index a, b, c and values with sequence index $\alpha, \beta, 0$.

$$f_{\alpha\beta 0} = T^{-1} f_{abc} \quad (6.168)$$

$$\text{where } T = \begin{bmatrix} 1 & 1 & 1 \\ 1 & a^2 & a \\ 1 & a & a^2 \end{bmatrix}, \quad a = \exp(j\frac{2\pi}{3}).$$

(6.169)-(6.170) show the relationship between the phase voltages and currents and the sequence voltages and currents respectively.

$$V_{\alpha\beta 0} = T^{-1}V_{abc} \quad (6.169)$$

$$I_{\alpha\beta 0} = T^{-1}I_{abc} \quad (6.170)$$

where

$$V_{\alpha\beta 0} = \begin{bmatrix} V_{\alpha} \\ V_{\beta} \\ V_0 \end{bmatrix}, \quad I_{\alpha\beta 0} = \begin{bmatrix} I_{\alpha} \\ I_{\beta} \\ I_0 \end{bmatrix}, \quad V_{abc} = \begin{bmatrix} V_a \\ V_b \\ V_c \end{bmatrix}, \quad I_{abc} = \begin{bmatrix} I_a \\ I_b \\ I_c \end{bmatrix}$$

(6.171)-(6.172) show the relationship between the phase impedance/admittance matrix and the sequence impedance/ admittance matrix. The sequence impedance matrix is not diagonal for untransposed TL. This means that the positive sequence impedance depends on all three (positive, negative and zero) sequence components which increase the computation complexity. The sequence impedance/admittance matrix has the following form :-

$$Z_{\alpha\beta 0} = T^{-1}Z_{abc}T \quad (6.171)$$

$$Y_{\alpha\beta 0} = T^{-1}Y_{abc}T \quad (6.172)$$

where:

$$Z_{\alpha\beta 0} = \begin{bmatrix} Z_{\alpha} & 0 & 0 \\ 0 & Z_{\beta} & 0 \\ 0 & 0 & Z_0 \end{bmatrix}, Y_{\alpha\beta 0} = j \begin{bmatrix} B_{\alpha} & 0 & 0 \\ 0 & B_{\beta} & 0 \\ 0 & 0 & B_0 \end{bmatrix}$$

The following assumptions are taken for obtaining sequence quantities of transposed NTL as :-

$$\begin{aligned}
 L &= L_a = L_b = L_c, R = R_a = R_b = R_c, C = C_a = C_b = C_c, \\
 G &= G_{ab} = G_{ac} = G_{bc}, G_g = G_{ag} = G_{bg} = G_{cg}, \\
 M &= M_{ab} = M_{ac} = M_{bc} = M_{ba} = M_{cb} = M_{ca}, \\
 C_m &= C_{ab} = C_{ac} = C_{bc} = C_{ba} = C_{cb} = C_{ca}
 \end{aligned} \tag{6.173}$$

substituting (6.173), (6.169) and (6.170) into (6.162)-(6.167), we obtain the SDE for NTL. They are :-

$$\frac{\partial}{\partial x} v_i + L_i(x) i_i' + R(x) i_i = w_{v_i} \tag{6.174}$$

$$\frac{\partial}{\partial x} i_i + C(x) v_i' + G_g(x) v_i = w_{i_i} \tag{6.175}$$

where $i = \alpha, \beta, 0$. w_{v_i} and w_{i_i} are zero mean exponential correlation process. R_i , L_i , C_i and G_i denote the positive sequence resistance, inductance, capacitance and admittance respectively. These values are :-

$L_0 = L + 2M$, $L_\alpha = L_\beta = L - M$, $C_\alpha = C_\beta = C + 3C_m$, $R_0 = R + 3R_g$, $G_\alpha = G_\beta = 3G + G_g$. Now, considering ζ is the parameters R, L, C, G as :-

$$\zeta_i(x) = \zeta_i(x|\theta) = \sum_{m=1}^p \theta[m] \zeta_{i,m}(x) \tag{6.176}$$

Representing v_i , i_i , w_{v_i} and w_{i_i} in terms of spatial Fourier series as :-

$$\xi_i = \sum_n \xi_{i,n}(t) \exp\left(\frac{j2\pi nx}{d}\right) \tag{6.177}$$

where ξ denotes v, i, w_v, w_i . d is the total length of the transmission line.

Representing (6.177) in matrix form as :-

$$\xi_i(x) = \sum_N \xi_i(n) \mathbf{W}_N^{nx} \tag{6.178}$$

where $\xi_i(x)$ denotes N point DFT at $n = 0, \dots, (N - 1)$. Weight matrix (\mathbf{W}_N) is simply defined as :-

$$\mathbf{W}_N = e^{j2\pi/N} = \begin{bmatrix} \mathbf{W}_N^0 & \mathbf{W}_N^0 & \mathbf{W}_N^0 & \dots & \mathbf{W}_N^0 \\ \mathbf{W}_N^0 & \mathbf{W}_N^1 & \mathbf{W}_N^2 & \dots & \mathbf{W}_N^{N-1} \\ \vdots & \vdots & \vdots & \dots & \vdots \\ \mathbf{W}_N^0 & \mathbf{W}_N^{N-1} & \mathbf{W}_N^{2N-1} & \dots & \mathbf{W}_N^{(N-1)^2} \end{bmatrix} \quad (6.179)$$

(6.179) can be represented by sparse matrix factorization using Kronecker product [127] as:-

$$\mathbf{W}_N = \left\{ \mathbf{B} \right\}_{N/2} \otimes \mathbf{W}_{N/2}, \mathbf{W}_1 = 1 \quad (6.180)$$

where N is a power of two, and $\left\{ \mathbf{B} \right\}_{N/2}$ has $N/2$ matrices in the set, with the k^{th} matrix $k = 0$ to $(N/2 - 1)$ given by

$$\mathbf{B}_k = \left\{ \begin{array}{l} \begin{bmatrix} 1 & 1 \\ 1 & j \end{bmatrix}, \quad k = 1 \\ \begin{bmatrix} 1 & 1 \\ 1 & -1 \end{bmatrix}, \quad \text{otherwise} \end{array} \right\}$$

Therefore, (6.178) is rearranged as :-

$$\xi_i(x) = \sum_N \xi_i(n) \times \left\{ \mathbf{B} \right\}_{N/2} \otimes \mathbf{W}_{N/2} \quad (6.181)$$

From (6.176), the value of $\zeta_{i,m}(x)$ can be expressed in terms of truncated Fourier series as :-

$$\left(\left(\zeta_i[n - m|\theta] \right) \right)_{-N \leq n, l \leq N} = \zeta_i(\theta) = \sum_{m=1}^p \theta[m] \zeta_{i_m} \quad (6.182)$$

Substituting (6.176) along with (6.182) into (6.174)-(6.175) and equating both sides coefficients, we have

$$\mathbf{R}[\theta]\mathbf{i}_\alpha(t) + \mathbf{L}_\alpha[\theta]\mathbf{i}'_\alpha(t) + j\mathbf{D}\mathbf{v}_\alpha(t) = \mathbf{w}_{v_\alpha}(t) \quad (6.183)$$

$$\mathbf{R}[\theta]\mathbf{i}_\beta(t) + \mathbf{L}_\beta[\theta]\mathbf{i}'_\beta(t) + j\mathbf{D}\mathbf{v}_\beta(t) = \mathbf{w}_{v_\beta}(t) \quad (6.184)$$

$$\mathbf{R}_0[\theta]\mathbf{i}_0(t) + \mathbf{L}_0[\theta]\mathbf{i}'_0(t) + j\mathbf{D}\mathbf{v}_0(t) = \mathbf{w}_{v_0}(t) \quad (6.185)$$

$$\mathbf{G}_\alpha[\theta]\mathbf{v}_\alpha(t) + \mathbf{C}_\alpha[\theta]\mathbf{v}'_\alpha(t) + j\mathbf{D}\mathbf{i}_\alpha(t) = \mathbf{w}_{i_\alpha}(t) \quad (6.186)$$

$$\mathbf{G}_\beta[\theta]\mathbf{v}_\beta(t) + \mathbf{C}_\beta[\theta]\mathbf{v}'_\beta(t) + j\mathbf{D}\mathbf{i}_\beta(t) = \mathbf{w}_{i_\beta}(t) \quad (6.187)$$

$$\mathbf{G}_0[\theta]\mathbf{v}_0(t) + \mathbf{C}_0[\theta]\mathbf{v}'_0(t) + j\mathbf{D}\mathbf{i}_0(t) = \mathbf{w}_{i_0}(t) \quad (6.188)$$

where $\mathbf{D} = \text{diag}[\frac{2\pi n}{d}; -N \leq n \leq N]$. Rearranging (6.183)-(6.188) to find their state space model, we get

$$\frac{\partial}{\partial t}\xi(t) = F(\theta)\xi(t) + P(\theta)w(t) \quad (6.189)$$

State transition matrix $F(\theta)$ obtained from (6.189) is defined in real and imaginary terms as :-

$$-F(\theta) = -F_R(\theta) - jF_I(\theta) = \begin{bmatrix} C_\alpha^{-1}[\theta]G_\alpha[\theta] & 0 & 0 & jC_\alpha^{-1}[\theta]D & 0 & 0 \\ 0 & C_\beta^{-1}[\theta]G_\beta[\theta] & 0 & 0 & jC_\beta^{-1}[\theta]D & 0 \\ 0 & 0 & C^{-1}[\theta]G_g[\theta] & 0 & 0 & jC^{-1}[\theta]D \\ jL_\alpha^{-1}[\theta]D & 0 & 0 & L_\alpha^{-1}[\theta]R[\theta] & 0 & 0 \\ 0 & jL_\beta^{-1}[\theta]D & 0 & 0 & L_\beta^{-1}[\theta]R[\theta] & 0 \\ 0 & 0 & jL_0^{-1}[\theta]D & 0 & 0 & L_0^{-1}[\theta]R_0[\theta] \end{bmatrix} \quad (6.190)$$

State vector matrix denoted by $\xi(t)$ is represented as :-

$$\xi(t) = \xi_R(t) + j\xi_I(t) = \left[v_\alpha(t), v_\beta(t), v_0(t), i_\alpha(t), i_\beta(t), i_0(t) \right]^T \quad (6.191)$$

Here, $\xi_R(t)$ and $\xi_I(t)$ denote real and imaginary terms respectively. Also, process noise matrix is

$$P(\theta) = P_R(\theta) + jP_I(\theta)$$

$$= \begin{bmatrix} C_\alpha^{-1}[\theta] & 0 & 0 & 0 & 0 & 0 \\ 0 & C_\beta^{-1}[\theta] & 0 & 0 & 0 & 0 \\ 0 & 0 & C^{-1}[\theta] & 0 & 0 & 0 \\ 0 & 0 & 0 & L_\alpha^{-1}[\theta] & 0 & 0 \\ 0 & 0 & 0 & 0 & L_\beta^{-1}[\theta] & 0 \\ 0 & 0 & 0 & 0 & 0 & L_0^{-1}[\theta] \end{bmatrix} \quad (6.192)$$

$$w(t) = w_R(t) + jw_I(t) =$$

$$\left[w_{i_\alpha}(t), w_{i_\beta}(t), w_{i_0}(t), w_{v_\alpha}(t), w_{v_\beta}(t), w_{v_0}(t) \right]^T \quad (6.193)$$

Substituting (6.190)-(6.193) into (6.189), the line equation are :-

$$(\xi'_R(t) + j\xi'_I(t)) = (F_R(\theta) + jF_I(\theta))(\xi_R(t) + j\xi_I(t))$$

$$+ (P_R(\theta) + jP_I(\theta))(w_R(t) + jw_I(t)) \quad (6.194)$$

The real and imaginary parts are :-

$$\xi'_R(t) = F_R(\theta)\xi_R(t) - F_I(\theta)\xi_I(t) + P_R(\theta)w_R(t)$$

$$- P_I(\theta)w_I(t) \quad (6.195)$$

$$\xi'_I(t) = F_R(\theta)\xi_I(t) + F_I(\theta)\xi_R(t) + P_R(\theta)w_I(t)$$

$$+ P_I(\theta)w_R(t) \quad (6.196)$$

The combined augmented state space model is

$$\frac{\partial}{\partial t} \begin{bmatrix} \xi_R(t) \\ \xi_I(t) \\ \theta(t) \end{bmatrix} = \begin{bmatrix} F_R[\theta] & -F_I[\theta] & 0 \\ F_I[\theta] & F_R[\theta] & 0 \\ 0 & 0 & I \end{bmatrix} \begin{bmatrix} \xi_R(t) \\ \xi_I(t) \\ \theta(t) \end{bmatrix}$$

$$+ \begin{bmatrix} P_R[\theta] & -P_I[\theta] & 0 \\ P_I[\theta] & P_R[\theta] & 0 \\ 0 & 0 & I \end{bmatrix} \begin{bmatrix} w_R(t) \\ w_I(t) \\ \varepsilon_\theta(t) \end{bmatrix} \quad (6.197)$$

where I is the unitary matrix of sample size $2N + 1$. The measurement model is

$$\partial \xi_{v_i,n}(t) = v_i(t, \mathbf{x}_n) \partial t + \partial w_{v_i,n}(t), \quad n = 1, 2, \dots, m \quad (6.198)$$

$$\partial \xi_{i_i,n}(t) = i_i(t, \mathbf{x}_n) \partial t + \partial w_{i_i,n}(t), \quad n = 1, 2, \dots, m \quad (6.199)$$

where $i = \alpha, \beta, 0$. Now noting that $v_i(t, \mathbf{x}_n)$ and $i_i(t, \mathbf{x}_n)$ can be expressed as linear combinations of the Fourier series components of the line voltage and current, i.e.

$$v_i(t, \mathbf{x}_n) = \sum_n v_{i,n}(t) \exp(j2\pi n x / d), \quad n = 1, 2, \dots, m \quad (6.200)$$

$$i_i(t, \mathbf{x}_n) = \sum_n i_{i,n}(t) \exp(j2\pi n x / d), \quad n = 1, 2, \dots, m \quad (6.201)$$

When the measurement of Fourier component is not possible, then measurement of the current and voltage vector at a finite set of spatial points along the line can be used. Thus H gets modified. The measurement model in vector form is as follows :-

$$\begin{aligned} \partial Z(t) &= (H_1 \xi_R(t) + H_2 \xi_I(t)) \partial t + \partial V(t) \\ &= H \eta(t) \partial t + \partial V(t) \end{aligned} \quad (6.202)$$

where $Z(t) = [\xi_{v_i,1}(t), \dots, \xi_{v_i,m}(t), \xi_{i_i,1}(t), \dots, \xi_{i_i,m}(t)]^T$ is a $6m \times 1$ real vector.

$$H = [H_1, \dots, H_6, 0] \quad (6.203)$$

6.2.3 Modeling of NTL using Frequency Domain Analysis

Expanding line voltage v_i and line current i_i in frequency domain using Fourier transform as :-

$$-\frac{\partial}{\partial x}V_\alpha = [R(x|\theta) + j\omega L_\alpha(x|\theta)]I_\alpha + W_{v_\alpha} \quad (6.204)$$

$$-\frac{\partial}{\partial x}V_\beta = [R(x|\theta) + j\omega L_\beta(x|\theta)]I_\beta + W_{v_\beta} \quad (6.205)$$

$$-\frac{\partial}{\partial x}V_0 = [R_0(x|\theta) + j\omega L_0(x|\theta)]I_0 + W_{v_0} \quad (6.206)$$

$$-\frac{\partial}{\partial x}I_\alpha = [G_\alpha(x|\theta) + j\omega C_\alpha(x|\theta)]V_\alpha + W_{i_\alpha} \quad (6.207)$$

$$-\frac{\partial}{\partial x}I_\beta = [G_\beta(x|\theta) + j\omega C_\beta(x|\theta)]V_\beta + W_{i_\beta} \quad (6.208)$$

$$-\frac{\partial}{\partial x}I_0 = [G_0(x|\theta) + j\omega C(x|\theta)]V_0 + W_{i_0} \quad (6.209)$$

where

$$Z_i(x) = Z_i(x|\theta) = R_i(x|\theta) + j\omega L_i(x|\theta) = \sum_n Z_{i,n}(\omega|\theta)e^{j2\pi nx/d}$$

$$Z_{i,n}(\omega|\theta) = R_{i,n}(\theta) + j\omega L_{i,n}(\theta)$$

Similarly,

$$Y_i(z) = Y_i(z|\theta) = G_i(z|\theta) + j\omega C_i(z|\theta) = \sum_n Y_{i,n}(\omega|\theta)e^{j2\pi nx/d}$$

$$Y_{i,n}(\omega|\theta) = G_{i,n}(\theta) + j\omega C_{i,n}(\theta)$$

Using (6.176) and (6.217)-(6.201) into (6.204)-(6.209) and apply the perturbation theory to consider the nonlinearity of the Transmission line. We express line voltage and current in terms of σ , the perturbation parameter.

$$V_{i,n}(\omega) = V_{i,n}^{(0)}(\omega) + \sigma V_{i,n}^{(1)}(\omega) + \sigma^2 V_{i,n}^{(2)}(\omega) + \dots \quad (6.210)$$

$$I_{i,n}(\omega) = I_{i,n}^{(0)}(\omega) + \sigma I_{i,n}^{(1)}(\omega) + \sigma^2 I_{i,n}^{(2)}(\omega) + \dots \quad (6.211)$$

where $V_{i,n}^{(0)}(\omega)$ and $I_{i,n}^{(0)}(\omega)$ are linear terms. $\sigma V_{i,n}^{(1)}(\omega)$ and $\sigma I_{i,n}^{(1)}(\omega)$ are nonlinear terms.

Measurement model is represented as :-

$$\begin{bmatrix} jD & 0 & 0 & Z_\alpha(\omega|\theta) & 0 & 0 \\ 0 & jD & 0 & 0 & Z_\beta(\omega|\theta) & 0 \\ 0 & 0 & jD & 0 & 0 & Z_0(\omega|\theta) \\ Y_\alpha(\omega|\theta) & 0 & 0 & jD & 0 & 0 \\ 0 & Y_\beta(\omega|\theta) & 0 & 0 & jD & 0 \\ 0 & 0 & Y_0(\omega|\theta) & 0 & 0 & jD \end{bmatrix} \otimes I_n \times \begin{bmatrix} v_\alpha(\omega) \\ v_\beta(\omega) \\ v_0(\omega) \\ i_\alpha(\omega) \\ i_\beta(\omega) \\ i_0(\omega) \end{bmatrix} = 0 \quad (6.212)$$

For simulations, measurements have been done using (6.212).

6.2.4 State Estimation for Transmission Line

(6.189) has been discretized to implement the state estimation technique. The discrete model of the NTL is represented as :-

$$\mathcal{X}_{k+1} = \mathcal{F}_k \mathcal{X}_k + \mathcal{B}_k \mathcal{U}_k + \mathcal{G}_k \mathcal{W}_k \quad (6.213)$$

$$\mathcal{Z}_k = \mathcal{H}_k \mathcal{X}_k + \mathcal{V}_k \quad (6.214)$$

where \mathcal{F}_k

$$= \begin{bmatrix} 1-T_s C_\alpha^{-1}[\theta] G_\alpha[\theta] & 0 & 0 & -T_s j C_\alpha^{-1}[\theta] D & 0 & 0 \\ 0 & 1-T_s C_\beta^{-1}[\theta] G_\beta[\theta] & 0 & 0 & -T_s j C_\beta^{-1}[\theta] D & 0 \\ 0 & 0 & 1-T_s C^{-1}[\theta] G_g[\theta] & 0 & 0 & -T_s j C^{-1}[\theta] D \\ -T_s j L_\alpha[\theta]^{-1} D & 0 & 0 & 1-T_s L_\alpha^{-1}[\theta] R[\theta] & 0 & 0 \\ 0 & -T_s j L_\beta^{-1}[\theta] D & 0 & 0 & 1-T_s L_\beta^{-1}[\theta] R[\theta] & 0 \\ 0 & 0 & -T_s j L_0^{-1}[\theta] D & 0 & 0 & 1-T_s L_0^{-1}[\theta] R_0[\theta] \end{bmatrix} \in \mathbb{R}^{6 \times 6},$$

$$\mathcal{H}_k = \begin{bmatrix} 1 & 0 & 0 & 0 & 0 & 0 \\ 0 & 1 & 0 & 0 & 0 & 0 \\ 0 & 0 & 1 & 0 & 0 & 0 \\ 0 & 0 & 0 & 1 & 0 & 0 \\ 0 & 0 & 0 & 0 & 1 & 0 \\ 0 & 0 & 0 & 0 & 0 & 1 \end{bmatrix} \in \mathbb{R}^{6 \times 6}, \mathcal{G}_k = \begin{bmatrix} C_\alpha^{-1}[\theta] & 0 & 0 & 0 & 0 & 0 \\ 0 & C_\beta^{-1}[\theta] & 0 & 0 & 0 & 0 \\ 0 & 0 & C^{-1}[\theta] & 0 & 0 & 0 \\ 0 & 0 & 0 & L_\alpha^{-1}[\theta] & 0 & 0 \\ 0 & 0 & 0 & 0 & L_\beta^{-1}[\theta] & 0 \\ 0 & 0 & 0 & 0 & 0 & L_0^{-1}[\theta] \end{bmatrix} \in \mathbb{R}^{6 \times 6}$$

$\mathcal{X}_k \in \mathbb{R}^{6 \times 1}$ denotes the state vector as :-

$$\mathcal{X}_k = \begin{bmatrix} v_{\alpha,k} & v_{\beta,k} & v_{0,k} & i_{\alpha,k} & i_{\beta,k} & i_{0,k} \end{bmatrix}^T \quad (6.215)$$

The state model is given as :-

$$\begin{aligned}
\begin{bmatrix} \mathbf{V}_{\alpha,k+1} \\ \mathbf{V}_{\beta,k+1} \\ \mathbf{V}_{0,k+1} \\ \mathbf{i}_{\alpha,k+1} \\ \mathbf{i}_{\beta,k+1} \\ \mathbf{i}_{0,k+1} \end{bmatrix} &= \begin{bmatrix} K_1 & 0 & 0 & K_2 & 0 & 0 \\ 0 & K_3 & 0 & 0 & K_4 & 0 \\ 0 & 0 & K_5 & 0 & 0 & K_6 \\ K_7 & 0 & 0 & K_8 & 0 & 0 \\ 0 & K_9 & 0 & 0 & K_{10} & 0 \\ 0 & 0 & K_{11} & 0 & 0 & K_{12} \end{bmatrix} \begin{bmatrix} \mathbf{V}_{\alpha,k} \\ \mathbf{V}_{\beta,k} \\ \mathbf{V}_{0,k} \\ \mathbf{i}_{\alpha,k} \\ \mathbf{i}_{\beta,k} \\ \mathbf{i}_{0,k} \end{bmatrix} \\
&+ \begin{bmatrix} C_{\alpha}^{-1}[\theta] & 0 & 0 & 0 & 0 & 0 \\ 0 & C_{\beta}^{-1}[\theta] & 0 & 0 & 0 & 0 \\ 0 & 0 & C^{-1}[\theta] & 0 & 0 & 0 \\ 0 & 0 & 0 & L_{\alpha}^{-1}[\theta] & 0 & 0 \\ 0 & 0 & 0 & 0 & L_{\beta}^{-1}[\theta] & 0 \\ 0 & 0 & 0 & 0 & 0 & L_0^{-1}[\theta] \end{bmatrix} \begin{bmatrix} \mathbf{W}_{i_{\alpha,k}} \\ \mathbf{W}_{i_{\beta,k}} \\ \mathbf{W}_{i_{0,k}} \\ \mathbf{W}_{v_{\alpha,k}} \\ \mathbf{W}_{v_{\beta,k}} \\ \mathbf{W}_{v_{0,k}} \end{bmatrix} \tag{6.216}
\end{aligned}$$

where

$$\begin{aligned}
K_1 &= 1 - T_s C_{\alpha}^{-1}[\theta] G_{\alpha}[\theta], & K_2 &= -T_s j C_{\alpha}^{-1}[\theta] D, & K_3 &= 1 - T_s C_{\beta}^{-1}[\theta] G_{\beta}[\theta] \\
K_4 &= -T_s j C_{\beta}^{-1}[\theta] D, & K_5 &= 1 - T_s C^{-1}[\theta] G_g[\theta], & K_6 &= -T_s j C^{-1}[\theta] D, \\
K_7 &= -T_s j L_{\alpha}^{-1}[\theta]^{-1} D, & K_8 &= 1 - T_s L_{\alpha}^{-1}[\theta] R[\theta], & K_9 &= -T_s j L_{\beta}^{-1}[\theta] D \\
K_{10} &= 1 - T_s L_{\beta}^{-1}[\theta] R[\theta], & K_{11} &= -T_s j L_0^{-1}[\theta] D, & K_{12} &= 1 - T_s L_0^{-1}[\theta] R_0[\theta].
\end{aligned}$$

T_s is the sampling time. \mathbf{V}_{in} is the measurement vector of line voltage and line current respectively.

$$\mathcal{Z}_k \in \mathbb{R}^{6 \times 6} = \begin{bmatrix} 1 & 0 & 0 & 0 & 0 & 0 \\ 0 & 1 & 0 & 0 & 0 & 0 \\ 0 & 0 & 1 & 0 & 0 & 0 \\ 0 & 0 & 0 & 1 & 0 & 0 \\ 0 & 0 & 0 & 0 & 1 & 0 \\ 0 & 0 & 0 & 0 & 0 & 1 \end{bmatrix} \begin{bmatrix} \mathbf{V}_{\alpha,n} \\ \mathbf{V}_{\beta,n} \\ \mathbf{V}_{0,n} \\ \mathbf{i}_{\alpha,n} \\ \mathbf{i}_{\beta,n} \\ \mathbf{i}_{0,n} \end{bmatrix} + \begin{bmatrix} V_{1n} \\ V_{2n} \\ V_{3n} \\ V_{4n} \\ V_{5n} \\ V_{6n} \end{bmatrix} \tag{6.217}$$

As the equation (6.217) is a linear estimation problem, KF method has been used to estimate line voltage and line current. The number of unknown parameters can be identified by considering whether the estimation is being performed in the real or complex domain. This is illustrated in Table 6.4. For transposed TL, a ninth order parameter vector $\theta_k \in \mathbb{R}^{9 \times 1} = [R_{\alpha}(k), R_{\beta,k}, R_{0,k}, X_{\alpha,k}, X_{\beta,k}, X_{0,k}, B_{\alpha,k}, B_{\beta,k}, B_{0,k}]^T$

Table 6.4: Unknown Parameters of Estimation Methods.

	Complex Domain	Real Domain
Transposed Line	Z_1, Y_1	R_1, X_1, B_1
Untransposed Line	Z_i, Y_i	R_i, X_i, B_i

$$i = \alpha, \beta, 0, \alpha\beta, \alpha 0, \beta 0.$$

is defined for parameter identification. The parameters to be estimated must be added in (6.216) to obtain the augmented matrix as :-

$$\mathcal{X}_k^a = [\mathcal{X}_k^T, \boldsymbol{\theta}_k^T]^T \in \mathbb{R}^{15 \times 1} \quad (6.218)$$

The augmented state model is :-

$$\mathcal{X}_{k+1}^a = \mathcal{F}_k^a \mathcal{X}_k^a + \mathcal{B}_k^a \mathcal{U}_k + \mathcal{G}_k^a \mathcal{W}_k^a \quad (6.219)$$

$$\mathcal{Z}_k^a = \mathcal{H}_k^a \mathcal{X}_k^a + \mathcal{V}_k^a \quad (6.220)$$

where

$$\mathcal{G}_k^a = \begin{bmatrix} [\mathcal{G}_k] & [0] \\ [0] & [0] \end{bmatrix} \in \mathbb{R}^{15 \times 15}, \mathcal{W}_k^a = \begin{bmatrix} \mathcal{W}_s^T \\ \mathcal{W}_\theta^T \end{bmatrix} \in \mathbb{R}^{15 \times 1}$$

$$\mathcal{H}_k^a = \begin{bmatrix} 1 & 0 & 0 & 0 & 0 & 0 & 0 & 0 & 0 & 0 & 0 & 0 & 0 & 0 & 0 \\ 0 & 1 & 0 & 0 & 0 & 0 & 0 & 0 & 0 & 0 & 0 & 0 & 0 & 0 & 0 \\ 0 & 0 & 1 & 0 & 0 & 0 & 0 & 0 & 0 & 0 & 0 & 0 & 0 & 0 & 0 \\ 0 & 0 & 0 & 1 & 0 & 0 & 0 & 0 & 0 & 0 & 0 & 0 & 0 & 0 & 0 \\ 0 & 0 & 0 & 0 & 1 & 0 & 0 & 0 & 0 & 0 & 0 & 0 & 0 & 0 & 0 \\ 0 & 0 & 0 & 0 & 0 & 1 & 0 & 0 & 0 & 0 & 0 & 0 & 0 & 0 & 0 \end{bmatrix} \in \mathbb{R}^{6 \times 15} \text{ and } \mathcal{V}_k^a = \begin{bmatrix} \mathcal{V}_x^T \\ \mathcal{V}_\theta^T \end{bmatrix} \in \mathbb{R}^{6 \times 15}$$

$\mathcal{F}_k^a \in \mathbb{R}^{15 \times 15}$ is nonlinear function of \mathcal{X}_k and $\boldsymbol{\theta}_k$. Therefore, EKF algorithm can be used to linearize \mathcal{F}_k matrix using Jacobian transform as :-

$$\mathcal{F}_k = -\frac{\partial}{\partial \boldsymbol{\theta}(m)} \begin{bmatrix} C_\alpha^{-1}[\boldsymbol{\theta}]G_\alpha[\boldsymbol{\theta}] & 0 & 0 & jC_\alpha^{-1}[\boldsymbol{\theta}]D & 0 & 0 \\ 0 & C_\beta^{-1}[\boldsymbol{\theta}]G_\beta[\boldsymbol{\theta}] & 0 & 0 & jC_\beta^{-1}[\boldsymbol{\theta}]D & 0 \\ 0 & 0 & C^{-1}[\boldsymbol{\theta}]G_g[\boldsymbol{\theta}] & 0 & 0 & jC^{-1}[\boldsymbol{\theta}]D \\ jL_\alpha[\boldsymbol{\theta}]^{-1}D & 0 & 0 & L_\alpha^{-1}[\boldsymbol{\theta}]R[\boldsymbol{\theta}] & 0 & 0 \\ 0 & jL_\beta^{-1}[\boldsymbol{\theta}]D & 0 & 0 & L_\beta^{-1}[\boldsymbol{\theta}]R[\boldsymbol{\theta}] & 0 \\ 0 & 0 & jL_0^{-1}[\boldsymbol{\theta}]D & 0 & 0 & L_0^{-1}[\boldsymbol{\theta}]R_0[\boldsymbol{\theta}] \end{bmatrix} \quad (6.221)$$

$$\mathcal{X}_k^a = \left[\mathbf{V}_{\alpha,k}, \mathbf{V}_{\beta,k}, \mathbf{V}_{0,k}, \mathbf{i}_{\alpha,k}, \mathbf{i}_{\beta,k}, \mathbf{i}_{0,k}, R_{\alpha,k}, R_{\beta,k}, R_{0,k}, X_{\alpha,k}, X_{\beta,k}, X_{0,k}, B_{\alpha,k}, B_{\beta,k}, B_{0,k} \right]^T.$$

For untransposed line, all of the following 6 different complex entries ($Z_\alpha, Z_{\alpha\beta}, Z_{\alpha 0}, Z_\beta, Z_{\beta 0}$ and Z_0) in $Z_{\alpha\beta 0}$ are considered to be unknown. The total number of real unknown parameters will be 12. Similarly, $Y_{\alpha\beta 0}$ has 6 real unknown parameters by excluding G_i term due to negligible effect (discussed above).

So therefore, total 18 unknown parameters for a three-phase untransposed transmission line. These parameter are defined as $\theta_k \in \mathbb{R}^{18 \times 1}$. Then the dimension of augmented matrices are $\mathcal{X}_k^a \in \mathbb{R}^{24 \times 1}$, $\mathcal{G}_k^a \in \mathbb{R}^{24 \times 24}$, $\mathcal{W}_k^a \in \mathbb{R}^{24 \times 1}$, $\mathcal{F}_k^a \in \mathbb{R}^{24 \times 24}$ and $\mathcal{H}_k^a \in \mathbb{R}^{6 \times 24}$.

6.2.5 Simulation Results

In general, TL are classified into three section: 1) short TL ($d \leq 80$ km), 2) medium TL ($80 \leq d \leq 250$ km) and 3) long TL ($250 \leq d$ km). Among all, long TL is considered to get high accuracy of calculating the line parameters modeled in distributed form. MATLAB software has been used to implement the derived equations. The conductance G is neglected as the value of line conductor is very low. This is due to the power lost in the insulation resistance is very small as compared to the other line losses.

We estimate line resistance R , reactance X and susceptance B . We consider a 300-km three-phase long transmission line. On the sending terminal, a balanced 440 KV/60 Hz three-phase source is attached. The receiving terminal of the transmission line is connected to a three-phase load of 500 kVA with a power factor (PF) of 0.97 [118]. The parameters's value for simulation are given as :-

$$\begin{aligned} [Z_{\alpha\beta 0}] &= \begin{bmatrix} 0.058 + j0.636 & 0.471 + j0.326 & 0.470 + j0.273 \\ 0.471 + j0.326 & 0.058 + j0.636 & 0.471 + j0.326 \\ 0.470 + j0.273 & 0.470 + j0.326 & 0.058 + j0.636 \end{bmatrix} \Omega/km \\ [Y_{\alpha\beta 0}] &= \begin{bmatrix} j4.261 & -j0.922 & -j0.309 \\ -j0.922 & j4.439 & -j0.922 \\ -j0.309 & -j0.922 & j4.261 \end{bmatrix} \mu S/km \end{aligned} \quad (6.222)$$

The initial values of variance of process noise and measurement noise are 0.005 and 1.0 respectively. The line currents and voltages at α , β , 0 of NTL have been estimated using RLS, KF and UKF methods for different noisy inputs as shown in Fig. 6.5 to 6.10. Further, we estimated the behaviour of the circuit parameters along the line. Table 6.5 and 6.6 show the comparison of RMSE and standard deviation of the parameter errors for state vectors in NTL using RLS, KF and UKF methods. Table 6.7 and 6.8 show comparison of RMSE for different parameters in transposed and untransposed line using RLS, KF

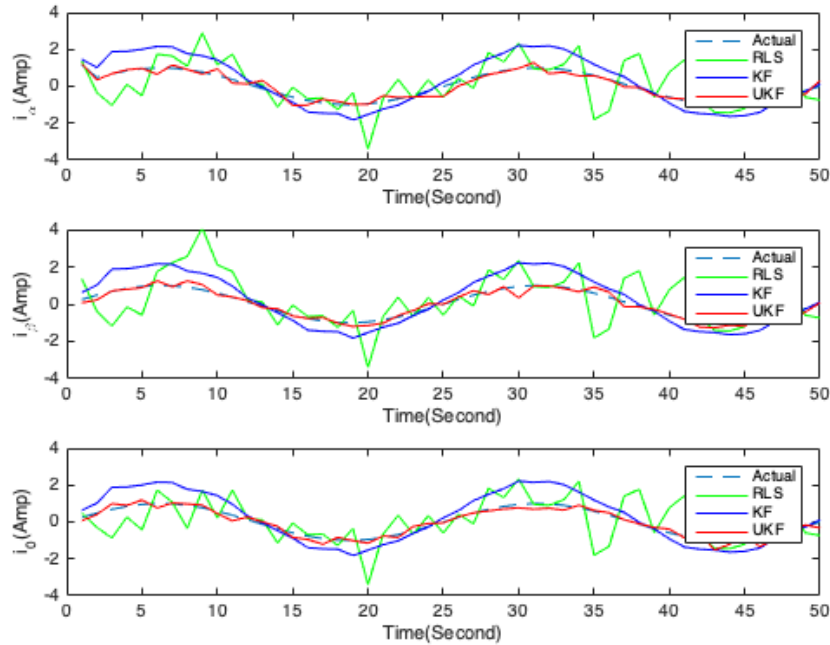


Figure 6.5: Comparison of line currents using Gaussian noisy input ($\mu = 0$ and $\sigma^2 = 0.1$) with RLS, KF and UKF methods.

and UKF methods. It shows UKF method has less variability in the parameter estimates compared to RLS and EKF methods.

Remarks: The limitation of this work are:

- (a) The parameters of the transposed/untransposed NTL have been estimated by excluding mutual effects among phase conductors and ground as it increases the mathematical complexity.
- (b) Higher order perturbation theory can be used, as it will present more accurate nonlinear mathematical expressions but it will increase the mathematical complexity.

6.2.6 Conclusions

This chapter estimates the states and parameters of a transposed and untransposed three-phase nonuniform transmission line circuit using KF, EKF and UKF methods and compared the results with the classical RLS method. To implement the various Kalman filtering algorithms, we used Kirchhoff's current law, Fourier series expansion and Clarke transformation matrix to derive the

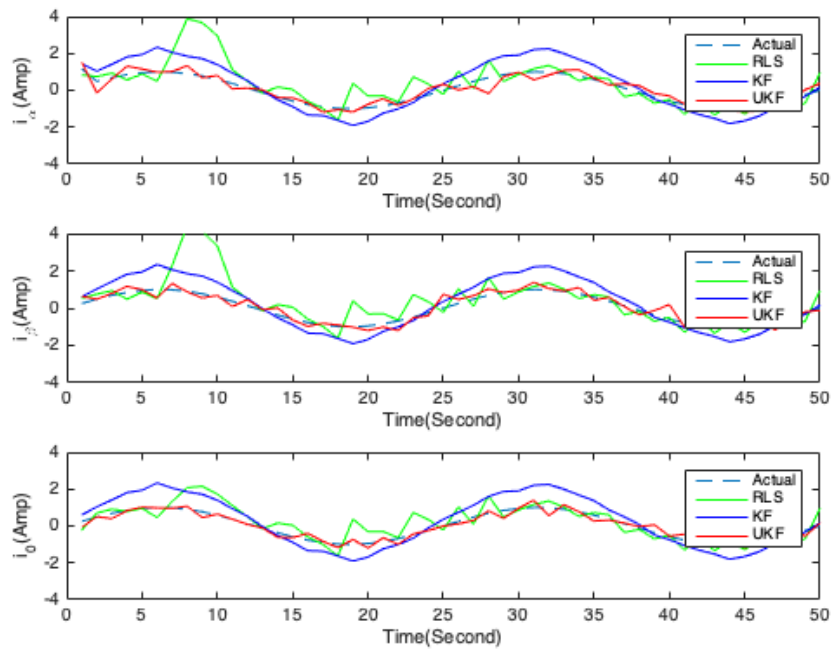


Figure 6.6: Comparison of line currents using Gaussian noisy input ($\mu = 0$ and $\sigma^2 = 0.25$) with RLS, KF and UKF methods.

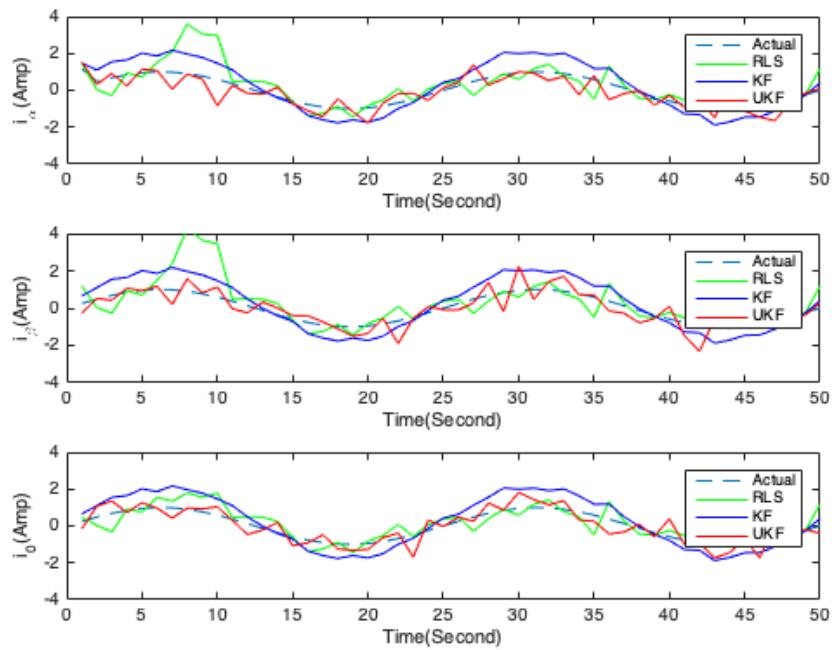


Figure 6.7: Comparison of line currents using Gaussian noisy input ($\mu = 0$ and $\sigma^2 = 0.5$) with RLS, KF and UKF methods.

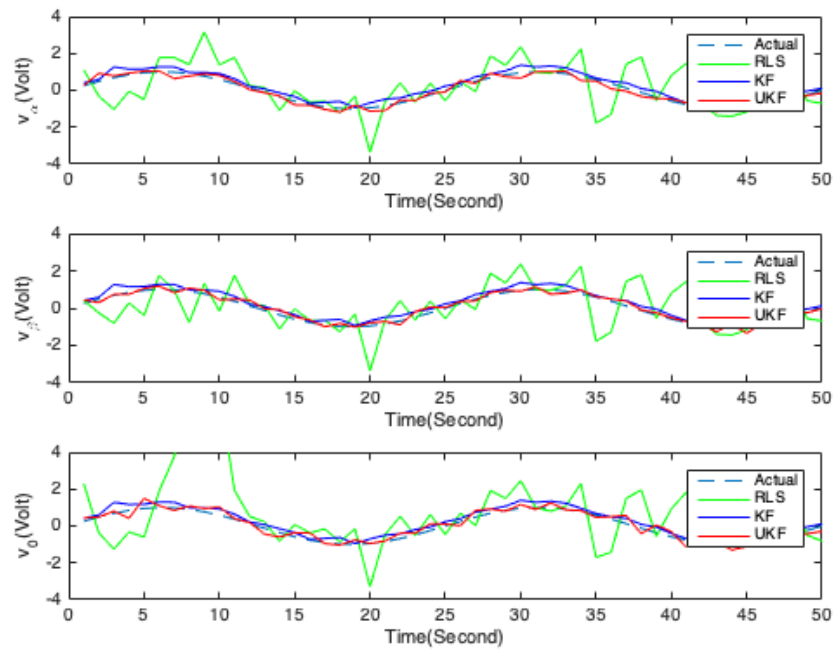


Figure 6.8: Comparison of line voltages using Gaussian noisy input ($\mu = 0$ and $\sigma^2 = 0.1$) with RLS, KF and UKF methods.

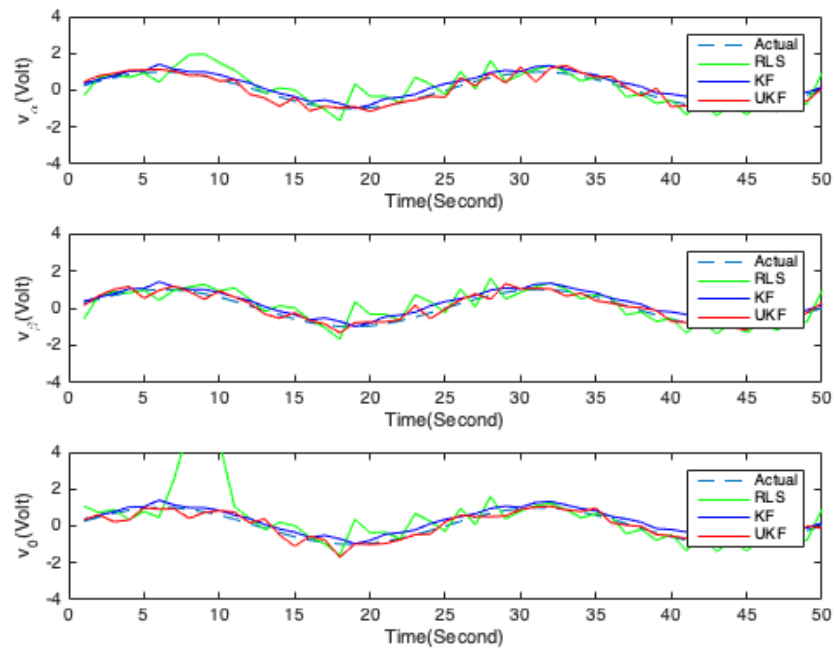


Figure 6.9: Comparison of line voltages using Gaussian noisy input ($\mu = 0$ and $\sigma^2 = 0.25$) with RLS, KF and UKF methods.

Table 6.5: Comparison of RMSE for line currents and line voltages using RLS, KF and UKF methods.

S. no.	Gaussian noise at input source	State	RMSE using RLS method	RMSE using KF method	RMSE using UKF method
1	$\mu = 0$ $\sigma = 0.0$	i_α	0.6738	0.4482	0.0932
		i_β	0.6415	0.4297	0.0982
		i_0	0.7010	0.2321	0.0782
		v_α	0.5890	0.2723	0.0992
		v_β	0.6894	0.3882	0.1092
		v_0	0.6404	0.5841	0.1321
2	$\mu = 0$ $\sigma = 0.1$	i_α	0.7328	0.5181	0.1031
		i_β	0.7409	0.5260	0.1006
		i_0	0.8304	0.4122	0.0889
		v_α	0.6819	0.3821	0.1019
		v_β	0.8012	0.4281	0.1132
		v_0	0.7194	0.6349	0.2387
3	$\mu = 0$ $\sigma = 0.25$	i_α	0.8118	0.6780	0.2531
		i_β	0.9109	0.6619	0.1326
		i_0	0.9201	0.6125	0.1018
		v_α	0.7610	0.4521	0.1329
		v_β	0.9411	0.5129	0.2332
		v_0	0.8791	0.7719	0.5487
4	$\mu = 0$ $\sigma = 0.5$	i_α	0.9411	0.8781	0.6532
		i_β	1.3401	0.7854	0.2521
		i_0	1.0921	0.7224	0.2211
		v_α	0.9811	0.6522	0.6529
		v_β	1.5112	0.7221	0.3532
		v_0	0.9931	0.8211	0.6687

Table 6.6: Comparison of standard deviation of the parameter errors (σ_e) for line currents and line voltages using RLS, KF and UKF methods.

S. no.	Gaussian noise at input source	State	σ_e using RLS method	σ_e using KF method	σ_e using UKF method
1	$\mu = 0$ $\sigma = 0.0$	i_α	0.6738	0.3488	0.1218
		i_β	0.6415	0.3927	0.1910
		i_0	0.7010	0.2319	0.1109
		v_α	0.5890	0.2714	0.0912
		v_β	0.6894	0.3690	0.3690
		v_0	0.6404	0.5001	0.1060
2	$\mu = 0$ $\sigma = 0.1$	i_α	0.7718	0.5481	0.5511
		i_β	0.7811	0.5127	0.2511
		i_0	0.9012	0.3620	0.2310
		v_α	0.6710	0.4314	0.1012
		v_β	0.7719	0.4312	0.4409
		v_0	0.8810	0.7019	0.2310
3	$\mu = 0$ $\sigma = 0.25$	i_α	0.8782	0.6182	0.6232
		i_β	0.9101	0.6117	0.3940
		i_0	1.1011	0.5121	0.3632
		v_α	0.8710	0.5514	0.4510
		v_β	0.9019	0.5710	0.5701
		v_0	0.9912	0.9120	0.3611
4	$\mu = 0$ $\sigma = 0.5$	i_α	0.9910	0.7880	0.9901
		i_β	0.9561	0.7210	0.5441
		i_0	1.3101	0.7220	0.6732
		v_α	0.9610	0.7602	0.4032
		v_β	0.9920	0.6540	0.7712
		v_0	1.0232	1.0820	0.4510

Table 6.7: Comparison of RMSE for different parameters in transposed line using RLS, EKF and UKF methods.

Parameter	RMSE of R using RLS	RMSE of R using EKF	RMSE of R using UKF	RMSE of X or B using RLS	RMSE of X or B using EKF	RMSE of X or B using UKF
$Z_\alpha(\Omega)$	1.06881	0.22543	0.01543	0.25786	0.00676	0.00176
$Z_\beta(\Omega)$	1.06881	0.22543	0.09543	0.25786	0.00676	0.00176
$Z_0(\Omega)$	1.96154	0.25530	0.17530	0.97765	0.24439	0.09439
$B_\alpha(\Omega)$	-	-	-	0.09376	0.00576	0.00110
$B_\beta(\Omega)$	-	-	-	0.10983	0.00410	0.00410
$B_0(\Omega)$	-	-	-	1.05154	0.03512	0.01012

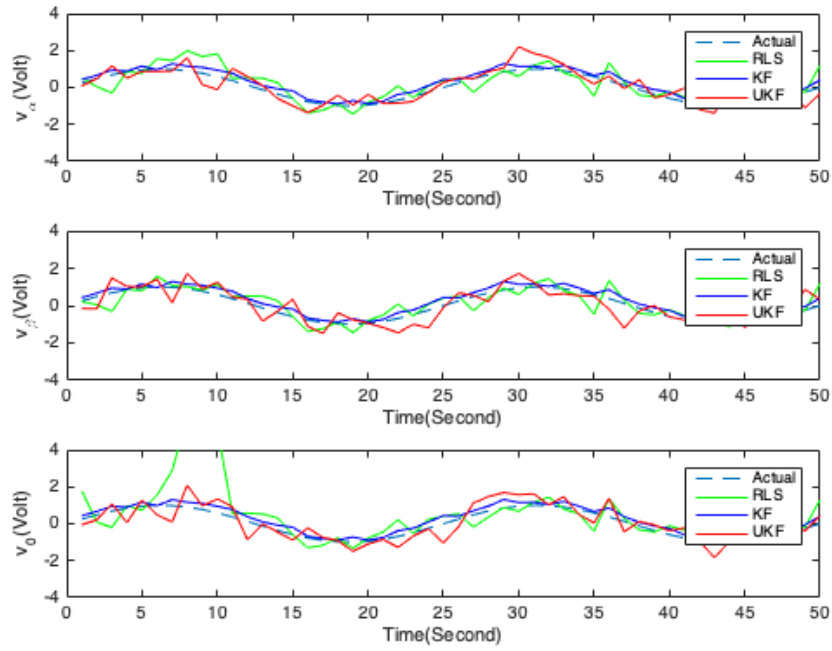


Figure 6.10: Comparison of line voltages using Gaussian noisy input ($\mu = 0$ and $\sigma^2 = 0.5$) with RLS, KF and UKF methods.

Table 6.8: Comparison of RMSE for different parameters in untransposed line using RLS, EKF and UKF methods.

Parameter	RMSE of R using RLS	RMSE of R using EKF	RMSE of R using UKF	RMSE of X or B using RLS	RMSE of X or B using EKF	RMSE of X or B using UKF
$Z_\alpha(\Omega)$	2.00664	0.00619	0.00109	0.34771	0.00481	0.00101
$Z_\beta(\Omega)$	1.98566	0.00986	0.00326	0.34778	0.00481	0.00101
$Z_0(\Omega)$	1.06765	0.00988	0.00198	0.78781	0.00676	0.00326
$B_\alpha(\Omega)$	-	-	-	0.18098	0.00771	0.00221
$B_\beta(\Omega)$	-	-	-	0.18123	0.00347	0.00097
$B_0(\Omega)$	-	-	-	0.18118	0.00347	0.00121
$Z_{\alpha\beta}(\Omega)$	3.78118	0.00587	0.00120	1.34778	0.00118	0.001001
$Z_{\alpha 0}(\Omega)$	1.78718	0.00485	0.00325	2.34781	0.00718	0.00532
$Z_{\beta 0}(\Omega)$	5.77658	0.00604	0.00094	1.11801	0.00781	0.00342
$B_{\alpha\beta}(\Omega)$	-	-	-	0.81981	0.00347	0.00121
$B_{\alpha 0}(\Omega)$	-	-	-	0.78118	0.00781	0.00432
$B_{\beta 0}(\Omega)$	-	-	-	0.78110	0.00781	0.00398

Telegrapher's equation of NTL and used perturbation theory to include line currents and voltages. Further, implementation of Kronecker product has been utilized to obtain the sparse matrix formulation. Simulation results show better precision in estimated values using UKF method with actual values as compared with RLS, KF and EKF methods. For state estimation, RMSE values of parameters using UKF method are smaller than KF and RLS methods. UKF method provide better estimations than RLS and EKF methods since UKF method is accurate to the third order for any nonlinearity. Further, EKF and UKF methods are real-time estimation methods for estimating the states and parameter of TL in space-time which demonstrates the superiority of these methods over RLS method.

Chapter 7

Conclusions and Future Scope

7.1 Conclusions

We have studied the state and parameter estimation of linear and nonlinear systems described by SDE using KF, EKF, IEKF and UKF methods. We recapitulate the salient features of this investigation study and results obtained for real-time state estimation and parameter estimation in the following points :-

- (a) As a first problem, we used the classical mathematical model, namely, Ebers-Moll model together with perturbation theory to obtain closed-form Volterra expressions between input and output of SCR. The derived equations can be used as a model for designing, analysis and development of new integrated circuits in advance before the formation of chips. The closed form expressions can also be used for circuit parameter estimation purposes. The derived equations are useful as a model in any simulation software such as SIMULINK, as this software provides direct access to circuit parameters. The main advantage of the method is that the use of nonlinear expressions obtained using perturbation theory instead of using the linear expression represents distortion which shows the importance of nonlinear expression. Percentage distortion for SCR circuit is approximately 0.5028 % for 1 V input voltage.

- (b) As a second problem, we estimated the states of higher-order RC LPF and RC HPF circuits using EKF and UKF methods. It also compared the estimation results with LMS method. The EKF method presents better estimate than LMS method as EKF method accounts for measurement noise. Also, the maximal precision of simulation requires the modeling of circuit in terms of device parameters and circuit elements, so the method is able to provide good estimation. The method presents real-time estimation. For sinusoidal signal, SNR for RC LPF circuit using EKF method is 43.769 dB and using LMS method is 32.737 dB approximately. For sinusoidal signal, SNR for RC HPF circuit using EKF method is 58.144 dB and using LMS method is 26.886 dB approximately. Also, for square wave, SNR for RC LPF circuit using EKF method is 55.994 dB and using LMS method is 34.314 dB approximately. For square wave, SNR for RC HPF circuit using EKF method is 62.650 dB and using LMS method is 60.480 dB approximately. While using UKF method for state estimation, we obtained better closeness of estimated capacitor voltage and diode current with PSPICE simulated values as compared to the EKF method. This is due to smaller linearization error of UKF method. Also, the SNR value of UKF method is better than EKF method. UKF method presents smaller RMSE as compared to EKF method as UKF method is accurate to the third order for any non-linearity.
- (c) As a third problem, we estimated the states of single phase rectifier circuit using different versions of KF method. The results show that for noiseless sinusoidal signal, the SNR (dB) value of capacitor voltage v_c using LMS, EKF, IEKF and UKF methods are 0.42 dB, 1.07 dB, 1.42 dB and 2.42 dB respectively whereas, for noisy input signal with zero mean and 1.0 variance, the SNR (dB) values using LMS, EKF, IEKF and UKF methods are 0.26 dB, 0.90 dB, 1.06 dB and 1.26 dB respectively. Further, for noiseless sinusoidal signal, the RMSE value of capacitor voltage v_c using LMS, EKF, IEKF and UKF methods are 1.24, 0.86, 0.24 and 0.40 respectively whereas, for noisy input signal with zero mean and 1.0 variance, the RMSE values using LMS, EKF, IEKF and UKF methods are 2.55, 1.82, 1.10 and 0.55 respectively. This shows the significance of nonlinearity within the system. The simulation results show that the SNR value for UKF method is higher

compared to LMS, EKF and IEKF methods. Also, UKF method has small RMSE value than the other methods and also less affected by noise. The UKF method presents better estimate than other versions of KF method.

(d) As a fourth problem, the states of following transistor circuits have been estimated :-

(ii) CE BJT circuit.

(iv) BJT DA circuit.

The output voltage of CE BJT circuit using EKF and IEKF methods are compared with the simulated value. For noisy input signal with zero mean and 1.0 variance, the SNR (dB) values using EKF and IEKF methods are 27.82 dB, 28.43 dB respectively. The result shows that IEKF method provides a higher SNR than EKF method because it reduces the linearization error by taking measurement into account when the measurement model is linearized. Performance and stability are not guaranteed for all operating conditions with the EKF approach since nonlinear systems are linearized around the operating points of states. Both transistor states and transistor model parameters can be estimated using the derived extended state equation. Results indicate that because IEKF method takes linearization error into account, it is better able to track the state than EKF method. Further, The voltage estimation of a DA using UKF method is presented in this paper and the results have been compared with EKF and IEKF methods. Simulation results using UKF method show the better closeness of estimated output voltage with actual simulated values as compared to the EKF and IEKF methods. UKF method presents smaller MSE value as compared to EKF and IEKF methods as UKF method is accurate to the third order for any nonlinearity. As the modeling of the circuit has been performed using transistor model and circuit elements, the proposed method is able to provide the maximal precision of simulation. Also, the use of Gummel-Poon model presents more accurate modeling as compared to the Ebers-Moll model. This is due to secondary effects of the transistor being taken into account by the Gummel-Poon.

(e) As a fifth problem, we present the formulation of NTL dynamics modeling using Fourier series expansion and Kronecker product along with the state and parameter estimation using KF, EKF and UKF methods. The following

circuits have been used for estimation purposes :-

- (i) Single-phase NTL circuit.
- (ii) Three-phase transposed and untransposed NTL circuit.

In the first problem, state-space model of the single-phase NTL circuit has been derived. As Telegrapher's equations used for modeling the NTL are a function of space and time, the Fourier series expansion of the voltage and current have been used to obtain the time-dependent equations. Further, Kronecker product has been used for representation of Fourier unitary transform. The measurements have been obtained by solving the eigenvector problem. The frequency-domain analysis is used to obtain the state-space equations. For this, the four distributed parameters of the line are expanded in Fourier series.

Secondly, we presented KF-based state estimation and EKF and UKF-based parameter estimation for three-phase NTL. For this, state space model for three-phase transposed and untransposed NTL has been obtained by including Fourier series expansion of state and Gaussian noise vectors in the stochastic differential equations. Clarke transformation matrix has been utilized for phase to sequence transformation which allows to represent the three-phase TL into fully transposed TL. The measurement model for current and voltage vectors along the line are expressed in terms of Fourier series. Also, the frequency domain analysis is used to obtain the eigenvalue and eigenvector for measurement model. The voltage and current of NTL are expanded in Fourier series to obtain the sparse matrix formulation using Kronecker product. Kronecker product representation of discrete unitary transforms results in computer efficient implementation. This work implements the analysis of nonlinearity effect in transmission line using perturbation theory. For this, the nonlinearity of the transmission line is included by perturbing the voltage and current of the line. Also, we compared the estimation performances with RLS method. This chapter also discusses few recent methods used for state and parameter estimation and their disadvantages.

7.2 Scope for Future Work

For working with nanotechnology-based circuits both with lumped and distributed parameters, we require to formulate circuit or transmission line dynamics in terms of quantum stochastic differential equations in the sense of Hudson and Parthasarathy. Noisy Heisenberg dynamics for circuit observables like current and voltage can be derived from noisy Schrodinger dynamics. For this, one must first start with a circuit Hamiltonian based on the total electrostatic energy in capacitors plus total magnetic energy in inductors and then include Lindblad noise terms so that the corresponding Heisenberg quantum stochastic differential equation (QSDE) generalised a classical situation. Then by taking non-demolition measurements, in the sense of V. P. Belavkin, we use the Belavkin quantum filter to estimate parameters and the system state on a real-time basis. This has direct applications to devices like quantum tunnelling diodes, nanomotors and more generally quantum electromagnetic fields enclosed within nanocavities. Molecular dynamics in the presence of radiation can also be controlled using this approach which enables us to alter the chemical properties of compounds leading to the manufacture of new kinds of drugs a science well known by the name molecular medicine.

List of Publications

- (a) **Amit Kumar Gautam**, Sudipta Majumdar and Harish Parthasarathy, "State and parameter estimation of non-uniform transmission line using Kronecker product based modeling," IEEE Transactions on Power Delivery, ISSN no. 1937-4208, vol. 37, no. 5, pp. 4291-4302, 2022.
- (b) **Amit Kumar Gautam** and Sudipta Majumdar, "Application of stochastic filter to three-phase nonuniform transmission lines," International Journal of Electronics, ISSN no. 1362-3060, 2023.
- (c) **Amit Kumar Gautam** and Sudipta Majumdar, "Kronecker product based modeling of Darlington amplifier and state estimation using unscented Kalman filter," International Journal of Electronics Letters, ISSN no. 2168-1732, 2022.
- (d) **Amit Kumar Gautam** and Sudipta Majumdar, "State estimation of RC filter using unscented Kalman filters," International Journal of Innovative Technology and Exploring Engineering, ISSN no. 2278-3075, vol. 9, no. 9, pp. 91-96, 2020.
- (e) **Amit Kumar Gautam** and Sudipta Majumdar, "State estimation of common emitter amplifier using iterated extended Kalman filters," International Journal of Innovative Technology and Exploring Engineering, ISSN no. 2278-3075, vol. 8, no. 9, pp. 1784-1789, 2019.
- (f) **Amit Kumar Gautam** and Sudipta Majumdar, "Parameter estimation of RC circuits using extended Kalman filter," International Journal of Advanced in Management, Technology and Engineering Sciences, ISSN no. 2249-7455, vol. 8, no. 1, pp. 83-91, 2018.
- (g) **Amit Kumar Gautam** and Sudipta Majumdar, "Parameter estimation of diode circuit using extended Kalman filter," World Academy of Science, Engineering and Technology International Journal of Electronics and Commu-

nication Engineering, ISSN no. 1307- 6892, vol. 12, no. 9, pp. 605-610, 2018.

- (h) **Amit Kumar Gautam** and Sudipta Majumdar, "Iterated extended Kalman filter based state estimation of diode circuit," in Journal of Physics: Conference Series 2070 (2021) 012092, pp. 1-10, 2021.
 - (i) **Amit Kumar Gautam** and Sudipta Majumdar, "State estimation of single-phase rectifier based load using unscented Kalman filter," in 2nd IEEE International Conference on Power Electronics, Intelligent Control and Energy Systems (ICPEICES-2018), pp. 1172-1177, 2018.
 - (j) **Amit Kumar Gautam** and Sudipta Majumdar, "Volterra model of silicon controlled rectifier," in International Conference on Functional Materials, Characterization, Solid State Physics, Power, Thermal and Combustion Energy, AIP Conference Proceedings 1859, 020060 , pp.1-8, 2017.
-

References

- [1] H. Kuntman, "Application of modified Ebers Moll model to nonlinear distortion analysis of transistor amplifier," *Electronics Letters*, vol. 19, no. 4, pp. 126–127, 1983.
- [2] K. L. Fong and R. G. Meyer, "High frequency nonlinear analysis of common emitter and differential pair transconductance stages," *IEEE Journal of Solid State circuits*, vol. 33, no. 4, pp. 548–555, 1998.
- [3] B. Song, S. He, J. Peng and Y. Zhao, "Dynamic deviation memory polynomial model for digital predistortion," *Electronics Letters*, vol. 53, no. 9, pp. 606-607, 2017.
- [4] X. Wu, F. Grassi, P. Manfredi and D. V. Ginste, "Perturbative analysis of differential to common mode conversion in asymmetric nonuniform interconnects," *IEEE Transactions on Electromagnetic Compatibility*, vol. 60, no. 1, pp. 7-15, 2018.
- [5] S. Afifi and R. Dusseaux, "Scattering from 2-D perfect electromagnetic conductor rough surface: analysis with the small perturbation method and the small slope approximation," *IEEE Transactions on Antennas and Propagation*, vol. 66, no. 1, pp. 340-346, 2018.
- [6] S. Mishra and R. D. S. Yadava, "A method for chaotic self-modulation in nonlinear colpitts oscillator and its potential applications," *Circuits, Systems, and Signal Processing*, pp. 1-21, 2017.
- [7] W. Q. Liu, X. M. Wang and Z. L. Deng, "Robust centralized and weighted measurement fusion Kalman predictors with multiplicative noises, uncertain noise variances, and missing measurements," *Circuits, Systems, and Signal Processing*, pp. 1-40, 2017.
- [8] M. V. Thuan and D. C. Huong, "New Results on Exponential Stability and Passivity Analysis of Delayed Switched Systems with Nonlinear

Perturbations," *Circuits, Systems, and Signal Processing*, pp. 1-24, 2017.

- [9] A. Buonomo and A. L. Schiavo, "Predicting nonlinear distortion in multistage amplifiers and gm-C filters. *Analog Integrated Circuits and Signal Processing*, vol. 77, no. 3, pp. 483-493, 2013.
- [10] H. Wang, M. Qi and B. Wang, "PPV modeling of memristor-based oscillators and application to ONN pattern recognition," *IEEE Transactions on Circuits and Systems II: Express Briefs*, vol. 64, no. 6, pp. 610-614, 2017.
- [11] W. Wang, S. K. Nguang, S. Zhong and H. Y. Liu, "New delay-dependent stability criteria for uncertain neutral system with time-varying delays and nonlinear perturbations", *Circuits, Systems, and Signal Processing*, vol. 33, no. 9, pp. 2719- 2740, 2014.
- [12] S. Lakshmanan, J. H. Park and H. Y. Jung, "Robust delay-dependent stability criteria for dynamic systems with nonlinear perturbations and leakage delay," *Circuits, systems, and signal processing*, vol. 32, no. 4, pp. 1637-1657, 2013.
- [13] F. Auger, M. Hilaret, J. M. Guerrero, E. Monmasson, T. Orłowska-Kowalska and S. Katsura, "Industrial applications of the Kalman filter: A review," *IEEE Transactions on Industrial Electronics*, vol. 60, no. 12, pp.5458-5471, 2013.
- [14] R. Diversi, R. Guidorzi and U. Soverini, "Kalman filtering in extended noise environments," *IEEE Transactions on Automatic Control*, vol. 50, no. 9, pp. 1396-1402, 2005.
- [15] A. A. Girgis and D. G. Hart, "Implementation of Kalman and adaptive Kalman filtering algorithms for digital distance protection on a vector signal processor," *IEEE Transactions on Power Delivery*, vol. 4, no. 1, pp.141-156, 1989.
- [16] D. F. Crouse, P. Willett and Y. Bar-Shalom, "A low-complexity sliding-window Kalman FIR smoother for discrete-time models," *IEEE Signal Processing Letters*, vol. 17, no. 2, pp.177-180, 2009.
- [17] J. Sarmavuori and S. Sarkka, "Fourier-hermite kalman filter," *IEEE Transactions on Automatic Control*, vol. 57, no. 6, pp.1511-1515, 2011.

- [18] L. Hong, G. Cheng and C. K. Chui, "A filter-bank-based Kalman filtering technique for wavelet estimation and decomposition of random signals," *IEEE Transactions on Circuits and Systems II: Analog and Digital Signal Processing*, vol. 45, no. 2, pp.237-241, 1998.
- [19] J. R. Macias and A. G. Exposito, "Self-tuning of Kalman filters for harmonic computation," *IEEE transactions on power delivery*, vol. 21, no. 1, pp.501-503, 2005.
- [20] L. Reggiani, L. Dossi, L. Barletta and A. Spalvieri, "Extended Kalman filter for MIMO phase noise channels with independent oscillators," *IEEE Communications Letters*, vol. 22, no. 6, pp.1200-1203, 2018..
- [21] K. Reif and R. Unbehauen, "The extended Kalman filter as an exponential observer for nonlinear systems," *IEEE Transactions on Signal processing*, vol. 47, no. 8, pp.2324-2328, 1999.
- [22] C. Pantaleon and A. Souto, " An aperiodic phenomenon of the extended Kalman filter in filtering noisy chaotic signals," *IEEE transactions on signal processing*, vol. 53, no. 1, pp.383-384, 2004.
- [23] Y. S. Shmaliy, "Suboptimal FIR filtering of nonlinear models in additive white Gaussian noise," *IEEE Transactions on Signal Processing*, vol. 60, no. 10, pp.5519-5527, 2012.
- [24] P. Stano, Z. Lendek, J. Braaksma, R. Babuška, C. de Keizer and J. Arnold, "Parametric Bayesian filters for nonlinear stochastic dynamical systems: A survey," *IEEE transactions on cybernetics*, vol. 43, no. 6, pp.1607-1624, 2013.
- [25] S. J. Julier, J. K. Uhlmann and H. F. Durrant-Whyte, "A new approach for filtering nonlinear systems," In *Proceedings of 1995 American Control Conference-ACC'95 IEEE*, Vol. 3, pp. 1628-1632, 1995.
- [26] D. Simon, "Optimal state estimation: Kalman, H infinity, and nonlinear approaches," *John Wiley and Sons*, 2006.
- [27] S. J. Julier and J. K. Uhlmann, "New extension of the Kalman filter to nonlinear systems," In *Signal processing, sensor fusion, and target recognition VI, International Society for Optics and Photonics*, Vol. 3068, pp. 182-193, 1997.
- [28] S. Julier, J. Uhlmann and H.F. Durrant-Whyte, "A new method for the nonlinear transformation of means and covariances in filters and

estimators," *IEEE Transactions on automatic control*, vol. 45, no. 3, pp.477-482, 2000.

- [29] M. Ahmeid, M. Armstrong, S. Gadoue, M. Al-Greer and P. Missailidis, "Real-time parameter estimation of dc–dc converters using a self-tuned Kalman filter," *IEEE Transactions on Power Electronics*, vol. 32, no. 7, pp.5666-5674, 2016.
- [30] N. Hoffmann and F. W. Fuchs, "Minimal invasive equivalent grid impedance estimation in inductive–resistive power networks using extended Kalman filter," *IEEE Transactions on Power Electronics*, vol. 29, no. 2, pp.631-641, 2013.
- [31] S. Nadarajan, S. K. Panda, B. Bhangu and A. K. Gupta, "Online model-based condition monitoring for brushless wound-field synchronous generator to detect and diagnose stator windings turn-to-turn shorts using extended Kalman filter," *IEEE Transactions on Industrial Electronics*, vol. 63, no. 5, pp.3228-3241, 2016.
- [32] M. Yazdani, A. Mehrizi-Sani and M. Mojiri, "Estimation of electromechanical oscillation parameters using an extended Kalman filter," *IEEE Transactions on Power Systems*, vol. 30, no. 6, pp.2994-3002, 2015.
- [33] K. Bogdanski and M. C. Best, "Kalman and particle filtering methods for full vehicle and tyre identification," *Vehicle System Dynamics*, vol. 56, no. 5, pp.769-790.
- [34] Y. Tian, B. Xia, W. Sun, Z. Xu and W. Zheng, "A modified model based state of charge estimation of power lithiumion batteries using unscented Kalman filter," *Journal of power sources*, vol. 270, pp.619-626, 2014.
- [35] E. Ghahremani and I. Kamwa, "Online state estimation of a synchronous generator using unscented Kalman filter from phasor measurements units," *IEEE Transactions on Energy Conversion*, vol. 26, no. 4, pp.1099-1108.
- [36] A. H. Jazwinski, "Stochastic Processes and Filtering Theory," *New York: Academic Press*, 1970.
- [37] A. K. Gautam and S. Majumdar, "Parameter estimation of RC circuits using extended Kalman filter," *International Journal of Advanced in*

Management, Technology and Engineering Sciences, vol. 8, no. 1, pp. 83-91, 2018.

- [38] R. Bansal and S. Majumdar, "Implementation of extended Kalman filter on stochastic model of LPF," *International Journal of Advanced in Management, Technology and Engineering Sciences*, vol. 7, no. 12, 2017.
- [39] S. J. Julier and J. K. Uhlmann, "Unscented filtering and nonlinear estimation," *roceedings of the IEEE*, vol. 92, no. 3, pp.401-422, 2004.
- [40] A. Buonomo and A. L. Schiavo, "Perturbation analysis of nonlinear distortion in analog integrated circuits," *IEEE Transactions on Circuits and Systems I: Regular Papers*, vol. 52, no. 8, pp.1620-1631, 2005.
- [41] S. Majumdar and H. Parthasarathy, "Perturbation approach to Ebers-Moll equations for transistor circuit analysis," *Circuits, Systems and Signal Processing*, vol. 29, no. 3, pp.431-448, 2010.
- [42] A. Rathee and H. Parthasarathy, "Perturbation-Based Fourier Series Analysis of Transistor Amplifier," *Circuits, Systems, and Signal Processing*, vol. 31, no. 1, pp. 313-328, 2012.
- [43] A. Rathee and H. Parthasarathy, "Perturbation-based stochastic modeling of nonlinear circuits," *Circuits, Systems, and Signal Processing*, vol. 32, no. 1, pp. 123-141, 2013.
- [44] Y. Dang, Y. Liang, B. Bie, J. Ding and Y. Zhang, "A Range Perturbation Approach for Correcting Spatially Variant Range Envelope in Diving Highly Squinted SAR With Nonlinear Trajectory," *IEEE Geoscience and Remote Sensing Letters*, vol. 15, no. 6, pp.858-862, 2018.
- [45] H. Bulow, V. Aref, and L. Schmalen, "Modulation on discrete nonlinear spectrum: Perturbation sensitivity and achievable rates," *IEEE Photonics Technology Letters*, vol. 30, no. 5, pp.423-426, 2018.
- [46] W. A. Ali, D. A. Mohamed and A. H. Hassan, "Performance analysis of least mean square sample matrix inversion algorithm for smart antenna system," In *Antennas and Propagation Conference (LAPC) IEEE*, pp. 624-629, 2013.
- [47] D. Z. Feng, Z. Bao and L. C. Jiao, "Total least mean squares algorithm," *IEEE Transactions on Signal Processing*, vol. 46, no. 8, pp. 2122-2130, 1998.

- [48] A. K. Pradhan, A. Routray and A. Basak, "Power system frequency estimation using least mean square technique," *IEEE transactions on power delivery*, vol. 20, no. 3, pp. 1812-1816, 2005.
- [49] W. Edmonson, J. Principe, K. Srinivasan and C. Wang, "A global least mean square algorithm for adaptive IIR filtering," *IEEE Transactions on Circuits and Systems II: Analog and Digital Signal Processing*, vol. 45, no. 3, pp. 379-384, 1998.
- [50] I. Lakkis and D. McLernon, "Least mean squares algorithm for fractionally spaced blind channel estimation," *IEE Proceedings-Vision, Image and Signal Processing*, vol. 146, no. 4, pp. 181-184, 1999.
- [51] Y. Wang, R. Pan, C. Liu, Z. Chen and Q. Ling, "Power capability evaluation for lithium iron phosphate batteries based on multi-parameter constraints estimation," *Journal of Power Sources*, vol. 374, pp. 12-23, 2018..
- [52] B. Fridholm, T. Wik, H. Kuusisto and A. Klintberg, "Estimating power capability of aged lithiumion batteries in presence of communication delays," *Journal of Power Sources*, vol. 383, pp. 24-33, 2018.
- [53] Z. Wei, S. Meng, K. J. Tseng, T. M. Lim, B. H. Soong and M. Skyllas-Kazacos, "An adaptive model for vanadium redox flow battery and its application for online peak power estimation," *Journal of Power Sources*, vol. 344, pp. 195-207, 2017.
- [54] R. Xiong, F. Sun, H. He and T. D. Nguyen, "A data-driven adaptive state of charge and power capability joint estimator of lithiumion polymer battery used in electric vehicles," *Energy*, vol. 63, pp. 295-308, 2013.
- [55] S. Haykin, "Adaptive filter theory", 1991.
- [56] L. Lou, J. J. Liou, S. Dong and Y. Han, "Silicon controlled rectifier (SCR) compact modeling based on VBIC and Gummel–Poon models," *Solid-state electronics*, vol. 53, no. 2, pp.195-203, 2009.
- [57] L. Lou and J. J. Liou, "An improved compact model of silicon-controlled rectifier (SCR) for electrostatic discharge (ESD) applications," *IEEE transactions on electron devices*, vol. 55, no. 12, pp.3517-3524, 2008.
- [58] C. Y. Lin and R. K. Chang, "Design of ESD Protection Device for K/Ka -Band Applications in Nanoscale CMOS Process," *IEEE Transactions*

on Electron Devices, vol. 62, no. 9, pp.2824-2829, 2015.

- [59] C. Y. Lin and M. L. Fan, "Design of ESD protection diodes with embedded SCR for differential LNA in a 65-nm CMOS process," *IEEE Transactions on microwave theory and techniques*, vol. 62, no. 11, pp.2723-2732, 2014.
- [60] Y. Yang, P. Davari, F. Zare and F. Blaabjerg, "A DC-link modulation scheme with phase-shifted current control for harmonic cancellations in multidrive applications," *IEEE Transactions on Power Electronics*, vol. 31, no. 3, pp.1837-1840, 2015.
- [61] J. Solanki, N. Frohleke, J. Bocker, G. Duppe, A. Averberg and P. Wallmeier, "Voltage Sequence Control Based High Current Rectifier System," *IEEE Transactions on Industry Applications*, vol. 51, no. 5, pp.3995-4005, 2015.
- [62] T. Ghanbari, E. Farjah, and N. Tashakor, "Thyristor based bridge-type fault current limiter for fault current limiting capability enhancement," *IET Generation, Transmission and Distribution*, vol. 10, no. 9, pp.2202-2215, 2016.
- [63] S. L. Chen and Y. T. Huang, "Design and layout strategy in the 60-V power PLDMOS with drain-end modulated engineering of reliability considerations," *IEEE Transactions on Power Electronics*, vol. 31, no. 7, pp. 5113-5121, 2015.
- [64] R. C. Sun, Z. Wang, M Klebanov, W. Liang, J. J. Liou, and Liu, D.G., 2015. Silicon-controlled rectifier for electrostatic discharge protection solutions with minimal snapback and reduced overshoot voltage. *IEEE Electron Device Letters*, 36(5), pp.424-426.
- [65] H. Liang, X. Gu, S. Dong and J. J. Liou, "RC-embedded LDMOS-SCR with high holding current for high-voltage I/O ESD protection," *IEEE Transactions on Device and Materials Reliability*, vol. 15, no. 4, pp. 495-499, 2015.
- [66] Q. Cui, J. A. Salcedo, S. Parthasarathy, Y. Zhou, J. J. Liou and J. J. Hajjar, "High-robustness and low-capacitance silicon-controlled rectifier for high-speed I/O ESD protection," *IEEE electron device letters*, vol. 34, no. 2, pp.178-180, 2013.

- [67] C. T. Dai and M. D. Ker, "ESD protection design with stacked high-holding-voltage SCR for high-voltage pins in a battery-monitoring IC," *IEEE Transactions on Electron Devices*, vol. 63, no. 5, pp.1996-2002, 2016.
- [68] T. Onchi, D. McColl, A. Rohollahi, C. Xiao, A. Hirose, M. Dreval and S. Wolfe, "Development toward a repetitive compact torus injector," *IEEE Transactions on Plasma Science*, vol. 44, no. 2, pp.195-200, 2015.
- [69] F. A. Altolaquirre and M. D. Ker, "Quad-SCR device for cross-domain ESD protection," *IEEE Transactions on Electron Devices*, vol. 63, no. 8, pp.3177-3184, 2016.
- [70] Z. Ali, K. Saleem, N. Christofides, A. Rashid, H. Zaman, M. Tahir and U. Younas, "Performance analysis of fuzzy logic control and six-pulse line-commutated converter in dc motor drive application," *In 2015 International Conference on Emerging Technologies (ICET) IEEE*, pp. 1-6, 2015.
- [71] P. Nabatia and R. Farnooshb, "Stochastic perspective and parameter estimation for RC and RLC electrical circuits," *Int. J. Nonlinear Anal. Appl*, vol. 6, no. 1, pp.153-161, 2015.
- [72] Y. Trachi, E. Elbouchikhi, V. Choqueuse, M. E. H. Benbouzid and T. Wang, "A novel induction machine fault detector based on hypothesis testing," *IEEE Transactions on Industry Applications*, vol. 53, no. 3, pp.3039-3048, 2016.
- [73] J. Pan, X. Jiang, X. Wan and W. Ding, "A filtering based multi-innovation extended stochastic gradient algorithm for multivariable control systems," *International Journal of Control, Automation and Systems*, vol. 15, no. 3, pp.1189-1197, 2017.
- [74] Z. H. Liu, H. L. Wei, Q. C. Zhong, K. Liu, X. S. Xiao and L. H. Wu, "Parameter estimation for VSI-fed PMSM based on a dynamic PSO with learning strategies," *IEEE Transactions on Power Electronics*, vol. 32, no. 4, pp.3154-3165, 2016.
- [75] M. S. Arefin, J. M. Redouté and M. R. Yuce, "A low-power and wide-range MEMS capacitive sensors interface IC using pulse-width modulation for biomedical applications," *IEEE Sensors Journal*, vol. 16(17), pp.6745-6754.

- [76] P. Mitros, "Filters with decreased passband error." *IEEE Transactions on Circuits and Systems II: Express Briefs*, vol. 63, no. 2, pp.131-135, 2015.
- [77] X. Yang, "A Flexible Continuous-Time? S ADC With Programmable Bandwidth Supporting Low-Pass and Complex Bandpass Architectures," *IEEE Transactions on Very Large Scale Integration (VLSI) Systems*, vol. 25, no. 3, pp.872-880, 2016.
- [78] T. Moy, L. Huang, W. Rieutort-Louis, C. Wu, P. Cuff, S Wagner, J. C. Sturm and N. Verma, "An EEG acquisition and biomarker-extraction system using low noise amplifier and compressive-sensing circuits based on flexible, thin-film electronics," *IEEE Journal of Solid-State Circuits*, vol. 52, no. 1, pp.309-321, 2016.
- [79] J. Li, W. X. Zheng, J. Gu, and L. Hua, "Parameter estimation algorithms for Hammerstein output error systems using Levenberg–Marquardt optimization method with varying interval measurements," *Journal of the Franklin Institute*, vol. 354, no. 1, pp.316-331, 2017.
- [80] W. Zhu, K. Zhou, M. Cheng and F. Peng, "A high-frequency-link singlephase PWM rectifier," *IEEE Transactions on Industrial Electronics*, vol. 62, no. 1, pp. 289-298, January 2015.
- [81] M. S. Ortmann, T. B. Soeiro and M. L. Heldwein, "High switches utilization single-phase PWM boost-type PFC rectifier topologies multiplying the switching frequency," *IEEE Transactions on Power Electronics*, vol. 29, no. 11, pp. 5749-5760, November 2014.
- [82] B. Gou, X. Ge, S. Wang, X. Feng, J. B. Kuo and T. G. Habetler, "An open-switch fault diagnosis method for single-phase PWM rectifier using a model-based approach in high-speed railway electrical traction drive system," *IEEE Transactions on Power Electronics*, vol. 31, no. 5, pp. 3816-3826, May 2016.
- [83] S. Zeinolabedinzadeh, H. Ying, Z. E. Fleetwood, N. J. H. Roche, A. Khachatryan, D. McMorrow, S.P. Buchner, J. H. Warner, P. Paki-Amouzou and J. D. Cressler, "Single-event effects in high-frequency linear amplifiers: experiment and analysis," *IEEE Transactions on Nuclear Science*, vol. 64, no. 1, pp. 125-132, 2016.

- [84] S. Zeinolabedinzadeh, A. Ç. Ulusoy, M.A. Oakley, N. E. Lourenco and J.D. Cressler, "A 0.3–15 GHz SiGe LNA with 1 THz gain-bandwidth product," *IEEE Microwave and Wireless Components Letters*, vol. 27, no. 4, pp.380-382, 2017.
- [85] S. P. Voinigescu, , Shopov, S., Bateman, J., Farooq, H., Hoffman, J. and Vasilakopoulos, K., 2017. Silicon millimeter-wave, terahertz, and high-speed fiber-optic device and benchmark circuit scaling through the 2030 ITRS horizon. *Proceedings of the IEEE*, 105(6), pp.1087-1104.
- [86] C. R. Chappidi and K. Sengupta, "Frequency reconfigurable mm-wave power amplifier with active impedance synthesis in an asymmetrical non-isolated combiner: Analysis and design," *IEEE Journal of Solid-State Circuits*, vol. 52, no. 8, pp.1990-2008, 2017.
- [87] S. Y. Mortazavi and K. J. Koh, "Integrated inverse class-F silicon power amplifiers for high power efficiency at microwave and mm-wave," *IEEE Journal of Solid-State Circuits*, vol. 51, no. 10, pp.2420-2434, 2016.
- [88] K. Greene, A. Sarkar and B. Floyd, "A 60-GHz dual-vector Doherty beamformer," *IEEE Journal of Solid-State Circuits*, vol. 52, no. 5, pp.1373-1387, 2017.
- [89] M. D. Luong, R. Ishikawa, Y. Takayama and K. Honjo, "Microwave characteristics of an independently biased 3-stack InGaP/GaAs HBT configuration," *IEEE Transactions on Circuits and Systems I: Regular Papers*, vol. 64, no. 5, pp.1140-1151, 2016.
- [90] B. Moeneclaey, F. Blache, J. Van Kerrebrouck, R. Brenot, G. Coudyzer, M. Achouche, X.Z. Qiu, J. Bauwelinck and X. Yin, "40-Gb/s TDM-PON downstream link with low-cost EML transmitter and APD-based electrical duobinary receiver," *Journal of Lightwave Technology*, vol. 35, no. 4, pp.1083-1089, 2017.
- [91] J. Lee and J. D. Cressler, "Analysis and design of an ultra-wideband low-noise amplifier using resistive feedback in SiGe HBT technology," *IEEE transactions on microwave theory and techniques*, vol. 54, no. 3, pp.1262-1268, 2006.
- [92] M. D. Tsai, C. S. Lin, C. H. Lien, H. and Wang, "Broad-band MMICs based on modified loss-compensation method using 0.35- μm

SiGe BiCMOS technology," *IEEE transactions on microwave theory and techniques*, vol. 53, no. 2, pp.496-505, 2005.

- [93] C. W. Kuo, H. K. Chiou and H. Y. Chung, "An 18 to 33 GHz Fully-Integrated Darlington Power Amplifier With Guanella-Type Transmission-Line Transformers in 0.18 μ m CMOS Technology," *IEEE microwave and wireless components letters*, vol. 23, no. 12, pp.668-670, 2013.
- [94] S. H. Weng, H.Y.Chang and C. C. Chiong, "A DC-21 GHz low imbalance active balun using darlington cell technique for high speed data communications," *IEEE microwave and wireless components letters*, vol. 19, no. 11, pp.728-730, 2009.
- [95] A. Mukherjee, C. Lin and M. Schröter, "The broadband Darlington amplifier as a simple benchmark circuit for compact model verification at mm-wave frequency," *In 2016 IEEE Bipolar/BiCMOS Circuits and Technology Meeting (BCTM) IEEE*, pp. 102-105, 2016.
- [96] S. Shukla and B. Pandey, "Two-stage small-signal amplifier with Darlington and Sziklai pairs," *In 2014 IEEE International Conference on Semiconductor Electronics (ICSE2014) IEEE*, pp. 13-16, 2014.
- [97] A. Mojab and S. K. Mazumder, "Design and characterization of high-current optical darlington transistor for pulsed-power applications," *IEEE Transactions on Electron Devices*, vol. 64, no. 3, pp. 769-778, 2016.
- [98] S. H. Weng, H. Y. Chang, C. C. Chiong and Y. C. Wang, "Gain-bandwidth analysis of broadband Darlington amplifiers in HBT-HEMT process," *IEEE transactions on microwave theory and techniques*, vol. 60, no. 11, pp. 3458-3473, 2012.
- [99] J. Lee and J. D. Cressler, "A 3-10 GHz SiGe resistive feedback low noise amplifier for UWB applications," *In 2005 IEEE Radio Frequency integrated Circuits (RFIC) Symposium-Digest of Papers IEEE*, pp. 545-548, 2005.
- [100] S. H. Weng, H. Y. Chang and C.C. Chiong, "Design of a 0.5–30 GHz Darlington amplifier for microwave broadband applications," *In 2010 IEEE MTT-S International Microwave Symposium IEEE*, pp. 137-140, 2010.

- [101] A. Bernardini, K. J. Werner, A. Sarti and J. O. Smith III, "Modeling nonlinear wave digital elements using the Lambert function," *IEEE Transactions on Circuits and Systems I: Regular Papers*, Vol. 63, No. 8, pp. 1231-1242, 2016.
- [102] Y. Laamari, K. Chafaa and B. Athamena, "Particle swarm optimization of an extended Kalman filter for speed and rotor flux estimation of an induction motor drive," *Electrical Engineering*, vol. 97, no. 2, pp. 129-138, 2015.
- [103] S. M. Ghiasi, M. Abedi and S. H. Hosseinian, "A new approach for the estimation of transient voltage profile along transmission line," *Canadian Journal of Electrical and Computer Engineering*, vol. 40, no. 4, pp. 295- 302, 2017.
- [104] R. Fan, Y. Liu, R. Huang, R. Diao and S. Wang, "Precise fault location on transmission lines using ensemble Kalman filter," *IEEE Transactions on Power Delivery*, vol. 33, no. 6, pp. 3252-3255, 2018.
- [105] C. Rakpenthai and S. Uatrongjit, "Power system state and transmission line conductor temperature estimation," *IEEE Transactions on Power Systems*, vol. 32, no. 3, pp. 1818-1827, 2017.
- [106] S. Malhara and V. Vittal, "Mechanical state estimation of overhead transmission lines using tilt sensors," *IEEE Transactions on Power Systems*, vol. 25, no. 3, pp. 1282-1290, 2010.
- [107] Y. Liu, A. S. Meliopoulos, R. Fan, L. Sun and Z. Tan, "Dynamic state estimation based protection on series compensated transmission lines," *IEEE Transactions on Power Delivery*, vol. 32, no. 5, pp. 2199-2209, 2017.
- [108] P. Ramachandran, V. Vittal and G. T. Heydt, "Mechanical state estimation for overhead transmission lines with level spans," *IEEE Transactions on Power Systems*, vol. 23, no. 3, pp. 908-915, 2008.
- [109] Y. Liu, A. P. Meliopoulos, L. Sun and R. Fan, "Dynamic state estimation based protection of mutually coupled transmission lines," *CSEE Journal of Power and Energy Systems*, vol. 2, no. 4, pp. 6-14, 2016.

- [110] Y. Liu, A. S. Meliopoulos, Z. Tan, L. Sun and R. Fan, "Dynamic state estimation-based fault locating on transmission lines," *IET Generation, Transmission and Distribution*, vol. 11, no. 17, pp. 4184-4192, 2017.
- [111] Y. Liu, B. Wang, X. Zheng, D. Lu, M. Fu and T. NengLing, "Fault Location Algorithm for Non-Homogeneous Transmission Lines Considering Line Asymmetry," *IEEE Transactions on Power Delivery*, vol. 35, no. 5, pp. 2425-2437, 2020.
- [112] J. Yang, W. A. Zhang and F. Guo, "Dynamic State Estimation for Power Networks by Distributed Unscented Information Filter," *IEEE Transactions on Smart Grid*, vol. 11, no. 3, pp. 2162-2171, 2020.
- [113] Q. Li, L. Cheng, W. Gao and D. W. Gao, "Fully Distributed State Estimation for Power System with Information Propagation Algorithm," *Journal of Modern Power Systems and Clean Energy*, vol. 8, no. 4, pp. 627-635, 2020.
- [114] I. Mohammed, S. J. Geetha, S. S. Shinde, K. Rajawat and S. Chakrabarti, "Modified Re-Iterated Kalman Filter for Handling Delayed and Lost Measurements in Power System State Estimation," *IEEE Sensors Journal*, vol. 20, no. 7, pp. 3946-3955, 2020.
- [115] H. H. Alhelou, M. E. Golshan and N. D. Hatziargyriou, "Deterministic dynamic state estimation-based optimal LFC for interconnected power systems using unknown input observer," *IEEE Transactions on Smart Grid*, vol. 11, no. 2, pp. 1582-1592, 2020.
- [116] A. S. Dobakhshari, S. Azizi, M. Paolone and V. Terzija, "Ultra fast linear state estimation utilizing SCADA measurements," *IEEE Transactions on Power Systems*, vol. 34, no. 4, pp. 2622-2631, 2019.
- [117] D. Ritzmann, P. S. Wright, W. Holderbaum, B. Potter, "A method for accurate transmission line impedance parameter estimation," *IEEE Transactions on instrumentation and measurement*, vol. 65, no. 10, pp. 2204-2213, 2016.
- [118] A. Bendjabeur, A. Kouadri and S. Mekhilef, "Novel technique for transmission line parameters estimation using synchronised sampled data," *IET Generation, Transmission and Distribution*, vol. 14, no. 3, pp. 506-515, 2020.

- [119] I. Tolić, K. Miličević, N. Šuvak and I. Biondić, "Non-linear least squares and maximum likelihood estimation of probability density function of cross-border transmission losses," *IEEE Transactions on Power Systems*, vol. 33, no. 2, pp. 2230-2238, 2018.
- [120] M. Yang, J. Wang, H. Diao, J. Qi, X. Han, "Interval estimation for conditional failure rates of transmission lines with limited samples," *IEEE Transactions on Smart Grid*, vol. 9, no. 4, pp. 2752-2763, 2018.
- [121] M. Asprou and E. Kyriakides, "Identification and estimation of erroneous transmission line parameters using PMU measurements," *IEEE transactions on power delivery*, vol. 32, no. 6, pp. 2510-2519, 2018.
- [122] C. Wang, V. A. Centeno, K. D. Jones and D. Yang, "Transmission lines positive sequence parameters estimation and instrument transformers calibration based on PMU measurement error model," *IEEE Access.*, vol. 7, pp. 145104-145117, 2019.
- [123] W. Sima, Y. Li, V. A. Rakov, Q. Yang, T. Yuan and M. Yang, "An analytical method for estimation of lightning performance of transmission lines based on a leader progression model," *IEEE Transactions on Electromagnetic Compatibility*, vol. 56, no. 6, pp. 1530-1539, 2014.
- [124] G. Sivanagaraju, S. Chakrabarti and S. C. Srivastava, "Uncertainty in transmission line parameters: Estimation and impact on line current differential protection," *IEEE Transactions on Instrumentation and Measurement*, vol. 63, no. 6, pp. 1496-1504, 2014.
- [125] M. S. Halligan and D. G. Beetner, "Maximum crosstalk estimation in weakly coupled transmission lines," *IEEE transactions on electromagnetic compatibility*, vol. 56, no. 3, pp. 736-44, 2014.
- [126] P. Ren, H. Lev-Ari and A. Abur, "Tracking three-phase untransposed transmission line parameters using synchronized measurements," *IEEE Transactions on Power Systems*, vol. 33, no. 4, pp. 4155-63, 2018.
- [127] P. A. Regalia, M. K. Sanjit, "Kronecker products, unitary matrices and signal processing applications," *SIAM review*, vol. 31, no. 4, pp. 586-613, 1989.

- [128] L. Kumar, V. S. Pandey, H. Parthasarathy, V. Shrimali, "Hysteresis Effects on a Non-uniform Transmission Line with Induced Quantum Mechanical Atomic Transitions," *Journal of Superconductivity and Novel Magnetism*, vol. 31, no. 5, pp. 1587-1605, 2017.
- [129] O.Nelles, "Nonlinear System Identification: From Classical Approaches to Neural Networks, Fuzzy Models, and Gaussian Processes," *Springer Nature*, pp. 60-66, 2020.
- [130] B. Gustavsen, "Frequency-dependent transmission line modeling utilizing transposed conditions," *IEEE transactions on power delivery* vol. 17, no. 3, pp. 834-839, 2002.
-